1-1-2013

Injectable Hydrogels for Local Protein Delivery to Engineer Myocardial Remodeling

Brendan Patrick Purcell
University of Pennsylvania, brendan.p.purcell@gmail.com

Injectable Hydrogels for Local Protein Delivery to Engineer Myocardial Remodeling

Abstract

The endogenous tissue remodeling events that occur following a myocardial infarction (MI) are inadequate to maintain left ventricular (LV) function, and the progression towards heart failure is often inevitable. Our increased understanding of protein regulators of post MI remodeling provides the opportunity to intervene and engineer tissue remodeling through exogenous protein delivery. The global hypothesis of this dissertation was that the local delivery of therapeutic proteins (SDF-1alpha and TIMP-3) from injectable hyaluronic acid (HA) hydrogels attenuates adverse post MI remodeling processes by providing sustained concentrations of bioactive signals within the remodeling myocardium.

To test this hypothesis, HA based hydrogels were designed with crosslinking chemistries to allow hydrogel formation and protein encapsulation in situ upon injection through a syringe, negatively charged polymer backbones to bind encapsulated proteins through electrostatic interactions and sustain protein release, and degradable crosslinks to release proteins in a controlled fashion. Using these injectable hydrogel systems, adverse post MI remodeling events were attenuated following experimental MI in animals by enhancing endogenous cell homing to the myocardium through SDF-1alpha delivery and inhibiting matrix metalloproteinase activity through TIMP-3 delivery.

Our results demonstrate the utility of implantable biomaterials to localize and sustain biological signals to engineer tissue remodeling processes, and provide insight into novel biological therapeutics to treat LV remodeling following MI.

Degree Type
Dissertation

Degree Name
Doctor of Philosophy (PhD)

Graduate Group
Bioengineering

First Advisor
Jason A. Burdick

Keywords
Drug Delivery, Hyaluronic Acid, Hydrogel, Myocardial Infarction, Polymer, Protein

Subject Categories
Biology | Biomedical | Mechanics of Materials

INJECTABLE HYDROGELS FOR LOCAL PROTEIN DELIVERY TO

ENGINEER MYOCARDIAL REMODELING

Brendan P. Purcell

A DISSERTATION

in Bioengineering

Presented to the Faculties of the University of Pennsylvania

In Partial Fulfillment of the Requirements for the Degree of Doctor of Philosophy

2013

Supervisor of Dissertation

_____

Jason A. Burdick, PhD
Professor of Bioengineering

Graduate Group Chairperson

_____

Jason A. Burdick, PhD
Professor of Bioengineering

Dissertation Committee
Andrew Tsourkas, PhD, Associate Professor of Bioengineering (Chair)
Kenneth Margulies, MD, Professor of Medicine
Robert Gorman, MD, Professor of Surgery

ACKNOWLEDGEMENTS

ABSTRACT

INJECTABLE HYDROGELS FOR LOCAL PROTEIN DELIVERY TO ENGINEER MYOCARDIAL REMODELING

Brendan P. Purcell

Jason A. Burdick, PhD

The endogenous tissue remodeling events that occur following a myocardial infarction (MI) are inadequate to maintain left ventricular (LV) function, and the progression towards heart failure is often inevitable. Our increased understanding of protein regulators of post MI remodeling provides the opportunity to intervene and engineer tissue remodeling through exogenous protein delivery. The global hypothesis of this dissertation was that the local delivery of therapeutic proteins (SDF-1α and TIMP-3) from injectable hyaluronic acid (HA) hydrogels attenuates adverse post MI remodeling processes by providing sustained concentrations of bioactive signals within the remodeling myocardium.

To test this hypothesis, HA based hydrogels were designed with crosslinking chemistries to allow hydrogel formation and protein encapsulation *in situ* upon injection through a syringe, negatively charged polymer backbones to bind encapsulated proteins through electrostatic interactions and sustain protein release, and degradable crosslinks to release proteins in a controlled fashion. Using these injectable hydrogel systems, adverse post MI remodeling events were attenuated following experimental MI in animals by enhancing endogenous cell homing to the myocardium through SDF-1α delivery and inhibiting matrix metalloproteinase activity through TIMP-3 delivery.

Our results demonstrate the utility of implantable biomaterials to localize and sustain biological signals to engineer tissue remodeling processes, and provide insight into novel biological therapeutics to treat LV remodeling following MI.

TABLE OF CONTENTS

CHAPTER 1

Introduction

1.1. Significance

The loss of functional tissue following a myocardial infarction (MI) is detrimental to heart function. Over 3 million people in the United States currently suffer from heart failure caused by MI[1] and more than 1 million MIs occur each year[2]. These troubling statistics amount to an economic burden of over $30 billion in the United States[2]. Current clinical treatments for MI include coronary stents and bypass surgeries to overcome the blocked artery and reperfuse the ischemic tissue. In addition, current pharmacological treatments lessen the workload of the injured heart. While these treatments delay the onset of heart failure following MI, they do little to alter the tissue remodeling process initiated after coronary artery occlusion. The changes in myocardial tissue structure during post MI remodeling cause global changes to left ventricle (LV) geometry, compromise LV function, and lead to the progression of heart failure. Unfortunately, whole organ-transplants remain the only current treatment for patients with end-stage heart failure, and these are severely limited by the low number of donor hearts.

1.2. Post MI remodeling

An MI occurs when arterial blood flow to the myocardium is interrupted, typically by a ruptured atherosclerotic plaque in the coronary arteries. The lack of oxygen supply (hypoxia) to the highly aerobic myocardium following coronary artery occlusion induces the expression of proteins active in tissue remodeling. These include surface adhesion molecules and soluble factors that activate the coronary endothelium and signal the infiltration of endogenous cells[3-6]. Within the first few hours post MI, neutrophils accumulate in the ischemic myocardium and release ROS and proteolytic enzymes that damage both vasculature and

parenchymal cells in the myocardium[6-9]. In addition, marrow derived monocytes infiltrate the myocardium and differentiate into macrophages upon adherence to the damaged ECM[10, 11]. These matured macrophages phagocytize necrotic cells, provide a major source of proteases, and secrete growth factors to activate fibroblast proliferation[10]. Proliferating fibroblasts within the MI region also express a number of proteins and proteolytic enzymes that contribute to tissue remodeling[12-15]. Together, proteins expressed from both recruited cells and cells native to the myocardium orchestrate the post MI remodeling process that occurs locally in the MI region of the myocardium. While there are potentially hundreds of proteins that contribute to tissue remodeling post MI, the following two sections will highlight two families of proteins that are particularly important post MI and the focus of the research that follows.

1.3. Matrix metalloproteinases (MMPs)

The abundance of protease activity in the setting of MI contributes to ECM degradation, instability in the MI region, and myocardial expansion. A family of proteolytic enzymes that contribute to MI expansion are the MMPs[16, 17]. MMPs hydrolyze peptide bonds with a high level of amino acid specificity and regulation. Under normal physiological conditions, MMP activity is precisely controlled to maintain a low level of structural protein, cell receptor, and growth factor turnover. However, following a stimulus such as an injury, there is a loss of control over MMP activity which causes maladaptive changes to tissue architectures and functions, often resulting in the progression of disease[18]. For example, MMP dysregulation has been observed in patients during post MI remodeling and heart failure[19, 20]. Specifically, MMP expression was upregulated following MI, while the expression of endogenous tissue inhibitors of MMPs (TIMPs) was not. Subsequent clinical studies quantified MMP/TIMP levels in the circulation and found that plasma levels of MMPs increased following MI without a concomitant increase in plasma TIMPs. In particular, plasma TIMP-3 levels significantly decreased in the early post MI period, at a time when maximal MMP

2

induction and release was occurring [21-26]. This prolonged MMP/TIMP dysregulation was correlated with myocardial expansion in patients following MI. Further, regional MMP/TIMP expression has been quantified in the myocardium following experimental MI in pigs[27, 28,17,29-31]. LV samples were harvested 8 weeks following induced MI, and immunoblotting revealed a significant induction of the representative classes of MMPs whereas the relative levels of the 4 TIMPs (TIMP-1,2,3,4) were decreased or remained the same following MI. Further, to quantify MMP activity within the remote, border and MI regions, a fluorogenic-microdialysis assay was developed and revealed that induction of MMP activity is highly localized to the MI region[29-31].

1.4. Stromal cell-derived factor-1 alpha (SDF-1α)

SDF-1α chemokine mediates steady state homing of progenitor cells to the bone marrow by binding to the CXCR4 receptor, but is also expressed by endothelial cells in ischemic tissue through activation of hypoxia inducible transcription factors[32, 33]. SDF-1α expression is upregulated in the myocardium during the first few days following MI, but is quickly downregulated[34-36]. Separate studies have shown a concomitant increase in CXCR4+ circulating cells during the first few days following MI suggesting that these cells are mobilized and respond to the myocardial SDF-1α homing signal[37-39]. In addition, the mobilized CXCR4+ cells express cardiac specific markers suggesting that the SDF-1α/CXCR4 homing axis contributes to myocardial repair following MI[37-40]. The importance of this homing axis in post MI remodeling was shown by systemic administration of a pharmacological CXCR4 antagonist[41]. A single dose of the antagonist following MI increased progenitor cell numbers in the circulation and in the heart, promoted myocardial vascularity, reduced fibrosis, and improved cardiac function and survival. Continuous antagonist infusion increased circulating progenitor cell numbers, but blocked their engraftment in the myocardium, leading to worsened outcomes. Therefore, enhancing endogenous cell homing involves both mobilizing cells from their native niche and sustaining

local signals to promote their engraftment in the myocardium. Sustaining SDF-1α levels in the myocardium through exogenous delivery of recombinant SDF-1α has been shown to increase myocardial c-kit+ and CXCR4+ progenitor cells densities, increased vascular structures and improved cardiac function[36, 42, 43].

1.5. Engineered proteins

Collectively, endogenous protein expression following MI is inadequate to prevent maladaptive changes to myocardial tissue structure, which ultimately cause a gradual loss of LV function. However, our increased understanding of these protein regulators provides an opportunity to intervene and engineer tissue remodeling through exogenous delivery of protein based therapeutics. Delivery of proteins over small pharmaceutical drugs has several advantages including the highly specific functions of proteins that cannot be mimicked by chemical compounds, and the well-tolerated immunological response to proteins because of their natural amino acid composition[44]. In addition, advances in genetic engineering and chemical ligation technologies have allowed for large-scale production of proteins for therapeutic use.

Recombinant proteins are produced by isolating a human gene for the protein of interest, then expressing the gene in a cell culture platform using recombinant DNA technology[45]. A variety of cell types have been used for recombinant protein production including bacteria, yeast, insect cells, and mammalian cells[46-48]. In addition, transgenic animals and plants have been used for recombinant protein production. This technique has proven to be a powerful way to produce many of the thousands of sequenced human proteins in large quantities, as primary sources of human tissues are limited. In addition, while protein sequences are often conserved between species, isolation of proteins for therapeutic use from animal sources can be problematic. Tissue extraction and purification processes are difficult and costly, and the purified product still carries the risk of disease and immunological rejection in humans[44]. While more efficient and less expensive than extraction of proteins from tissues, recombinant proteins

for therapeutic use are still very expensive, with estimates up to $100,000 per patient per year for some disease treatments[49].

As an alternative to cell-based protein production, where the cell is used as a factory to synthesize proteins with its innate machinery, chemical synthesis technologies have been developed to produce proteins through purely synthetic routes[50]. For example, solid-phase peptide synthesis (SPPS) grows a polypeptide chain from a functionalized polymer resin by utilizing protecting groups to couple amino acids from C to N terminus, one at a time. The N-terminal amine of the growing polypeptide chain is deprotected and then reacted with the activated carboxylic acid of an N-protected amino acid. The coupling reactions are forced to completion by using an excess of activated soluble amino acid to improve yield of the final polypeptide chain. The solid-phase is then washed of excess amino aicds and the coupling reaction repeated for subsequent amino acids. Following completion of polypeptide synthesis, the polypeptide is cleaved from the polymer solid-phase and isolated for use. SPPS is typically limited to proteins that are shorter than approximately 30kDa. SPPS synthesis can proceed rapidly in an automated fashion, and produces large yields of purified product[50]. Longer proteins can be achieved using chemical ligation techniques to couple two SPPS synthesized proteins together[51]. One major advantage to SPPS over recombinant technologies is the ease with which proteins of almost any desired sequence can be generated. SPPS is commonly used to generate minimal peptide sequences designed from protein active sites in order to study protein interactions or to provide simpler mimics of the full-length protein for therapeutic use.

1.6. Limitations of protein therapeutics

These advances in protein engineering have led to more than 130 peptide or protein drugs approved for clinical use by the US Food and Drug Administration (FDA), and many more are in development[44]. While proteins continue to be a major focus of drug development efforts, significant challenges

remain in maximizing their efficacy towards treating disease. Specifically, short half-lives and rapid clearance of systemically delivered proteins require frequent dosage to maintain protein concentrations within the therapeutic window to effectively treat the patient. In addition, diseases local to a specific organ (e.g., MI) present a challenge to provide physiologic concentrations of the protein in the organ, while limiting systemic actions of the protein. One attractive way to overcome these challenges is the use of a device that encapsulates proteins and protects them from degradation and rapid clearance, while releasing physiologic protein concentrations locally, and in a sustained fashion.

1.7. References

1. Gheorghiade M, Bonow RO. Chronic heart failure in the united states: A manifestation of coronary artery disease. *Circulation*. 1998;97:282-289
2. Rosamond W, Flegal K, Furie K, Go A, Greenlund K, Haase N, Hailpern SM, Ho M, Howard V, Kissela B, Kittner S, Lloyd-Jones D, McDermott M, Meigs J, Moy C, Nichol G, O'Donnell C, Roger V, Sorlie P, Steinberger J, Thom T, Wilson M, Hong Y. Heart disease and stroke statistics--2008 update: A report from the american heart association statistics committee and stroke statistics subcommittee. *Circulation*. 2008;117:e25-146
3. Frangogiannis NG, Smith CW, Entman ML. The inflammatory response in myocardial infarction. *Cardiovascular Research*. 2002;53:31-47
4. Rossen RD, Michael LH, Kagiyama A, Savage HE, Hanson G, Reisberg MA, Moake JN, Kim SH, Self D, Weakley S, Giannini E, Entman ML. Mechanism of complement activation after coronary-artery occlusion - evidence that myocardial ischemia in dogs causes release of constituents of myocardial subcellular origin that complex with human c1q invivo. *Circulation Research*. 1988;62:572-584
5. Birdsall HH, Green DM, Trial J, Youker KA, Burns AR, MacKay CR, LaRosa GJ, Hawkins HK, Smith CW, Michael LH, Entman ML, Rossen RD. Complement c5a, tgf-beta 1, and mcp-1, in sequence, induce migration of monocytes into ischemic canine myocardium within the first one to five hours after reperfusion. *Circulation*. 1997;95:684-692
6. Jaeschke H, Smith CW. Mechanisms of neutrophil-induced parenchymal cell injury. *Journal of Leukocyte Biology*. 1997;61:647-653
7. Romson JL, Hook BG, Kunkel SL, Abrams GD, Schork MA, Lucchesi BR. Reduction of the extent of ischemic myocardial injury by neutrophil depletion in the dog. *Circulation*. 1983;67:1016-1023
8. Jolly SR, Kane WJ, Hook BG, Abrams GD, Kunkel SL, Lucchesi BR. Reduction of myocardial infarct size by neutrophil depletion - effect of duration of occlusion. *American Heart Journal*. 1986;112:682-690
9. Litt MR, Jeremy RW, Weisman HF, Winkelstein JA, Becker LC. Neutrophil depletion limited to reperfusion reduces myocardial infarct size after 90 minutes of ischemia - evidence for neutrophil-mediated reperfusion injury. *Circulation*. 1989;80:1816-1827
10. Lambert JM, Lopez EF, Lindsey ML. Macrophage roles following myocardial infarction. *Int J Cardiol*. 2008;130:147-158
11. Singer AJ, Clark RA. Cutaneous wound healing. *N Engl J Med*. 1999;341:738-746
12. Erlebacher JA, Weiss JL, Weisfeldt ML, Bulkley BH. Early dilation of the infarcted segment in acute transmural myocardial infarction: Role of infarct expansion in acute left ventricular enlargement. *J Am Coll Cardiol*. 1984;4:201-208
13. Anversa P, Olivetti G, Capasso JM. Cellular basis of ventricular remodeling after myocardial infarction. *Am J Cardiol*. 1991;68:7D-16D
14. Olivetti G, Capasso JM, Sonnenblick EH, Anversa P. Side-to-side slippage of myocytes participates in ventricular wall remodeling acutely after myocardial infarction in rats. *Circ Res*. 1990;67:23-34
15. Cleutjens JP, Verluyten MJ, Smiths JF, Daemen MJ. Collagen remodeling after myocardial infarction in the rat heart. *Am J Pathol*. 1995;147:325-338
16. Wilson EM, Moainie SL, Baskin JM, Lowry AS, Deschamps AM, Mukherjee R, Guy TS, St John-Sutton MG, Gorman JH, 3rd, Edmunds LH, Jr., Gorman RC, Spinale FG. Region- and type-specific induction of matrix metalloproteinases in post-myocardial infarction remodeling. *Circulation*. 2003;107:2857-2863
17. Yarbrough WM, Mukherjee R, Escobar GP, Mingoia JT, Sample JA, Hendrick JW, Dowdy KB, McLean JE, Lowry AS, O'Neill TP, Spinale FG. Selective targeting and timing of matrix metalloproteinase inhibition in post-myocardial infarction remodeling. *Circulation*. 2003;108:1753-1759
18. Visse R, Nagase H. Matrix metalloproteinases and tissue inhibitors of metalloproteinases: Structure, function, and biochemistry. *Circ Res*. 2003;92:827-839
19. Spinale FG, Coker ML, Heung LJ, Bond BR, Gunasinghe HR, Etoh T, Goldberg AT,

Zellner JL, Crumbley AJ. A matrix metalloproteinase induction/activation system exists in the human left ventricular myocardium and is upregulated in heart failure. *Circulation*. 2000;102:1944-1949

20. Thomas CV, Coker ML, Zellner JL, Handy JR, Crumbley AJ, 3rd, Spinale FG. Increased matrix metalloproteinase activity and selective upregulation in lv myocardium from patients with end-stage dilated cardiomyopathy. *Circulation*. 1998;97:1708-1715

21. Webb CS, Bonnema DD, Ahmed SH, Leonardi AH, McClure CD, Clark LL, Stroud RE, Corn WC, Finklea L, Zile MR, Spinale FG. Specific temporal profile of matrix metalloproteinase release occurs in patients after myocardial infarction: Relation to left ventricular remodeling. *Circulation*. 2006;114:1020-1027

22. Hirohata S, Kusachi S, Murakami M, Murakami T, Sano I, Watanabe T, Komatsubara I, Kondo J, Tsuji T. Time dependent alterations of serum matrix metalloproteinase-1 and metalloproteinase-1 tissue inhibitor after successful reperfusion of acute myocardial infarction. *Heart*. 1997;78:278-284

23. Kai H, Ikeda H, Yasukawa H, Kai M, Seki Y, Kuwahara F, Ueno T, Sugi K, Imaizumi T. Peripheral blood levels of matrix metalloproteases-2 and -9 are elevated in patients with acute coronary syndromes. *J Am Coll Cardiol*. 1998;32:368-372

24. Fukuda D, Shimada K, Tanaka A, Kusuyama T, Yamashita H, Ehara S, Nakamura Y, Kawarabayashi T, Iida H, Yoshiyama M, Yoshikawa J. Comparison of levels of serum matrix metalloproteinase-9 in patients with acute myocardial infarction versus unstable angina pectoris versus stable angina pectoris. *Am J Cardiol*. 2006;97:175-180

25. Inokubo Y, Hanada H, Ishizaka H, Fukushi T, Kamada T, Okumura K. Plasma levels of matrix metalloproteinase-9 and tissue inhibitor of metalloproteinase-1 are increased in the coronary circulation in patients with acute coronary syndrome. *Am Heart J*. 2001;141:211-217

26. Inoue T, Kato T, Takayanagi K, Uchida T, Yaguchi I, Kamishirado H, Morooka S, Yoshimoto N. Circulating matrix metalloproteinase-1 and -3 in patients with an acute coronary syndrome. *Am J Cardiol*. 2003;92:1461-1464

27. Mukherjee R, Brinsa TA, Dowdy KB, Scott AA, Baskin JM, Deschamps AM, Lowry AS, Escobar GP, Lucas DG, Yarbrough WM, Zile MR, Spinale FG. Myocardial infarct expansion and matrix metalloproteinase inhibition. *Circulation*. 2003;107:618-625

28. Yarbrough WM, Mukherjee R, Brinsa TA, Dowdy KB, Scott AA, Escobar GP, Joffs C, Lucas DG, Crawford FA, Jr., Spinale FG. Matrix metalloproteinase inhibition modifies left ventricular remodeling after myocardial infarction in pigs. *J Thorac Cardiovasc Surg*. 2003;125:602-610

29. Deschamps AM, Yarbrough WM, Squires CE, Allen RA, McClister DM, Dowdy KB, McLean JE, Mingoia JT, Sample JA, Mukherjee R, Spinale FG. Trafficking of the membrane type-1 matrix metalloproteinase in ischemia and reperfusion: Relation to interstitial membrane type-1 matrix metalloproteinase activity. *Circulation*. 2005;111:1166-1174

30. Spinale FG, Koval CN, Deschamps AM, Stroud RE, Ikonomidis JS. Dynamic changes in matrix metalloprotienase activity within the human myocardial interstitium during myocardial arrest and reperfusion. *Circulation*. 2008;118:S16-23

31. Etoh T, Joffs C, Deschamps AM, Davis J, Dowdy K, Hendrick J, Baicu S, Mukherjee R, Manhaini M, Spinale FG. Myocardial and interstitial matrix metalloproteinase activity after acute myocardial infarction in pigs. *Am J Physiol Heart Circ Physiol*. 2001;281:H987-994

32. Ceradini DJ, Kulkarni AR, Callaghan MJ, Tepper OM, Bastidas N, Kleinman ME, Capla JM, Galiano RD, Levine JP, Gurtner GC. Progenitor cell trafficking is regulated by hypoxic gradients through hif-1 induction of sdf-1. *Nat Med*. 2004;10:858-864

33. Bernhardt WM, Warnecke C, Willam C, Tanaka T, Wiesener MS, Eckardt KU. Organ protection by hypoxia and hypoxia-inducible factors. *Methods Enzymol*. 2007;435:221-245

34. Askari AT, Penn MS. Stromal cell-derived factor-1 mediates stem cell homing and tissue regeneration. *Discov Med*. 2003;3:46-47

35. Ma J, Ge J, Zhang S, Sun A, Shen J, Chen L, Wang K, Zou Y. Time course of myocardial stromal cell-derived factor 1 expression and beneficial effects of intravenously administered bone marrow stem cells in rats with experimental myocardial infarction. *Basic Res Cardiol*. 2005;100:217-223

36. Abbott JD, Huang Y, Liu D, Hickey R, Krause DS, Giordano FJ. Stromal cell-derived factor-1alpha plays a critical role in stem cell recruitment to the heart after myocardial infarction but is not sufficient to induce homing in the absence of injury. *Circulation*. 2004;110:3300-3305

37. Wojakowski W, Tendera M, Michalowska A, Majka M, Kucia M, Maslankiewicz K, Wyderka R, Ochala A, Ratajczak MZ. Mobilization of cd34/cxcr4+, cd34/cd117+, c-met+ stem cells, and mononuclear cells expressing early cardiac, muscle, and endothelial markers into peripheral blood in patients with acute myocardial infarction. *Circulation*. 2004;110:3213-3220

38. Kucia M, Dawn B, Hunt G, Guo Y, Wysoczynski M, Majka M, Ratajczak J, Rezzoug F, Ildstad ST, Bolli R, Ratajczak MZ. Cells expressing early cardiac markers reside in the bone marrow and are mobilized into the peripheral blood after myocardial infarction. *Circ Res*. 2004;95:1191-1199

39. Agarwal U, Ghalayini W, Dong F, Weber K, Zou YR, Rabbany SY, Rafii S, Penn MS. Role of cardiac myocyte cxcr4 expression in development and left ventricular remodeling after acute myocardial infarction. *Circ Res*.107:667-676

40. Kucia M, Reca R, Jala VR, Dawn B, Ratajczak J, Ratajczak MZ. Bone marrow as a home of heterogenous populations of nonhematopoietic stem cells. *Leukemia*. 2005;19:1118-1127

41. Jujo K, Hamada H, Iwakura A, Thorne T, Sekiguchi H, Clarke T, Ito A, Misener S, Tanaka T, Klyachko E, Kobayashi K, Tongers J, Roncalli J, Tsurumi Y, Hagiwara N, Losordo DW. Cxcr4 blockade augments bone marrow progenitor cell recruitment to the neovasculature and reduces mortality after myocardial infarction. *Proc Natl Acad Sci U S A*.107:11008-11013

42. Zhang G, Nakamura Y, Wang XH, Hu QS, Suggs LJ, Zhang JY. Controlled release of stromal cell-derived factor-1alpha in situ increases c-kit(+) cell homing to the infarcted heart. *Tissue Engineering*. 2007;13:2063-2071

43. Segers VF, Tokunou T, Higgins LJ, MacGillivray C, Gannon J, Lee RT. Local delivery of protease-resistant stromal cell derived factor-1 for stem cell recruitment after myocardial infarction. *Circulation*. 2007;116:1683-1692

44. Leader B, Baca QJ, Golan DE. Protein therapeutics: A summary and pharmacological classification. *Nat Rev Drug Discov*. 2008;7:21-39

45. Zoller MJ. New molecular biology methods for protein engineering. *Curr Opin Biotechnol*. 1991;2:526-531

46. Brannigan JA, Wilkinson AJ. Protein engineering 20 years on. *Nat Rev Mol Cell Biol*. 2002;3:964-970

47. Wurm F, Bernard A. Large-scale transient expression in mammalian cells for recombinant protein production. *Curr Opin Biotechnol*. 1999;10:156-159

48. Baldi L, Hacker DL, Adam M, Wurm FM. Recombinant protein production by large-scale transient gene expression in mammalian cells: State of the art and future perspectives. *Biotechnol Lett*. 2007;29:677-684

49. Gross ML. Ethics, policy, and rare genetic disorders: The case of gaucher disease in israel. *Theor Med Bioeth*. 2002;23:151-170

50. Nilsson BL, Soellner MB, Raines RT. Chemical synthesis of proteins. *Annu Rev Biophys Biomol Struct*. 2005;34:91-118

51. Dawson PE, Kent SB. Synthesis of native proteins by chemical ligation. *Annu Rev Biochem*. 2000;69:923-960

CHAPTER 2

Research Overview

2.1. Objectives

As discussed in the Introduction to this dissertation (Chapter 1), there is a pressing need for treatment strategies that attenuate adverse left ventricular (LV) remodeling following myocardial infarction (MI). Injectable hydrogels are developing as a unique therapeutic platform to treat patients with MI, through a range of both biochemical and biomechanical signaling. Additionally, recombinant and chemically synthesized proteins offer an attractive source of biological therapeutics to modulate post MI tissue remodeling processes; however, their short half-lives in blood plasma and ubiquitous involvement in normal biological processes throughout the body make continuous, systemic delivery of the drugs problematic.

With this in mind, the goal of my dissertation work has been to develop hydrogels that can be injected onto or into the myocardium to encapsulate and sustain the release of protein therapeutics locally following MI. Generally, injectable hydrogel systems were designed using a hyaluronic acid (HA) backbone to mimic a hydrated tissue-like environment. These HA-based hydrogels were engineered for (1) *injectability* through formation of covalent bonds on or within myocardial tissue, (2) *controlled degradation* through either hydrolytic or enzymatic means, and (3) *interactions with proteins* through charge association, all features to alter the local release and presentation of therapeutics. More specifically, HA hydrogels were designed that form *in vivo* through either free-radical polymerization of methacrylate groups initiated with photo or re-dox mechanisms or via formation of a hydrozone bond through the combination of polymers with aldehyze or hydrazide functionality. Next, degradation was mediated through crosslinks that contained either hydrolytically degradable ester bonds for passive degradation or the incorporation of matrix

metalloproteinase (MMP) cleavable peptides for cell-mediated degradation. Finally, many proteins interact natively with HA due to charge interactions and these responses were enhanced by the incorporation of sulfated polysaccharides or by directly adding sulfate groups to HA.

Two proteins were chosen for delivery based on their roles in post MI remodeling and their natural association with polysaccharides in the ECM; (1) stromal-derived factor-1 alpha (SDF-1α) is a chemokine that regulates trafficking of cells between the bone marrow and ischemic tissues, as well as promotes angiogenic responses and enhances cell viability and (2) tissue inhibitor of matrix metalloproteinase-3 (TIMP-3) is a protease inhibitor that regulates MMP activity by forming a non-covalent complex with MMPs. Delivery of each molecule was investigated separately to determine efficacy of each therapeutic strategy (i.e., cell recruitment and MMP inhibition). In all studies, experiments were pursued both *in vitro*, to illustrate the release behavior and activity of either SDF-1α or TIMP-3, and *in vivo*, to illustrate the influence of local release on LV remodeling and cardiac function in animal models.

2.2. Specific Aims and Hypotheses

The *global hypothesis* of this dissertation was that the local delivery of therapeutic proteins (SDF-1α and TIMP-3) from injectable HA hydrogels modulates post MI remodeling processes by providing sustained concentrations of bioactive signals within the remodeling myocardium. To test this hypothesis, five specific aims were identified and completed.

Specific Aim 1: Demonstrate that local SDF-1α delivery from HA hydrogels homes mobilized bone marrow derived cells (BMCs) to the heart post MI.
Specific Hypothesis 1: Epicardial delivery of SDF-1α from adherent HA hydrogels will enhance engraftment of mobilized BMCs in the heart.
HA was modified with hydroxyethylmethacrylate (HEMA) groups to allow free-radical initiated crosslinking of hydrolytically degradable macromers for

encapsulation and delivery of SDF-1α. A visible light photo-initiator system was utilized to form hydrogels in the presence of light, which allowed *in situ* formation of HA gels on the epicardial surface of the myocardium through light exposure. SDF-1α binding affinity to HA macromers, along with photo-encapsulated SDF-1α release kinetics and hydrogel degradation was quantified *in vitro*. In addition, the activity of released molecules was assessed using BMCs in an *in vitro* chemotaxis assay. After demonstrating sustained release of active molecules *in vitro*, a mouse MI model (collaboration with Dr. Kenneth Margulies, UPenn) was developed to quantify and track systemically infused BMCs with epicardial delivery of SDF-1α from adherent HA hydrogel patches. The experiments were designed to demonstrate the utility of HA hydrogels to localize and sustain SDF-1α release and provide proof-of-concept that this system promotes endogenous BMC homing to the heart following MI.

<u>Specific Aim 2</u>: Assess the therapeutic benefit of an engineered SDF-1α analogue (ESA) delivery from injectable HA hydrogels post MI.

Specific Hypothesis 2: ESA delivery from injectable HA hydrogels will attenuate post MI remodeling by providing a sustained homing signal within the myocardium.

To expand on the work of Aim 1 that investigated the ability of local delivery of SDF-1α from degradable HA hydrogels to effectively home BMCs to the heart, these hydrogels were utilized for encapsulation and delivery of ESA, a truncated version of SDF-1α produced via chemical peptide synthesis (collaboration with Dr. Joseph Woo, UPenn). For therapeutic assessment, a redox-initiator system was used to form hydrogels within the myocardium via injection through a syringe. Kinetics of hydrogel formation was quantified using rheometry to ensure rapid gelation *in situ* for maximal ESA encapsulation. Release kinetics of encapsulated ESA and hydrogel degradation were quantified *in vitro*, along with released molecule activity using BMCs in a chemotaxis assay. After demonstrating sustained release of active molecules *in vitro,* encapsulated ESA

release was quantified *in vivo* using ESA labeled with a near-infrared tag and delivery from injectable HA hydrogels in a rat model of MI. Functional assessment of ESA delivery from HA hydrogels post MI was compared to MI only and hydrogel alone controls using echocardiography and hemodynamic analysis. In addition, myocardial tissue structure was analyzed with immunohistochemistry to provide a mechanistic understanding of any observed improvements in LV function.

Specific Aim 3: Investigate the effect of local TIMP-3 release from injectable HA hydrogels on MMP activity and LV remodeling following MI.

Specific Hypothesis 3: Local delivery of TIMP-3 from injectable HA hydrogels will reduce myocardial expansion and attenuate global LV remodeling through MMP inhibition within the MI region.

HEMA modified HA macromers, along with the redox-initiator system used in Aim 2 were used for encapsulation and delivery of TIMP-3 in this Aim. TIMP-3 binding to HA macromers was quantified as in Aim 1, and TIMP-3 release from redox-initiated hydrogels along with hydrogel degradation was quantified *in vitro*. In order to investigate the effects of TIMP-3 delivery post MI, a pig MI model (collaboration with Dr. Frank Spinale, University of South Carolina, and Dr. Robert Gorman, UPenn) was used to quantify regional MMP activity, infarct expansion, and LV function after injection. These metrics were compared between hydrogel/TIMP-3 group and control groups of MI only and hydrogel alone, and biochemical analysis of tissues from all groups was analyzed with immunohistochemistry and for the expression of a range of genes involved in the remodeling process to investigate the biological effects of TIMP-3 delivery.

Specific Aim 4: Develop sulfated HA macromers to incorporate high TIMP-3 binding affinity into injectable HA hydrogels.

Specific Hypothesis 4: Incorporation of sulfate groups into HA macromers will enhance binding of TIMP-3 and therefore allow control of TIMP-3 delivery from

injectable HA hydrogels.

HEMA modified HA macromers used in Aims 1-3 were synthetically sulfated using a method that maintains reactive group chemistry to allow incorporation of sulfated HA into injectable HA hydrogels. Sulfate content, charge, and TIMP-3 binding of HA macromers were analyzed before and after sulfation reaction and compared to the naturally sulfated heparin. Sulfated HA macromers were mixed with unsulfated HA macromers and hydrogel crosslinking was quantified with rheometry and compared to hydrogels consisting of only unsulfated HA macromers to confirm covalent incorporation of sulfated HA macromers. Further, TIMP-3 or bovine serum albumin (BSA) was encapsulated into the hydrogels and protein release along with hydrogel degradation were analyzed with incorporation of sulfated HA to investigate the influence of sulfation on protein release from HA hydrogels.

<u>Specific Aim 5</u>: Engineer injectable HA hydrogels with MMP sensitive degradation for localized TIMP-3 delivery as a function of MMP expression within the MI region.

Specific Hypothesis 5: Incorporation of MMP-sensitive crosslinks will permit TIMP-3 release based on local MMP concentrations and alter LV remodeling when injected into infarct tissue.

Based on our results in Aim 3 using HEMA modified HA hydrogels with hydrolytic degradation and therefore passive rTIMP-3 release to inhibit MMP activity post MI, we designed injectable HA hydrogels that degrade and release rTIMP-3 in direct proportion to local MMP activity. To accomplish this, hydrogels were developed with MMP degradable crosslinks that form stable networks in the absence of MMP activity, but degrade in the presence of MMP-2 and MMP-9. Based on our results in Aim 4 on sulfated polymers that bind and immobilize TIMP-3 within hydrogels, dextran sulfate was also incorporated into HA hydrogels for this Aim in order to limit passive TIMP-3 release. Further, polymers were modified with complimentary reactive groups to form hydrogels rapidly upon

injection through a dual-barrel syringe without the need for free-radical initiators, using hydrazone chemistry (formation through reaction of hydrazide and aldehyde containing polymers). TIMP-3 binding to sulfated polymers was quantified *in vitro* and compared to unsulfated HA and sulfated heparin controls. Hydrogel crosslinking was quantified using rheometry and MMP mediated hydrogel degradation was quantified *in vitro*. TIMP-3 release from the hydrogels was quantified and the effect of TIMP-3 encapsulation on MMP mediated hydrogel degradation was investigated *in vitro*. After demonstrating MMP-triggered release of encapsulated TIMP-3 *in vitro*, the injectable hydrogel system was applied in the pig MI model used in Aim 3 and the same outcomes were pursued to assess therapeutic efficacy of this unique delivery approach.

2.3. Chapter Outline

An extensive review of the use of injectable hydrogels for treating MI will be presented first in Chapter 3. Next, each Specific Aim of this dissertation will constitute its own chapter consisting of introduction, methods, results, and discussion sections in the following order: Specific Aim 1 - Chapter 4, Specific Aim 2 - Chapter 5, Specific Aim 3 - Chapter 6, Specific Aim 4 - Chapter 7, Specific Aim 5 - Chapter 8. Finally, the conclusions related to each Specific Aim along with any limitations of the studies will follow in Chapter 9.

CHAPTER 3

Injectable acellular hydrogels for cardiac repair: a review

3.1. Introduction

Left ventricular (LV) remodeling caused by a myocardial infarction (MI) is responsible for almost 70% of the 5 million cases of heart failure that have occurred in the United States in recent years[1]. Early infarct expansion or stretching has been associated with poor long-term prognosis[2-4] and has been identified as the mechanical phenomenon that initiates and sustains the process of adverse post-MI LV remodeling that leads to heart failure[5-10]. Infarct expansion causes abnormal stress distributions in myocardial regions outside the infarction, especially in the adjacent borderzone (BZ) region, putting this region at a mechanical disadvantage. With time, increased regional stress is the impetus for several maladaptive biologic processes, such as myocyte apoptosis and matrix metalloproteinase activation that inherently alter the contractile properties of normally perfused myocardium[11-13]. Once initiated, these maladaptive processes lead to a heart failure phenotype that is difficult to reverse by medical or surgical means.

Previous work has demonstrated that the use of ventricular restraints, such as polymeric meshes wrapped around the heart or sutured to the surface of the infarcted myocardium, reduces infarct expansion by mechanically stabilizing the heart and forcing it to maintain its original shape, thus limiting long-term global LV remodeling in large animal models[10,14-17] However, these approaches are limited by the invasive procedure in which they are applied and clinical adoption has not occurred. In order to circumvent the invasive surgical placement of restraining devices early post-MI, our group and others have begun to explore the use of injectable materials, and specifically hydrogels, to limit

infarct expansion and normalize the regional stress distribution[18-35].

Hydrogels are water-swollen polymer networks that exhibit many tissue-like properties and have been explored for numerous tissue engineering and drug delivery applications[36-38]. Hydrogels can form through numerous techniques, including via self-assembly, through non-covalent interactions with ionic species, through covalent crosslinking via chemical reaction, and through thermal transitions that lead to gelation[36-38]. These techniques are advantageous as they could potentially translate to catheter delivery for minimally-invasive, percutaneous therapies. Hydrogels are finding application in cardiac therapy alone as a means for thickening and stabilizing the myocardium via tissue bulking, as well as for the delivery of a wide variety of therapies, such as cells and growth factors[39, 40]. This review will specifically focus on the application of hydrogels for (1) tissue bulking and (2) molecule delivery approaches that may translate quickly to the clinic since difficulties related to finding an adequate cell source for transplantation are eliminated.

3.2. Injectable Hydrogels as Bulking Agents

Over the past decade it has become clear that the mechanical changes that occur after MI must be considered when developing post-MI therapies[35,41,42]. MI leads to extracellular matrix (ECM) breakdown and results in geometric changes in both the infarcted and healthy myocardium. LV dilation results in stretched cardiomyocytes in the border zone (BZ) and healthy myocardium, which subsequently lose the ability to efficiently contract[43]. Globally, this is manifested as a shift to a more spherical shape and a reduction in the transmural wall thickness. The Law of Laplace (Eq. 3.1) illustrates how the resulting dilation (increased radius) and thinning of the myocardium post-MI leads to increased stress; where stress (T) is directly proportional to pressure (P) and the radius of curvature (R), and inversely to the thickness of the myocardial wall (h).

$$T = \frac{P \cdot R}{h} \qquad \text{(Eq. 3.1)}$$

As mentioned above, past strategies to attenuate LV expansion have included surgeries to reconstruct the dilated ventricle and restraints placed around the myocardium or infarct to physically prevent dilation[16,44-47]. Injectable hydrogels may present a material system that is applied in a non-invasive manner (liquid to solid transition) and leads to limited LV expansion. In this section we will review common natural and synthetic hydrogels that have been investigated to this end, as well as comment on the underlying mechanisms of therapy. The reader should refer to Table 3.1 throughout this section, which summarizes the various materials that have been investigated in animal models of MI.

Table 3.1. Summary of injectable hydrogels and their assessment in animal models of MI.

Hydrogel Type	Animal/Model	Inject Time (post-MI)	Gelation Mechanism	Injection Volume	End Point
Fibrin [19,70,71]	Rat: LAD ligation/ reperfusion	1 wk	Peptide-self assembly	50 µL	6 wks
Fibrin, collagen, matrigel [72]	Rat: LAD ligation/ reperfusion	1 wk	Peptide-self assembly/Thermal	50 µL	6 wks
Fibrin and Alginate [73]	Rat: LAD ligation/ reperfusion	5 wks	Peptide-self assembly/Ionic		10 wks
Alginate [20]	Rat: LAD ligation/ reperfusion	5 wks	Ionic		10 wks
Alginate [21]	Rat: Ligation of proximal left coronary artery	1 wk	Ionic	130 µL	9 wks
Alginate [22]	Rat: Ligation of proximal left coronary artery	1 wk and 2 months	Ionic	100 to 150 µL	2 and 4 months
Alginate [23]	Swine: Transient balloon occlusion of LAD	4 days	Ionic	1,2, and 4 mL	2 months
Alginate/fibrin composite [74]	Swine: Ligation of OM1 and OM2	1 week	Peptide-self assembly/Ionic	200 µL x 25	4 wks
Chitosan [75]	Rat: LAD ligation	1 wk	Thermal	100 µL	5 wks
Hyaluronic Acid [77]	Rat: Ligation of left circumflex arteries	2 wks	Michael-type addition	50 µL	6 wks
Hyaluronic Acid [78]	Sheep: LAD ligation and 2nd diagonal coronary artery	30 min	Redox initiation	300 µL x 20	2 months
Collagen [79]	Rat: Ligation of proximal left coronary artery	1 wk	Thermal	100 µL	6 wks
Matrigel [80]	Mouse: LAD ligation	Immediately	Thermal	50 µL	2 wks
Matrigel [79]	Rat: LAD ligation/ heterotopic transplant	Immediately	Thermal	125 µL	2 wks
Naturally Derived ECM [81, 82]	Rat: no infarct	N/A	Thermal	90 µL	N/A
Dex-PCL-HEMA/PNIPAAm [83]	Rabbit: Ligation of the proximal left coronary artery	4 Days	Thermal	50 µL x 4	34 days
poly(NIPAAm-co-AAc-co-HEMAPTMC) [84]	Rat: LAD ligation	2 wk	Thermal	100 µL x 5	10 wks
αCD-MPEG-PCL-MPEG [36]	Rat: LAD ligation	5 min	Self assembly	100 µL x 3	1 month
αCD-MPEG-PCL-MPEG [24]	Rabbit: LAD ligation	1 wk	Self assembly	200 µL	5 wks
PEG-VS [41]	Rat: LAD ligation	2 min	Redox reaction	100 µL (via 2 or 3)	13 wks

Natural Hydrogels

Christman and colleagues pioneered the field of acellular injectable biomaterials by exploring the effects of fibrin glue as a bulking agent[18,23,34,49]. Fibrin has natural binding domains for soluble growth factors and cellular integrin receptors, motivating its use for wound healing applications. Although fibrin is commonly utilized for these biological properties, it can also be used as a mechanical support for the myocardium[18,29,34,49]. Specifically, fibrin forms a crosslinked 3-D hydrogel in the myocardium upon injection with a dual-barreled syringe. One barrel contains fibrinogen and aprotinin, a fibrinolysis inhibitor, and the second barrel contains thrombin, factor XIIIa, and $CaCl_2$[18,23,29,49]. Following a similar mechanism to that involved in the normal clotting cascade *in vivo*, when fibrinogen and thrombin are mixed, fibrinogen is converted to fibrin which self assembles and is crosslinked via the factor XIIIa.

Christman et al. injected these fibrin hydrogels into the ischemic LV one week following induced MI in rats (reperfusion- MI model) and animals were sacrificed 5 weeks later. Echocardiograph and explant data showed that fibrin is capable of maintaining fractional shortening (FS) and preserving infarct scar thickness after the material was resorbed[18]. In later studies, using the same model, Christman et al. demonstrated the ability of fibrin to substantially decrease infarct size and increase arteriole density in the infarct area compared to control BSA injections[49]. These results imply that in addition to its bulking effects, fibrin may also elicit a bioactive response that influences LV remodeling. Significant increases in neovasculature formation (capillary density) following fibrin injection in rat models of MI were later confirmed by Huang et al.[23].

Natural materials that are relatively bioinert such as alginate have also been explored as injectable hydrogels to treat MI. Alginate is a linear seaweed-derived copolymer consisting of linked β-D-mannuronate (M) and α-L-guluronate (G) residues and can be crosslinked into hydrogels with the addition of divalent cations [57]. Unlike fibrin, alginate must be modified with adhesive peptides to

facilitate cell binding. Both non-modified alginate and alginate modified with adhesive peptides such as Arg-Gly-Asp (RGD) or Tyr-Ile-Gly-Ser-Arg (YIGSR) have been explored as bulking agents[26,31,34,50,51] and comparisons have been performed between the two[31,50]. Yu et al. compared modified alginate to non-modified alginate using a rat reperfusion-MI model with injections 5 weeks post-MI, more indicative of a chronic response[50]. Five weeks after hydrogel injections, both alginate groups improved FS, reduced LV dimensions and significantly increased myocardial wall thickness compared to control BSA injections. Although both non-modified and modified groups also increased the number of arterioles in the infarct area, modified alginate resulted in higher densities, indicating the ability of adhesive peptide modifications to promote angiogenesis following MI. Tsur-Gang et al. also observed improved geometry and function following injection of non-modified alginate hydrogels; however, they observed conflicting data with modified alginate hydrogels[31]. Specifically, modified alginate showed a reduced benefit compared to non-modified alginate in terms of LV diastolic and systolic dimension (LVDD and LVSD), LV diastolic and systolic areas (LVDA and LVSA), FS, and fractional area change, although no significant differences in relative scar thickness or blood vessel densities were observed.

Utilizing a large animal swine model, Mukherjee et al. injected composite hydrogels containing both fibrin and alginate to prevent geometric LV remodeling[29]. One week post-MI, 200μL injections (25 total) were applied to the infarct area via a double barreled injection device; one component was comprised of fibrinogen, fibronectin, factor XIII, plasminogen and gelatin-grafted alginate dissolved in an aprotinin solution, while the second consisted of thrombin and 40mM $CaCl_2$. Therapeutic outcomes included increased posterior wall thickness 1 week post injection and a reduction in infarct expansion 21 and 28 days post-MI; however, no functional improvements were observed. Other interesting findings included a significant reduction of soluble collagen in the treatment groups, suggesting that collagen was less vulnerable to protease degradation. This observation was supported by a significant decrease in

protease levels (e.g., MMP-2) in the composite hydrogel injection group, which could favor infarct stiffening and, thus, attenuate maladaptive remodeling in the future.

Chitosan is a linear polysaccharide that is biocompatible and biodegradable and therefore has been used in a wide variety of tissue engineering applications[58]. Chitosan hydrogels can be formed upon mixing commercially produced chitosan with a glycerol phosphate and glyoxal solution. These gels exhibit a thermoresponsive gelation that is tuned to occur at 37°C by changing the glyoxal concentration, while hydrogel degradation is controlled by the degree of deacetylation[59,60]. In a rat infarct model, a thermally responsive chitosan was injected 1 week post-MI[28]. Four weeks after hydrogel injection, the myocardium thickness was significantly increased compared to PBS controls, even though the amount of chitosan present in the myocardium after 4 weeks had substantially decreased due to hydrogel degradation. There were also significant improvements in infarct size, FS, ejection fraction (EF), end systolic diameter (ESD), end diastolic diameter (EDD), and microvessel density. Although the material was not completely degraded at the end of this study, like fibrin, this is an example of a degradable material that was effective in not only preserving thickness but also function.

Hyaluronic acid (HA) is a polysaccharide that is abundant in the body and can play several biological roles that include angiogenesis, cell migration, and scar reduction depending on its molecular weight and the addition of function groups allows for tunability in material properties[61-66]. In one example, acrylated-HA was mixed with a thiol-terminated PEG crosslinker (PEG-SH$_4$) and crosslinked via Michael-type addition; the mixture was injected into a rat MI model 2 weeks post-MI[33]. Four weeks after treatment, heart function was evaluated; HA treatment led to significantly decreased infarct size, increased EF and increased arteriole and capillary density. Interestingly, results showed significant increases in infarct thickness while histology showed complete degradation of the HA gels. Improvements in this work were attributed to the

biological role of HA, which like fibrin has proven to play a large role in wound healing applications. Additional work with engineered HA hydrogels will be discussed in a section below on modulating hydrogel properties.

Collagen is a natural ECM protein that has been applied for LV remodeling therapies due to the ability to inject as a liquid, which subsequently gels at 37°C[19,23]. Collagen injections in 1 week old rat infarcts substantially increased infarct thickness, stroke volume (SV) and EF compared to saline inject controls; there was also a trend for improved end systolic volume (ESV)[19]. While this study did not show any evidence of angiogenesis or cell infiltration, Huang et al, using a reperfused model, were able to demonstrate both increased angiogenesis and myofibroblast infiltration in the infarct zone compared to controls[23]. Contradicting results may be attributed to variables in methodology (Table 1) or differences in collagen types and concentrations used. Dai et al. used a mixture of collagen I (95%) and collagen III (5%) at 65 mg/mL, while Huang et al. used a collagen I at 1 mg/mL. As an alternative to hydrogels composed solely of isolated collagen, Matrigel is commercially available hydrogel derived from the ECM that is primarily composed of collagen, but also contains numerous other molecules derived from the basement membrane. Studies with Matrigel alone in a mouse model showed trends towards increased scar thickening and improved function compared to infarct controls[25]; thickening and improved EDD were also observed in a rat model[54]. In addition, studies by Huang et al. showed significantly increased capillary density with Matrigel injection[23].

Extracellular matrix (ECM) components isolated from healthy myocardium have been recently explored to treat MI. Singelyn et al., decellularized and solubilized the ECM from pig hearts for use as an injectable scaffold[30]. The isolated ECM material maintained a complex composition including collagen and glyocosaminoglycan content and exhibited a natural thermoresponsive behavior as it self-assembled into a nanofibrous gel at 37°C from a liquid precursor at 25°C. Interestingly, the cocktail of isolated ECM components stimulated the migration of human coronary artery endothelial cells (HCAEC) and rat aortic

smooth muscle cells (RASMC) *in vitro.* For *in vivo* application, 90 μL hydrogels were successfully pushed through a catheter into the non-infarcted myocardium of rats where they induced a significant increase in arteriole formation 11 days post-injection. In later work, Seif-Naraghi et al. isolated both porcine and human pericardial ECM (PPM and HPM respectively) to evaluate their potential as autologous scaffolds for treating MI[55]. Similarly, these gels polymerized under thermal stimulation and maintained native components of the pericardial ECM. While *in vitro* results demonstrated that PPM was more effective in promoting migration of HCAEC, RASMC, and rat epicardial cells (RECs) compared to HPM, *in vivo* data 2 weeks post injection (90 μL) indicated that both PPM and HPM similarly promoted neovascularization (76 ±13 arterioles per mm^2 and 51±42 arterioles per mm^2, respectively). Interestingly, stem cell evaluation revealed that although very slight, c-kit+ cells were present within the injection regions, eluding to a role in endogenous homing of these materials. These studies demonstrate that providing cardiac-specific cues to the injured myocardium via decellularized ECM injectable hydrogels provides a useful strategy to promote cardiac-specific tissue formation.

Synthetic Hydrogels

Natural materials may provide numerous important cellular-interactive cues (e.g., adhesion and cell-mediated degradation), but are generally limited in the extent that their properties can be adjusted (ie: mechanics, degradation, and viscosity). In contrast, synthetic materials provide additional potential in engineering a variety of gelation mechanisms and physical properties. One synthetic thermosensitive polymer, comprised of dextran (Dex) grafted poly(caprolactone)-2-hydroxyethyl methacrylate (PCL-HEMA) and copolymerized with poly(N-isopropylacrylamide) (PNIPAAm) termed Dex-PCL-HEMA/PNIPAAm, was developed to gel *in situ*. Material injections were performed 4 days post-MI in a rabbit model and resulted in significant reductions in infarct scar and improvement in EF and LV end diastolic and systolic diameter (LVEDD and

LVSD) compared to PBS control injections when assessed 30 days after injection[32]. Significant thickening was observed despite no histological evidence of material remaining.

Similarly, Fujimoto et al. synthesized a biodegradable, temperature responsive hydrogel composed of N-PNIPAAm, acrylic acid, and hydroxyethyl methacrylate-poly(trimethylene carbonate) (poly(NIPAAm-co-AAc-co-HEMAPTMC)) with slower degradation than the previously discussed polymer (Figure 3.1)[22]. Like Dex-PCL-HEMA/PNIPAAm, poly(NIPAAm-co-AAc-co-HEMAPTMC) was engineered to undergo gelation at body temperature. In this particular study, a hydrogel with a maximum tensile strength of 6.1 kPa and complete hydrogel degradation after 5 months was evaluated for its efficacy in preventing LV remodeling in a rat MI model. The polymer was injected two weeks post-MI; after 8 weeks the myocardium thickness, EDA and fractional area change were significantly improved compared to PBS injection controls.
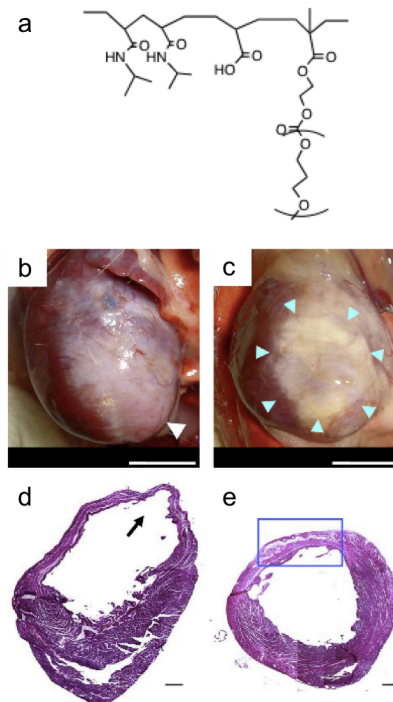

Figure 3.1. In vivo application of injectable synthetic polymers. Chemical structure of poly(NIPAAm-co-AAc-co-HEMAPTMC) (a), representative images of PBS (b) and gel (c) injected hearts at 8 weeks, and hematoxylin and eosin stained section of PBS control (d) and gel treatment (e) hearts at 8 weeks. Scale bar: 5 mm in (b,c), 500 μm in (d,e). Figure adapted from [22].

Another synthetic material consisting of αcyclodextrin (α-CD) and poly(ethylene glycol) (MPEG-PCL-PEG) triblock polymer that has the ability to gel *in situ* has also demonstrated therapeutic benefits when injected to target LV remodeling[24,32]. Degradation can be controlled by the PCL block and hydrogels were formed upon mixing the linear MPEG-PCL-MPEG polymer with α-CD. When injected 5 minutes post-MI in a rat model, the hydrogel-treated groups showed a significant reduction in infarct size, LVEDD, LVESD, and an increase in FS compared to PBS inject controls. No increase in neovascularization was observed[32]. In 1 week old infarcts in a rabbit model, significant improvements in thickness, infarct size, LVEDD, LVESD, and EF were observed with no increase in microvessel density[24].

The aforementioned synthetic materials have all been degradable. In contrast, a non-degradable vinyl sulfone derivatized PEG (PEG-VS) has also been investigated to treat MI[21]. PEG-based hydrogels are bioinert and can be tailored to have high mechanical properties. PEG-VS was polymerized upon combination with dithiothreitol (DTT) and injected into a rat MI model 2 minutes post-MI. PEG-VS significantly increased the wall thickness at 4 weeks, and although no longer significant, was still thicker than saline controls at 13 weeks. Despite PEG-VS thickening the myocardial wall, echocardiograph analysis showed significant improvements in EDD only 4 weeks after MI; this was not maintained at 13 weeks. FS was also not improved in treatment groups. Here, in this small animal model, it is observed that prolonged material presence (or stabilization) is not sufficient to attenuate LV remodeling.

Limitations of Experimental Assessment of Bulking Agents

From the above reviewed results, it is clear that bulking agents may attenuate remodeling post-MI; however, the mechanism involved in their success still remains to be elucidated. If anything, these results reveal the complexity in the material interaction with the myocardial tissue, including both the biological (e.g., material remodeling, inflammatory response) and mechanical (e.g., stress

reduction) responses. Variable results from these studies indicate that material thickness[21,26,29,34], infarct size[34], and/or increased angiogenesis[19,24,56] do not necessarily correlate directly with improved heart function. However, discrepancies in results could be due to inconsistencies in methodology (Table 3.1) (e.g., animal models, infarct, amount of material injected, timing of injection) and material properties and their importance should be considered when investigating LV remodeling. Specifically, several animal models have been used to study the efficacy of bulking agents. The most popular model is by far the rat model, possibly due to costs and ease of implementation; however, this model has several limitations. The most obvious is the lack of clinical relevance associated with a small animal model, as well as infarct consistency. In the clinical setting, factors such as the LV volume and structure, material injection volume, and method for injection will be very different than in the rat.

Material injection of bulking studies has been performed as early as immediately post-MI[21,25] as late at 8 weeks post-MI[26]. In separate studies with fibrin, injection at 1 week was more effective in improving myocardium function[18] versus injection 5 weeks post-MI[34]. Utilizing a permanent ligation rat model, Landa et al. directly compared injections into new (1 week post-MI) and old (2 months post-MI) infarcts and demonstrated the efficacy of alginate in both (although to different extents)[26]. Recent infarcts resulted in improvements in wall thickening and LV dilation; while older infarcts also showed improvements, results were more pronounced, implying that post-MI therapies are more effective when applied early in the LV remodeling process, potentially before irreversible processes have occurred. Similar to injection time, data collection time points are also important to consider. The longest study evaluated in this review was 3 months post treatment[21] and 4 months post-MI[26].

Material Optimization: Theoretical Evaluation

Theoretical models have implied that material properties, specifically mechanics and volume, are important to consider when selecting the type of

bulking agent to ameliorate dilation and increased stress in the myocardial wall[35,67-69]. Using a finite element (FE) model to simulate the effects of injecting a non-contractile material into the myocardium, Wall et al. showed that bulking the myocardium was sufficient to attenuate post-MI geometric changes and, thus, decrease stress in the myocardial wall[35]. More specifically, they demonstrated that injections of 4.5% of the LV wall volume and 20% of the stiffness of the natural myocardium into the BZ were able to decrease the fiber stress by 20% compared to control simulations with no injections. Other approaches have validated the importance of infarct compliance using FE, as well as lump-parameter models; results reveal similar overall beneficial outcomes[35,67,68]. FE models have also been employed to evaluate the effects of material volume and distribution in the myocardium and showed that they influence the extent of remodeling (Figure 3.2)[35,69]. After testing several injection patterns it was determined that the maximum number of injections leads to the highest reduction in fiber stress[69]. These simulations provide insight to the relevance of bulking material properties, specifically mechanics and volume distribution, and present more evidence to pursue injectable material therapies to control LV remodeling.
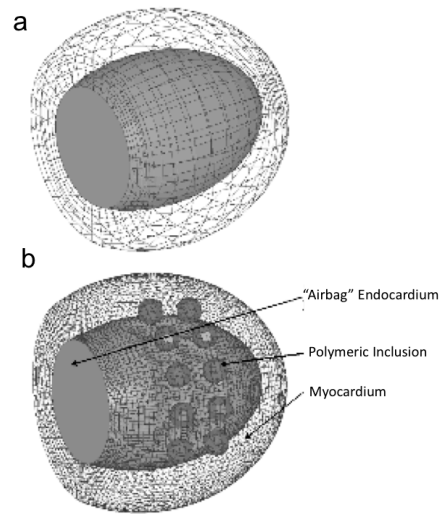

Figure 3.2. Finite element (FE) model of injected polymeric materials. Reference FE model for infarcted canine heart (a) and modified FE model with polymeric inclusion injection pattern into dilated LV (b) can be used to assess the effects of material volume and distribution on myofiber stress. Figure adapted from[69].

Material Optimization: Comparing Different Materials

Only two studies have directly compared different materials and their efficacy in preventing LV remodeling[23,34]. Utilizing an infarct-reperfusion rat model, Yu et al. compared non-modified alginate to fibrin with injections applied 5 weeks post-MI[34]. Two days after injection, both materials were similarly effective in improving FS, LV dimensions and wall thickness. However, 5 weeks post injection, alginate demonstrated greater improvements than fibrin in FS, LV dimensions, and wall thickness. This could be attributed to the extended presence of alginate in the myocardium while fibrin was no longer detectable; however, fibrin treatment did result in thicker myocardial walls when compared to BSA control injections. Interestingly, while unable to promote cell adhesion, alginate, like fibrin, resulted in significantly higher arteriole density. Despite alginate's superiority in long-term functional outcomes, fibrin treatment groups had significantly smaller infarcts compared to controls. This comparison highlights potential differences in the efficacy of material stabilization in preventing LV remodeling, due to differences in material degradation and biological activity. In another study, Huang et al. compared the extent of angiogenesis between fibrin, collagen and Matrigel post-MI and determined that while all three polymers significantly increased capillary density, only collagen significantly increased the degree of myofibroblast infiltration[23].

Material Optimization: Comparing Properties

Few studies have experimentally evaluated the role of material properties (e.g., volume and mechanics) on LV remodeling. A review of injectable materials illustrates that a wide range of volumes have been injected as bulking agents (Table 3.1). As a single example of differences in injected volumes, Leor et al. injected an alginate-calcium solution into the LAD 4 days post-MI via a coronary catheter in swine[51]. During this time post MI, the vasculature of the infarcted myocardium is leaky, allowing the alginate mixture to be delivered to the infarct site. Due to inadequate levels of calcium in the vasculature, the alginate solution

does not crosslink until released into the myocardium where levels of calcium suffice to stimulate gelation. Various volumes of 1, 2 and 4 mL were injected; 2 and 4 mL injections led to superior LVDA and LVSA with 2 mL injections resulting in significant thickening (despite material degradation) and more pronounced trends for functional improvements. These findings illustrate the importance of injection volume in stabilizing the myocardial wall[69]. Other parameters, such as number and pattern of injections, although relevant through theoretical analysis[69], have yet to be investigated in a clinically relevant model.

The influence of material properties may also be an important parameter to control, yet few studies have investigated this, particularly in a controlled manner. This may be due to limitations in material systems where various important properties can be decoupled. For example, fibrin properties can be varied by adjusting the concentration of fibrinogen and thrombin[70] and Martens et al. adjusted these parameters to optimize fibrin viscosity and gelation for catheter delivery[71]. Similarly, alginate properties can be adjusted by varying weight percent and the ratio of M and G units [72]. However, in both of these systems viscosity may be changed during injection and lead to differences in not only final mechanics, but also material dispersion and biomaterial concentration.

A recent study by Ifkovits et al. was the first to explore how the mechanical properties of injectable materials influence LV remodeling (Figure 3.3)[53]. A highly modified HA polymer (methacrylated HA, MeHA) with a high compressive modulus (43 kPa) was directly compared to lower modified MeHA with a low compressive modulus (7.7 kPa). This study demonstrated that although both materials similarly thickened, or bulked, the infarcted myocardial wall, high MeHA was able to also decrease infarct size and dilation as well as improve function under stress compared to the infarct control. This provides evidence that the mechanical properties of the injectable material are important to consider for attenuating LV remodeling. Studies with tunable injectable materials will broaden the understanding of factors, such as mechanics and degradation that should be regarded to target LV remodeling via bulking agents.
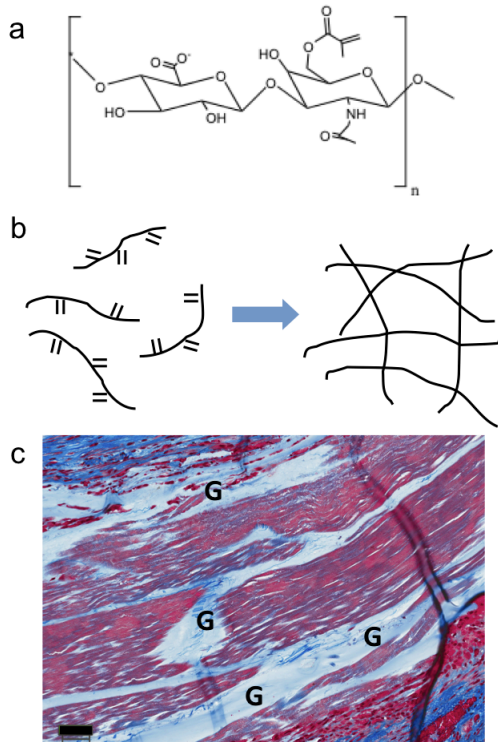
Figure 3.3. Injectable hyaluronic acid hydrogel. Chemical structure of methacrylated hyaluronic acid (a), schematic of gel formation process where functional macromers react via a radical polymerization to form a gel (b), and a representative Masson's Trichrome stain of the gel in myocardium 8 week post-MI (c). G=Gel, Scale Bar, 50 μm. Figure adapted from[53].

Likewise, the biological activity of materials cannot be overlooked.   A study by Ryan et al. injected a biocompatible dermal and soft tissue filler (Radiesse) composed of calcium hydroxyapatite microspheres suspended in an aqueous gel carrier of water, glycerin, and carboxymethylcellulose.   The uncrosslinked gel carrier allows endogenous cells to access the encapsulated microspheres to promote collagen synthesis[73].   Radiesse was injected into the myocardium 45 minutes after ligation in an ovine MI model and analyzed at 4 weeks; injection resulted in a thickened myocardial wall, increased global EF and reduced LV end systolic volumes compared to controls.   Unlike the previously mentioned hydrogel systems that directly bulk the myocardium through hydrogel crosslinking, this approach provides an effective means to induce tissue bulking by promoting the biological response to materials for attenuated LV remodeling and preserved cardiac function[52, 74-78].

3.3. Injectable Hydrogels for Molecule Delivery

In addition to mechanically supporting the injured myocardium as described above, injectable hydrogels provide a water-swollen matrix to encapsulate therapeutic molecules for targeted molecule delivery to the myocardium following MI. Exogenous delivery of therapeutic molecules including growth factors, cytokines and DNA plasmids can be used to manipulate endogenous post-MI remodeling processes; however, the high rates of diffusion and short half-life during which these molecules retain their biological activity *in vivo* make successful application of these molecules to treat MI difficult[79]. To this end, injectable hydrogels provide a useful platform to sustain the release of therapeutic molecules in the setting of MI. Molecules are encapsulated in the hydrogel matrix and released locally over time to sustain target levels of the molecule in the myocardium while preventing detrimental systemic effects. The pioneering work of Dr. Robert Langer and Dr. Judah Folkman showed that polymer matrices can be used to sustain the release of encapsulated molecules for up to 100 days[80]. Molecule release from these hydrogels exhibited an initial 'burst release' in which molecule release rates are rapid, followed by sustained released profiles with slower release rates (Figure 3.4). This initial burst release was significantly decreased with higher polymer concentrations (i.e., higher polymer-to-water ratios) and the overall release kinetics were unique for each polymer-molecule combination. Polymer-molecule interactions, polymer hydrophobicity, and hydrogel degradation all influence the diffusion of encapsulated molecules in the hydrogel matrix and therefore determine encapsulated molecule release kinetics[81]. The following sections will review the range of combinations of therapeutic molecules and injectable hydrogel formulations that have been applied to treat MI.
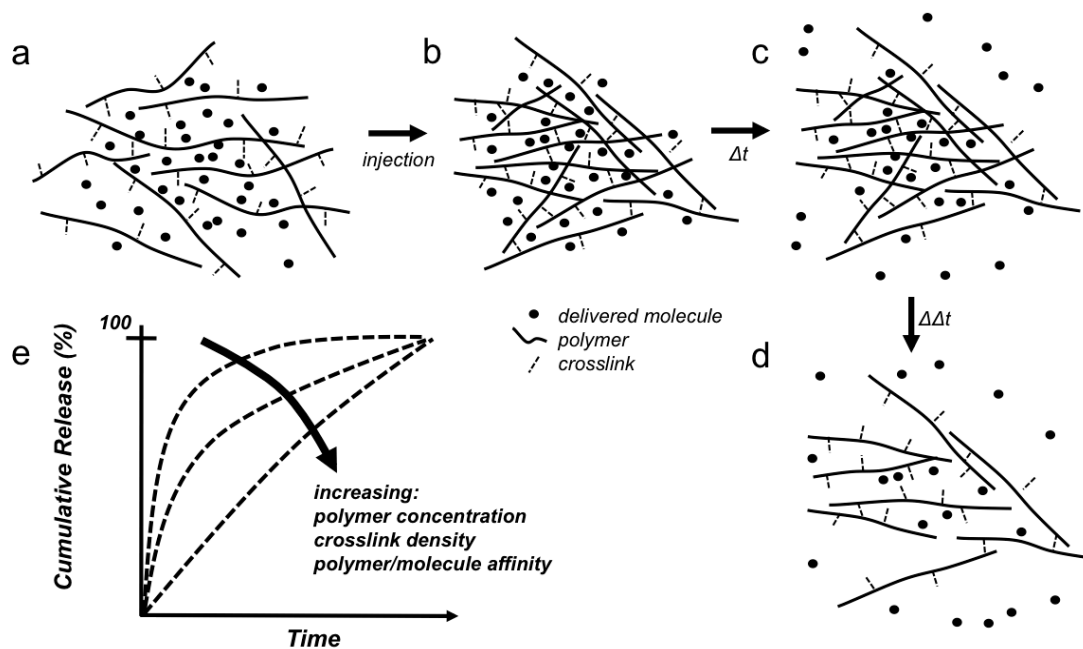
Figure 3.4. Representative release behavior from injectable hydrogels. Molecules are mixed into a hydrogel precursor solution (a), encapsulated after hydrogel formation upon injection (b), and are released from the network through both diffusion (c) and degradation (d) mechanisms. Molecule release from these systems can be controlled through polymer concentration, crosslink density and by incorporating affinity between the encapsulated molecule and hydrogel (e). Release profiles are unique for each polymer-molecule combination and are therefore often determined experimentally.

Anti-apoptotic Molecules

In order to attenuate the loss of viable myocardium following MI, protective growth factors have been delivered locally from injectable hydrogels to the at-risk myocardium. Ruvinov et al. developed alginate hydrogel microparticles with sulfate group modifications to affinity-bind encapsulated insulin-like growth factor-1 (IGF-1) and hepatocyte growth factor (HGF) for sustained molecule release in the setting of MI[82]. IGF-1 has been shown to be cytoprotective and HGF has been shown to be pro-angiogenic and anti-fibrotic; therefore, this group hypothesized that delivery of both of these molecules following MI would have an additive effect on preserving the viability and structure of the myocardium. Modifying hydrogels with negatively charged groups is a common way to mimic the natural affinity of glycosaminoglycans (GAGs) for proteins in order to localize and sustain the release of exogenously delivered proteins. In this particular

system, the modified alginate microparticles exhibited a dual release behavior with distinct release kinetics for IGF-1 and HGF (IGF-1 release was faster than HGF release), indicating a difference in the affinity of each molecule for the sulfate group modifications (Figure 3.5). Importantly, the molecules released from the microparticles remained active (confirmed *in vitro* with cell culture assays) and were protected by protease degradation when bound to the sulfate modified alginate (as evidenced by mass spectroscopy). When injected 1 week after induced MI in rats, the alginate microparticles facilitated significant improvements in IGF-1/HGF mediated repair compared to IGF-1/HGF injected in saline and alginate microparticles injected without growth factors. These improvements include reductions in fibrotic area (collagen staining), apoptotic cells (caspase-3 expression), and increases in vessel densities and areas (α-SMA expression), proliferating cardiomyocytes (Ki67 expression), and evidence of cardiogenesis (GATA4 expression) 4 weeks following injection.
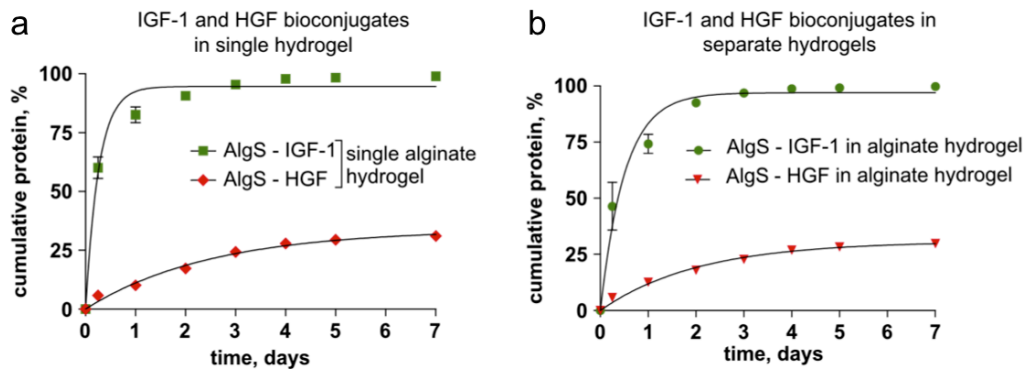
Figure 3.5. Molecule release from affinity-binding alginate hydrogels. Release kinetics of IGF-1 and HGF from the same hydrogel (a) and from separate hydrogels (b). Cumulative protein released (%) = (cumulative released protein up to each time point/total protein recovered from the hydrogel) × 100. Residual protein entrapped in the hydrogels at the end of the study was recovered with sodium citrate treatment. Figure adapted from[82].

In addition to GAG affinities, the natural affinity of streptavidin for biotin has been exploited to sustain the release of IGF-1 from injectable hydrogels[20]. Davis et al., biotinylated self-assembling (SA) oligopeptides and IGF-1 to form a streptavidin-biotin complex upon mixing the biotinylated oligopeptides and IGF-1

with tetravalent streptavidin. The oligopeptides were designed with alternating hydrophilic and hydrophobic amino acids in order to "self-assemble" into nanofibrous hydrogels upon exposure to physiologic pH and osmolarity. IGF-1 release from the hydrogels was sustained for up to 84 days *in vivo* after injection into the myocardium or rats. Tethering IGF-1 to the peptide scaffold using the streptavidin-biotin strategy had significant effects on improving cardiomyocyte survival *in vitro* (cardiomyocyte [^{3}H]phenylalanine incorporation) and *in vivo* (caspase-3 cleavage of implanted neonatal cardiac myocytes) confirming the activity of released IGF-1. Combining the IGF-1/SA peptide hydrogels with neonatal cardiac myocytes significantly improved functional outcomes post MI, however the contribution of the IGF-1/SA peptide hydrogels alone was not investigated.

These self-assembling peptide hydrogels have also been explored to deliver platelet derived growth factor (PDGF) to prevent cardiomyocyte apoptosis post MI[83]. The amphiphilic nature of the oligopeptides provided sustained release of PDGF through weak molecular interactions between the oligopeptides and PDGF. PDGF release was sustained from hydrogels for 14 days following injection into the myocardium of rats. The released PDGF activated its receptor (PDGFR-β) in cardiomyocytes adjacent to the injection areas and attenuated cardiomyocyte death (caspase-3 cleavage) 14 days after induced MI and PDGF/SA peptide hydrogel injection. In addition, global LV geometry and LV function (fractional shortening) was preserved 14 days following MI with the PDGF/SA peptide hydrogels. A subsequent study confirmed the therapeutic benefit of these PDGF releasing hydrogels[84]. LV geometry and function (hemodynamic parameters) and myocardial tissue structure (vascular density, regional blood flow, and infarct size) were significantly improved 4 months following induced MI in rats with injection of the PDGF/SA peptide hydrogels. Importantly, the locally delivered PDGF did not have adverse systemic effects (pulmonary hypertension) as confirmed by no observed change in pulmonary artery thickness.

Another group of proteins that can recover cell viability during periods of environmental stress, the heat shock family of proteins, have also been delivered in the setting of MI using injectable hydrogels. Lee et al. used calcium crosslinked alginate hydrogels as a delivery matrix for poly(lactic-*co*-glycolic acid) (PLGA) microspheres loaded with heat shock protein 27 (HSP27) fused to a transcriptional activator (TAT) (to facilitate cell uptake of HSP27)[85]. HSP27-TAT was encapsulated in the PLGA microspheres using water/oil/water emulsions, a frequently used method for preparing microspheres containing proteins, and these loaded microspheres were embedded in the alginate hydrogel during calcium crosslinking upon injection. Loading HSP27-TAT in the densely crosslinked microspheres prevented the burst release that is typical of proteins encapsulated in hydrogels. Released HSP27-TAT remained active as evidenced by reduced cardiomyocyte apoptosis and restored cardiomyocyte proliferation under ischemic conditions *in vitro*, although this system was not tested in the setting of MI.

Angiogenic Factors

Another common strategy to preserve viable myocardium following MI is to restore blood flow to the ischemic myocardium by stimulating neovasculature formation in the infarct area with localized release of pro-angiogenic growth factors. Sustained release of fibroblast growth factor (FGF) from injectable hydrogels has been extensively explored to stimulate angiogenesis following MI[60,86-91]. FGF is a powerful angiogenic molecule, but has a very short half-life *in vivo*. Sakakibara et al., showed that radiolabeled FGF delivered to the myocardium via bolus venous injections, intracoronary injections or intramyocardial injections is nearly undetectable 24 hrs after administration[89]. However, by using gelatin hydrogel microspheres as a carrier matrix, effective concentrations of radiolabeled FGF were sustained in the peri-infarct area of the myocardium 24 and 72 hrs after injection (all groups injected 4 weeks after induced MI in rats). To assess the therapeutic effects of sustaining FGF levels in

the myocardium with this hydrogel system, FGF loaded microspheres were injected 4 weeks after induced MI in swine. Upon evaluation at 4 weeks after injection, LV remodeling was significantly attenuated (echocardiography) and neovasculature was significantly increased (capillary density) compared to a control MI group. Other groups have also reported the efficacy of using gelatin microspheres to deliver FGF in the setting of MI[89,90]. In addition to gelatin microspheres, injectable chitosan hydrogels have been used to deliver FGF[86]. Wang et al. encapsulated FGF in thermoresponsive chitosan hydrogels upon injection into the myocardium by mixing FGF with the chitosan solution. This system significantly improved heart function compared to injecting FGF alone in a rat model of chronic MI (hydrogels injected 1 week post-MI).

While the sustained delivery of pro-angiogenic factors to ischemic tissue has stimulated neovasculature formation, as evidenced by increases in capillary densities, the stability and connectivity of these newly formed vessels has been a concern[92]. In order to form more stable vessels with supporting smooth muscles cells, dual delivery of angiogenic growth factors using injectable hydrogels has been explored to treat MI. Hao et al., encapsulated vascular endothelial growth factor (VEGF) and platelet derived growth factor (PDGF) in alginate hydrogels by mixing a solution of purified alginate and growth factors with a calcium sulfate solution upon injection into the myocardium[93]. The rationale for choosing these two molecules was to first stimulate endothelial vessel formation with VEGF delivery, followed by smooth muscle cell recruitment with PDGF delivery to support the immature vessels. To this end, VEGF release preceded PDGF release from the alginate hydrogels and release of both molecules was sustained for over 30 days *in vitro* as the hydrogel degraded. When applied 1 week following induced MI in rats, the dual growth factor releasing hydrogels significantly increased the number of α-SMA containing blood vessels around the injection site 4 weeks after injection compared to hydrogels loaded with each growth factor alone.

To further control VEGF delivery in the setting of MI, Wu et al. conjugated VEGF to *N*-hydroxysuccinimide (NHS) terminated PVL-*b*-PEG-*b*-PVL block copolymers (NHS reacts with primary amines on the protein)[94]. The block copolymers were designed to form a hydrogel at 37°C for injectability and completely degraded after 42 days when implanted subcutaneously in rats. When injected into the myocardium 1 week following induced MI in rats, the VEGF conjugated hydrogels showed significant improvements in heart function (FS, EF, LV EDV and ESV, dP/dt max, dP/dt min) and structure (scar area, capillary density) 4 weeks after injection compared to VEGF alone and VEGF injected with the hydrogel but not conjugated (Figure 3.6).
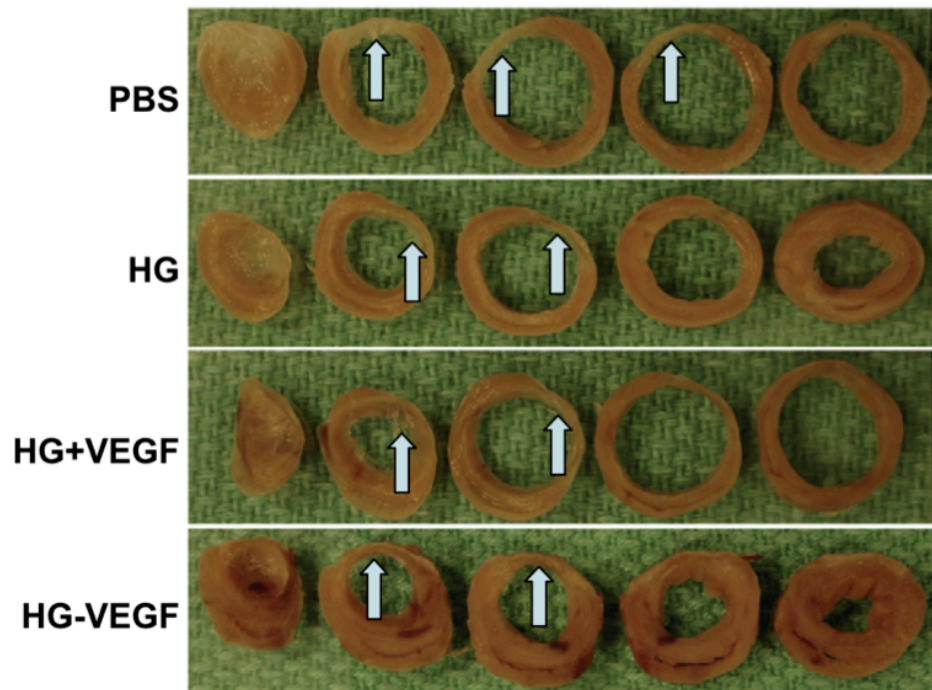
Figure 3.6. Tissue response to delivered growth factors. Representative heart slices obtained at 35 days after post-MI injection of PBS, hydrogel (HG), hydrogel with soluble VEGF (HG+VEGF), or hydrogel with VEGF tethered through covalent linkage (HG-VEGF). Arrows indicate the location of the infarct in individual slices. Figure adapted from[94].

Finally, plasmid DNA encoding angiogenic molecules has been delivered with injectable hydrogels. Kwon et al. synthesized multiblock copolymers with acid-labile acetal linkages (for controlled degradation) that form hydrogels at

37°C for VEGF plasmid delivery following MI[95]. The injectable hydrogels significantly enhanced the efficacy of the VEGF plasmid over injecting the naked plasmid, as confirmed by VEGF expression in the infarct area 2 weeks after injection. This enhanced expression was correlated with increases in capillary density and a more preserved myocardium in the infarct area. To further enhance angiogenesis, injectable hydrogels with adhesive sites can be used as a carrier of angiogenic plasmids to provide a matrix that facilitates cell migration. The combination of plasmid and adhesive matrix (termed gene-activated matrix) enhances gene transfection by localizing the plasmid until endogenous cells migrate into the implanted scaffold and become transfected to express the encoded protein[48,96,97]. For example, Christman et al. used an injectable fibrin glue that forms upon mixing fibrinogen and thrombin to localize a plasmid encoding the angiogenic molecule pleiotrophin (PTN) in the infarct myocardium[48]. Injecting the PTN plasmid in fibrin glue 1 week following induced MI in rats increased the formation of arterioles (α-SMA staining) that were functionally connected to existent coronary vasculature (confirmed with fluorescent microbead perfusion) 5 weeks after injection.

Chemoattractants

For control of endogenous cell recruitment, chemokines that selectively recruit stem/progenitor cells have been delivered from injectable hydrogels. For example, stromal derived factor-1 alpha (SDF-1α) has been locally delivered in the setting of MI using the injectable peptide hydrogels described in the previous section[98]. Release of SDF-1α was controlled by tethering the protein to the oligopeptide scaffold through a peptide sequence that is cleaved by endogenous proteases. The amino acid sequence of SDF-1α was engineered to resist protease degradation to ensure that active SDF-1α was released from the scaffold in the presence of proteases. Released SDF-1α was detectable for up to 7 days around the injection site *in vivo* and led to significant increases in cells expressing the receptor for SDF-1α in the MI region, which co-expressed

markers of stem/progenitor cells and endothelial cells. In addition, capillary (isolectin) and arteriole (α-SMA) densities increased significantly 4 weeks after injecting the SDF-1α containing hydrogels compared to MI controls in rats. These tissue-level observations were correlated with significant improvements in LV function.

3.4. Summary

Although only in its infancy, it is clear that the field of injectable hydrogels to treat cardiac tissue post-MI has high potential as a translatable therapy. The lack of a cell source needed for transplantation will only accelerate development of percutaneous delivered hydrogels, whether they act as tissue bulking agents or for the controlled delivery of therapeutic molecules. A wide range of both natural and synthetic materials have been investigated and each has unique properties, including mechanics, degradation, and cellular interactions. Future work should further investigate the various mechanisms in which these materials act, both biologically and mechanically, and focus on clinically relevant parameters, such as the animal model and mode of delivery. This information will lead to a clear understanding and illustration of the efficacy of injectable hydrogels to treat patients that have experienced an MI and to prevent the LV remodeling events that can lead to heart failure.

3.5. References

1. Gheorghiade M, Bonow RO. Chronic heart failure in the united states - a manifestation of coronary artery disease. *Circulation*. 1998;97:282-289
2. Eaton LW, Weiss JL, Bulkley BH, Garrison JB, Weisfeldt ML. Regional cardiac dilatation after acute myocardial-infarction - recognition by 2-dimensional echocardiography. *New England Journal of Medicine*. 1979;300:57-62
3. Erlebacher JA, Weiss JL, Weisfeldt ML, Bulkley BH. Early dilation of the infarcted segment in acute transmural myocardial-infarction - role of infarct expansion in acute left-ventricular enlargement. *Journal of the American College of Cardiology*. 1984;4:201-208
4. Weisman HF, Healy B. Myocardial infarct expansion, infarct extension, and reinfarction - pathophysiologic concepts. *Progress in Cardiovascular Diseases*. 1987;30:73-110
5. Epstein FH, Yang ZQ, Gilson WD, Berr SS, Kramer CM, French BA. Mr tagging early after myocardial infarction in mice demonstrates contractile dysfunction in adjacent and remote regions. *Magnetic Resonance in Medicine*. 2002;48:399-403
6. Jackson BM, Gorman JH, Moainie SL, Guy TS, Narula N, Narula J, John-Sutton MG, Edmunds LH, Gorman RC. Extension of borderzone myocardium in postinfarction dilated cardiomyopathy. *Journal of the American College of Cardiology*. 2002;40:1160-1167
7. Jackson BM, Gorman JH, Salgo IS, Moainie SL, Plappert T, St John-Sutton M, Edmunds LH, Gorman RC. Border zone geometry increases wall stress after myocardial infarction: Contrast echocardiographic assessment. *American Journal of Physiology-Heart and Circulatory Physiology*. 2003;284:H475-H479
8. Kramer CM, Lima JAC, Reichek N, Ferrari VA, Llaneras MR, Palmon LC, Yeh IT, Tallant B, Axel L. Regional differences in function within noninfarcted myocardium during left-ventricular remodeling. *Circulation*. 1993;88:1279-1288
9. Lima JAC, Becker LC, Melin JA, Lima S, Kallman CA, Weisfeldt ML, Weiss JL. Impaired thickening of nonischemic myocardium during acute regional ischemia in the dog. *Circulation*. 1985;71:1048-1059
10. Pilla JJ, Blom AS, Gorman JH, 3rd, Brockman DJ, Affuso J, Parish LM, Sakamoto H, Jackson BM, Acker MA, Gorman RC. Early postinfarction ventricular restraint improves borderzone wall thickening dynamics during remodeling. *Ann Thorac Surg*. 2005;80:2257-2262
11. Gorman RC, Jackson BM, Gorman JH. The potential role of ventricular compressive therapy. *Surgical Clinics of North America*. 2004;84:45-+
12. Mann DL. Mechanisms and models in heart failure - a combinatorial approach. *Circulation*. 1999;100:999-1008
13. Sutton MG, Sharpe N. Left ventricular remodeling after myocardial infarction: Pathophysiology and therapy. *Circulation*. 2000;101:2981-2988
14. Blom AS, Pilla JJ, Gorman RC, 3rd, Gorman JH, Mukherjee R, Spinale FG, Acker MA. Infarct size reduction and attenuation of global left ventricular remodeling with the corcap cardiac support device following acute myocardial infarction in sheep. *Heart Fail Rev*. 2005;10:125-139
15. Enomoto Y, Gorman JH, Moainie SL, Jackson BM, Parish LM, Plappert T, Zeeshan A, St John-Sutton MGS, Gorman RC. Early ventricular restraint after myocardial infarction: Extent of the wrap determines the outcome of remodeling. *Annals of Thoracic Surgery*. 2005;79:881-887

16. Kelley ST, Malekan R, Gorman JH, 3rd, Jackson BM, Gorman RC, Suzuki Y, Plappert T, Bogen DK, Sutton MG, Edmunds LH, Jr. Restraining infarct expansion preserves left ventricular geometry and function after acute anteroapical infarction. *Circulation*. 1999;99:135-142

17. Moainie SL, Guy S, Gorman JH, Plappert T, Jackson BM, St John-Sutton MG, Edmunds LH, Gorman RC. Infarct restraint attenuates remodeling and reduces chronic ischemic mitral regurgitation after postero-lateral infarction. *Annals of Thoracic Surgery*. 2002;74:444-449

18. Christman KL, Fok HH, Sievers RE, Fang QH, Lee RJ. Fibrin glue alone and skeletal myoblasts in a fibrin scaffold preserve cardiac function after myocardial infarction. *Tissue Engineering*. 2004;10:403-409

19. Dai WD, Wold LE, Dow JS, Kloner RA. Thickening of the infarcted wall by collagen injection improves left ventricular function in rats. *Journal of the American College of Cardiology*. 2005;46:714-719

20. Davis ME, Hsieh PCH, Takahashi T, Song Q, Zhang SG, Kamm RD, Grodzinsky AJ, Anversa P, Lee RT. Local myocardial insulin-like growth factor 1 (igf-1) delivery with biotinylated peptide nanofibers improves cell therapy for myocardial infarction. *Proceedings of the National Academy of Sciences of the United States of America*. 2006;103:8155-8160

21. Dobner S, Bezuidenhout D, Govender P, Zilla P, Davies N. A synthetic non-degradable polyethylene glycol hydrogel retards adverse post-infarct left ventricular remodeling. *J Card Fail*. 2009;15:629-636

22. Fujimoto KL, Ma ZW, Nelson DM, Hashizume R, Guan JJ, Tobita K, Wagner WR. Synthesis, characterization and therapeutic efficacy of a biodegradable, thermoresponsive hydrogel designed for application in chronic infarcted myocardium. *Biomaterials*. 2009;30:4357-4368

23. Huang NF, Yu J, Sievers R, Li S, Lee RJ. Injectable biopolymers enhance angiogenesis after myocardial infarction. *Tissue Eng*. 2005;11:1860-1866

24. Jiang XJ, Wang T, Li XY, Wu DQ, Zheng ZB, Zhang JF, Chen JL, Peng B, Jiang H, Huang C, Zhang XZ. Injection of a novel synthetic hydrogel preserves left ventricle function after myocardial infarction. *J Biomed Mater Res A*. 2009;90:472-477

25. Kofidis T, Lebl DR, Martinez EC, Hoyt G, Tanaka M, Robbins RC. Novel injectable bioartificial tissue facilitates targeted, less invasive, large-scale tissue restoration on the beating heart after myocardial injury. *Circulation*. 2005;112:I173-177

26. Landa N, Miller L, Feinberg MS, Holbova R, Shachar M, Freeman I, Cohen S, Leor J. Effect of injectable alginate implant on cardiac remodeling and function after recent and old infarcts in rat. *Circulation*. 2008;117:1388-1396

27. Leor J, Miller L, Feinberg MS, Shachar M, Landa N, Holbova R, Cohen S. A novel injectable alginate scaffold promotes angiogenesis and preserves left ventricular geometry and function after extensive myocardial infarction in rat. *Circulation*. 2004;110:279-279

28. Lu WN, Lu SH, Wang HB, Li DX, Duan CM, Liu ZQ, Hao T, He WJ, Xu B, Fu Q, Song YC, Xie XH, Wang CY. Functional improvement of infarcted heart by co-injection of embryonic stem cells with temperature-responsive chitosan hydrogel. *Tissue Eng Part A*. 2009;15:1437-1447

29. Mukherjee R, Zavadzkas JA, Saunders SM, McLean JE, Jeffords LB, Beck C, Stroud RE, Leone AM, Koval CN, Rivers WT, Basu S, Sheehy A, Michal G, Spinale FG. Targeted myocardial microinjections of a biocomposite material

reduces infarct expansion in pigs. *Ann Thorac Surg*. 2008;86:1268-1276

30. Singelyn JM, DeQuach JA, Seif-Naraghi SB, Littlefield RB, Schup-Magoffin PJ, Christman KL. Naturally derived myocardial matrix as an injectable scaffold for cardiac tissue engineering. *Biomaterials*. 2009;30:5409-5416

31. Tsur-Gang O, Ruvinov E, Landa N, Holbova R, Feinberg MS, Leor J, Cohen S. The effects of peptide-based modification of alginate on left ventricular remodeling and function after myocardial infarction. *Biomaterials*. 2009;30:189-195

32. Wang T, Wu DQ, Jiang XJ, Zhang XZ, Li XY, Zhang JF, Zheng ZB, Zhuo R, Jiang H, Huang C. Novel thermosensitive hydrogel injection inhibits post-infarct ventricle remodelling. *Eur J Heart Fail*. 2009;11:14-19

33. Yoon SJ, Fang, Y.H., Lim, C.H., Kim, B.S., Son, H.S., Park, Y., Sun K. Regeneration of ischemic heart using hyaluronic acid-based injectable hydrogel. *Journal of Biomedical Materials Research Part B: Applied Biomaterials*. 2008:9

34. Yu J, Christman KL, Chin E, Sievers RE, Saeed M, Lee RJ. Restoration of left ventricular geometry and improvement of left ventricular function in a rodent model of chronic ischemic cardiomyopathy. *J Thorac Cardiovasc Surg*. 2009;137:180-187

35. Wall ST, Walker JC, Healy KE, Ratcliffe MB, Guccione JM. Theoretical impact of the injection of material into the myocardium: A finite element model simulation. *Circulation*. 2006;114:2627-2635

36. Lee KY, Mooney DJ. Hydrogels for tissue engineering. *Chemical Reviews*. 2001;101:1869-1879

37. Minh KN, Lee DS. Injectable biodegradable hydrogels. *Macromolecular Bioscience*. 2010;10:563-579

38. Yu L, Ding JD. Injectable hydrogels as unique biomedical materials. *Chemical Society Reviews*. 2008;37:1473-1481

39. Nelson DM, Ma Z, Fujimoto KL, Hashizume R, Wagner WR. Intra-myocardial biomaterial injection therapy in the treatment of heart failure: Materials, outcomes and challenges. *Acta Biomater*. 2011;7:1-15

40. Shapira K, Dikovsky D, Habib M, Gepstein L, Seliktar D. Hydrogels for cardiac tissue regeneration. *Biomed Mater Eng*. 2008;18:309-314

41. Gupta KB, Ratcliffe MB, Fallert MA, Edmunds LH, Jr., Bogen DK. Changes in passive mechanical stiffness of myocardial tissue with aneurysm formation. *Circulation*. 1994;89:2315-2326

42. Holmes JW, Borg TK, Covell JW. Structure and mechanics of healing myocardial infarcts. *Annu Rev Biomed Eng*. 2005;7:223-253

43. Pfeffer MA, Pfeffer JM. Ventricular enlargement and reduced survival after myocardial infarction. *Circulation*. 1987;75:IV93-97

44. Batista R. Partial left ventriculectomy--the batista procedure. *Eur J Cardiothorac Surg*. 1999;15 Suppl 1:S12-19; discussion S39-43

45. Starling RC, Jessup M, Oh JK, Sabbah HN, Acker MA, Mann DL, Kubo SH. Sustained benefits of the corcap cardiac support device on left ventricular remodeling: Three year follow-up results from the acorn clinical trial. *Ann Thorac Surg*. 2007;84:1236-1242

46. Sartipy U, Albage A, Lindblom D. The dor procedure for left ventricular reconstruction. Ten-year clinical experience. *Eur J Cardiothorac Surg*. 2005;27:1005-1010

47. Klodell CT, Jr., Aranda JM, Jr., McGiffin DC, Rayburn BK, Sun B, Abraham WT, Pae WE, Jr., Boehmer JP, Klein H, Huth C. Worldwide surgical experience with

the paracor heartnet cardiac restraint device. *J Thorac Cardiovasc Surg*. 2008;135:188-195

48. Christman KL, Fang QZ, Yee MS, Johnson KR, Sievers RE, Lee RJ. Enhanced neovasculature formation in ischemic myocardium following delivery of pleiotrophin plasmid in a biopolymer. *Biomaterials*. 2005;26:1139-1144

49. Christman KL, Vardanian AJ, Fang Q, Sievers RE, Fok HH, Lee RJ. Injectable fibrin scaffold improves cell transplant survival, reduces infarct expansion, and induces neovasculature formation in ischemic myocardium. *J Am Coll Cardiol*. 2004;44:654-660

50. Yu J, Gu Y, Du KT, Mihardja S, Sievers RE, Lee RJ. The effect of injected rgd modified alginate on angiogenesis and left ventricular function in a chronic rat infarct model. *Biomaterials*. 2009;30:751-756

51. Leor J, Tuvia S, Guetta V, Manczur F, Castel D, Willenz U, Petnehazy O, Landa N, Feinberg MS, Konen E, Goitein O, Tsur-Gang O, Shaul M, Klapper L, Cohen S. Intracoronary injection of in situ forming alginate hydrogel reverses left ventricular remodeling after myocardial infarction in swine. *J Am Coll Cardiol*. 2009;54:1014-1023

52. Brown BN, Valentin JE, Stewart-Akers AM, McCabe GP, Badylak SF. Macrophage phenotype and remodeling outcomes in response to biologic scaffolds with and without a cellular component. *Biomaterials*. 2009;30:1482-1491

53. Ifkovits JL, Tous E, Minakawa M, Morita M, Robb JD, Koomalsingh KJ, Gorman JH, 3rd, Gorman RC, Burdick JA. Injectable hydrogel properties influence infarct expansion and extent of postinfarction left ventricular remodeling in an ovine model. *Proc Natl Acad Sci U S A*. 2010;107:11507-11512

54. Kofidis T, de Bruin JL, Hoyt G, Lebl DR, Tanaka M, Yamane T, Chang CP, Robbins RC. Injectable bioartificial myocardial tissue for large-scale intramural cell transfer and functional recovery of injured heart muscle. *J Thorac Cardiovasc Surg*. 2004;128:571-578

55. Seif-Naraghi SB, Salvatore MA, Schup-Magoffin PJ, Hu DP, Christman KL. Design and characterization of an injectable pericardial matrix gel: A potentially autologous scaffold for cardiac tissue engineering. *Tissue Eng Part A*.16:2017-2027

56. Wang T, Jiang XJ, Lin T, Ren S, Li XY, Zhang XZ, Tang QZ. The inhibition of postinfarct ventricle remodeling without polycythaemia following local sustained intramyocardial delivery of erythropoietin within a supramolecular hydrogel. *Biomaterials*. 2009;30:4161-4167

57. Rowley JA, Madlambayan G, Mooney DJ. Alginate hydrogels as synthetic extracellular matrix materials. *Biomaterials*. 1999;20:45-53

58. Kim IY, Seo SJ, Moon HS, Yoo MK, Park IY, Kim BC, Cho CS. Chitosan and its derivatives for tissue engineering applications. *Biotechnol Adv*. 2008;26:1-21

59. Ruel-Gariepy E, Shive M, Bichara A, Berrada M, Le Garrec D, Chenite A, Leroux JC. A thermosensitive chitosan-based hydrogel for the local delivery of paclitaxel. *Eur J Pharm Biopharm*. 2004;57:53-63

60. Chenite A, Chaput C, Wang D, Combes C, Buschmann MD, Hoemann CD, Leroux JC, Atkinson BL, Binette F, Selmani A. Novel injectable neutral solutions of chitosan form biodegradable gels in situ. *Biomaterials*. 2000;21:2155-2161

61. Chung C, Beecham M, Mauck RL, Burdick JA. The influence of degradation characteristics of hyaluronic acid hydrogels on in vitro neocartilage formation by mesenchymal stem cells. *Biomaterials*. 2009;30:4287-4296

62. Khetan S, Burdick J. Cellular encapsulation in 3d hydrogels for tissue engineering. *J Vis Exp*. 2009

63. Khetan S, Chung C, Burdick JA. Tuning hydrogel properties for applications in tissue engineering. *Conf Proc IEEE Eng Med Biol Soc*. 2009;2009:2094-2096

64. Laurent TC, Fraser JR. Hyaluronan. *FASEB J*. 1992;6:2397-2404

65. Sahoo S, Chung C, Khetan S, Burdick JA. Hydrolytically degradable hyaluronic acid hydrogels with controlled temporal structures. *Biomacromolecules*. 2008;9:1088-1092

66. Toole BP. Hyaluronan: From extracellular glue to pericellular cue. *Nat Rev Cancer*. 2004;4:528-539

67. Dang AB, Guccione JM, Mishell JM, Zhang P, Wallace AW, Gorman RC, Gorman JH, 3rd, Ratcliffe MB. Akinetic myocardial infarcts must contain contracting myocytes: Finite-element model study. *Am J Physiol Heart Circ Physiol*. 2005;288:H1844-1850

68. Pilla JJ, Gorman JH, 3rd, Gorman RC. Theoretic impact of infarct compliance on left ventricular function. *Ann Thorac Surg*. 2009;87:803-810

69. Wenk JF, Wall ST, Peterson RC, Helgerson SL, Sabbah HN, Burger M, Stander N, Ratcliffe MB, Guccione JM. A method for automatically optimizing medical devices for treating heart failure: Designing polymeric injection patterns. *J Biomech Eng*. 2009;131:121011

70. Sierra DH, Eberhardt AW, Lemons JE. Failure characteristics of multiple-component fibrin-based adhesives. *J Biomed Mater Res*. 2002;59:1-11

71. Martens TP, Godier AF, Parks JJ, Wan LQ, Koeckert MS, Eng GM, Hudson BI, Sherman W, Vunjak-Novakovic G. Percutaneous cell delivery into the heart using hydrogels polymerizing in situ. *Cell Transplant*. 2009;18:297-304

72. Augst AD, Kong HJ, Mooney DJ. Alginate hydrogels as biomaterials. *Macromol Biosci*. 2006;6:623-633

73. Ryan LP, Matsuzaki K, Noma M, Jackson BM, Eperjesi TJ, Plappert TJ, John-Sutton MGS, Gorman JH, Gorman RC. Dermal filler injection: A novel approach for limiting infarct expansion. *Annals of Thoracic Surgery*. 2009;87:148-155

74. Anderson JM. Biological responses to materials. *Annu. Rev. Mater. Res.* 2001;31:20

75. Anderson JM, Rodriguez A, Chang DT. Foreign body reaction to biomaterials. *Semin Immunol*. 2008;20:86-100

76. Badylak SF, Valentin JE, Ravindra AK, McCabe GP, Stewart-Akers AM. Macrophage phenotype as a determinant of biologic scaffold remodeling. *Tissue Eng Part A*. 2008;14:1835-1842

77. Rodriguez A, Meyerson H, Anderson JM. Quantitative in vivo cytokine analysis at synthetic biomaterial implant sites. *J Biomed Mater Res A*. 2009;89:152-159

78. Ziats NP, Miller KM, Anderson JM. In vitro and in vivo interactions of cells with biomaterials. *Biomaterials*. 1988;9:5-13

79. Epstein SE, Fuchs S, Zhou YF, Baffour R, Kornowski R. Therapeutic interventions for enhancing collateral development by administration of growth factors: Basic principles, early results and potential hazards. *Cardiovasc Res*. 2001;49:532-542

80. Langer R, Folkman J. Polymers for sustained-release of proteins and other macromolecules. *Nature*. 1976;263:797-800

81. Gombotz WR, Pettit DK. Biodegradable polymers for protein and peptide drug-delivery. *Bioconjugate Chemistry*. 1995;6:332-351

82. Ruvinov E, Leor J, Cohen S. The promotion of myocardial repair by the

sequential delivery of igf-1 and hgf from an injectable alginate biomaterial in a model of acute myocardial infarction. *Biomaterials*. 2011;32:565-578

83. Hsieh PCH, Davis ME, Gannon J, MacGillivray C, Lee RT. Controlled delivery of pdgf-bb for myocardial protection using injectable self-assembling peptide nanofibers. *Journal of Clinical Investigation*. 2006;116:237-248

84. Hsieh PCH, MacGillivray C, Gannon J, Cruz FU, Lee RT. Local controlled intramyocardial delivery of platelet-derived growth factor improves postinfarction ventricular function without pulmonary toxicity. *Circulation*. 2006;114:637-644

85. Lee J, Tan CY, Lee SK, Kim YH, Lee KY. Controlled delivery of heat shock protein using an injectable microsphere/hydrogel combination system for the treatment of myocardial infarction. *Journal of Controlled Release*. 2009;137:196-202

86. Wang HB, Zhang XL, Li YM, Ma YT, Zhang Y, Liu ZG, Zhou J, Lin QX, Wang YM, Duan CM, Wang CY. Improved myocardial performance in infarcted rat heart by co-injection of basic fibroblast growth factor with temperature-responsive chitosan hydrogel. *Journal of Heart and Lung Transplantation*. 2010;29:881-887

87. Sakakibara Y, Yamamoto M, Nishimura K, Nishina T, Miwa S, Handa N, Nomoto T, Tanbara K, Tabata Y, Komeda M. Prevasculrization using gelatin microsphere containing basic-fibroblast growth factor enhances the benefits of cardiomyocytes transplantation in rats with ischemic cardiomyopathy. *Circulation*. 2000;102:650-650

88. Yamamoto T, Suto N, Okubo T, Mikuniya A, Hanada H, Yagihashi S, Fujita M, Okumura K. Intramyocardial delivery of basic fibroblast growth factor-impregnated gelatin hydrogel microspheres enhances collateral circulation to infarcted canine myocardium. *Japanese Circulation Journal-English Edition*. 2001;65:439-444

89. Iwakura A, Fujita M, Kataoka K, Tambara K, Sakakibara Y, Komeda M, Tabata Y. Intramyocardial sustained delivery of basic fibroblast growth factor improves angiogenesis and ventricular function in a rat infarct model. *Heart and Vessels*. 2003;18:93-99

90. Liu Y, Sun LJ, Huan Y, Zhao HT, Deng JL. Effects of basic fibroblast growth factor microspheres on angiogenesis in ischemic myocardium and cardiac function: Analysis with dobutamine cardiovascular magnetic resonance tagging. *European Journal of Cardio-Thoracic Surgery*. 2006;30:103-107

91. Fujita M, Ishihara M, Morimoto Y, Simizu M, Saito Y, Yura H, Matsui T, Takase B, Hattori H, Kanatani Y, Kikuchi M, Maehara T. Efficacy of photocrosslinkable chitosan hydrogel containing fibroblast growth factor-2 in a rabbit model of chronic myocardial infarction. *Journal of Surgical Research*. 2005;126:27-33

92. Yancopoulos GD, Davis S, Gale NW, Rudge JS, Wiegand SJ, Holash J. Vascular-specific growth factors and blood vessel formation. *Nature*. 2000;407:242-248

93. Hao XJ, Silva EA, Mansson-Broberg A, Grinnemo KH, Siddiqui AJ, Dellgren G, Wardell E, Brodin LA, Mooney DJ, Sylven C. Angiogenic effects of sequential release of vegf-a(165) and pdgf-bb with alginate hydrogels after myocardial infarction. *Cardiovascular Research*. 2007;75:178-185

94. Wu J, Zeng FQ, Huang XP, Chung JCY, Konecny F, Weisel RD, Li RK. Infarct stabilization and cardiac repair with a vegf-conjugated, injectable hydrogel. *Biomaterials*. 2011;32:579-586

95. Kwon JS, Park IK, Cho AS, Shin SM, Hong MH, Jeong SY, Kim YS, Min JJ, Jeong MH, Kim WJ, Jo S, Pun SH, Cho JG, Park JC, Kang JC, Ahn Y. Enhanced

angiogenesis mediated by vascular endothelial growth factor plasmid-loaded thermo-responsive amphiphilic polymer in a rat myocardial infarction model. *Journal of Controlled Release*. 2009;138:168-176

96.   Bonadio J, Smiley E, Patil P, Goldstein S. Localized, direct plasmid gene delivery in vivo: Prolonged therapy results in reproducible tissue regeneration. *Nature Medicine*. 1999;5:753-759

97.   Shea LD, Smiley E, Bonadio J, Mooney DJ. DNA delivery from polymer matrices for tissue engineering. *Nature Biotechnology*. 1999;17:551-554

98.   Segers VF, Tokunou T, Higgins LJ, MacGillivray C, Gannon J, Lee RT. Local delivery of protease-resistant stromal cell derived factor-1 for stem cell recruitment after myocardial infarction. *Circulation*. 2007;116:1683-1692

CHAPTER 4

Synergy of SDF-1α and degradable hyaluronic acid hydrogels in directing bone marrow derived cell homing to the remodeling heart

(Adapted from: B.P. Purcell, J.A. Elser, A. Mu, K.B. Margulies, J.A. Burdick, *Biomaterials,* 2012, 33:7849-7857)

4.1. Introduction

Nearly 1 million Americans suffer a myocardial infarction (MI) each year and many patients progress to heart failure due to limited treatment options to attenuate the remodeling response post-MI[1]. Following MI, a dynamic tissue remodeling process, characterized by cell death and the formation of avascular scar tissue, induces global changes to ventricle geometry (i.e., wall thinning and chamber dilation), which ultimately compromise heart function[2]. In order to attenuate the progression to heart failure, therapeutics using bone marrow-derived cells (BMCs) are being widely explored to promote repair in the remodeling myocardium. In particular, autologous BMC transplantation has received the greatest attention in a clinical setting; yet, only modest improvements in ventricular function have been demonstrated after intracoronary BMC delivery, potentially due to limited cell engraftment in the myocardium[3]. Inconsistencies in cell isolation and storage procedures[4], the timing of BMC administration following MI[5], and the location of BMC administration[6] complicate outcomes by altering the delicate signaling mechanisms that are critical for cell engraftment.

BMC engraftment in the bone marrow microenvironment (i.e., BMC homing) is regulated by the expression of chemokines and extracellular matrix (ECM) molecules under steady state conditions. In response to injury or under pathological conditions, elevated concentrations of these regulatory molecules in the peripheral circulation mobilize BMCs and direct their engraftment in remodeling tissues to mediate repair. In particular, stromal-derived factor-1

alpha (SDF-1α), along with its receptor (CXCR4), are critical regulators of BMC homing to the bone marrow, but also orchestrate BMC mobilization into the peripheral circulation and local engraftment in the heart following MI[7]. Myocardial SDF-1α expression post MI is accompanied by a concomitant increase in bone marrow derived CXCR4+ circulating cells, suggesting that these cells are mobilized and respond to the myocardial SDF-1α signal[8].

Despite evidence that the mobilized BMCs home to the myocardium via SDF-1α and contribute to tissue repair, the extent of this endogenous response is insufficient to prevent the eventual onset of heart failure following MI. Enhancing endogenous BMC homing (and therefore repair) through myocardial delivery of SDF-1α increases progenitor cell markers in the heart, stimulates angiogenesis, and attenuates global ventricular remodeling[9]. However, due to its very low molecular weight (8kDa) and proteolytic susceptibility, SDF-1α delivery to the myocardium following MI is challenging. Researchers have addressed this challenge by covalently linking recombinant SDF-1α (rSDF-1α)[10] or SDF-1α peptide analogs[11] to scaffolds that incorporate sites for integrin mediated adhesion. Beyond integrin mediated interactions, there are other components of the bone marrow niche, such as interactions with glycosaminoglycans (GAGs) that might aid in SDF-1α delivery and BMC engraftment with improved efficacy.

Naturally, local concentrations of small, cationic chemokines like SDF-1α are regulated by GAGs in the ECM[12]. SDF-1α binds to GAGs through ionic interactions between basic amino acid residues and acidic groups along the disaccharide backbone[13]. The affinity between SDF-1α and GAGs plays an important role in localizing SDF-1α on the endothelium to direct cell homing[14] and sustaining SDF-1α activity in the presence of proteases[15]. In addition to their roles in chemokine presentation, some GAGs play a more direct role in BMC homing through receptor interactions. For example, hyaluronic acid (HA) is abundant in the bone marrow, where it serves as an anchoring molecule for BMC homing through binding to the CD44 receptor[16]. Interestingly, HA is localized to regions of SDF-1α expression in the bone marrow and HA and CD44 mediate

48

cell responsiveness to SDF-1α during cell migration *in vitro* and cell homing *in vivo*[17].

In this work, we exploit the cooperative roles of SDF-1α and HA in order to enhance endogenous BMC homing to the heart following MI. Specifically, recombinant SDF-1α was encapsulated in degradable HA hydrogels that form *in situ* on the heart, in order to localize SDF-1α and HA homing cues to the remodeling heart for enhanced engraftment of circulating BMCs in the myocardium.

4.2. Materials and Methods

Animals

Adult BALB/CAnNHsd mice (Charles River, Production) were housed in a dedicated vivarium under conventional conditions. Mice received a standard diet (LabDiet 5010) and water ad libitum. All experimental procedure were performed according to the NIH Guide for Care and Use of Laboratory Animals and approved by the Institutional Animal Care and Use Committee (IACUC) at the University of Pennsylvania.

Macromer synthesis

A degradable HA macromer with methacrylate functionality was synthesized through hydroxyethyl methacrylate (HEMA) modification of the HA backbone in a three step process. (1) Sodium hyaluronate (74 kDa, Lifecore) was converted to a tetrabutylammonium (TBA) salt by acidic ion exchange with Dowex resin (50W×8–200, Sigma), followed by neutralization with TBA-OH, and lyophilization. (2) 2-hydroxyethyl methacrylate was reacted with succinic anhydride in dichloroethane (DCE) via a ring opening reaction (65°C, 16hrs) in the presence of N-methylimidazole to obtain HEMA-COOH. HEMA-COOH was purified via hydrochloric acid wash, DI H_2O wash, and DCE evaporation with a rotary evaporator. (3) HEMA-COOH was coupled to HA-TBA in anhydrous dimethyl sulfoxide through an esterification reaction in the presence of 4-

dimethylaminopyridine (DMAP) and di-*tert*-butyl dicarbonate (BOC$_2$O) activating agents (45°C, 20hrs). The following molar ratios of reactants were used: HA-TBA (1), HEMA-COOH (1.4), BOC$_2$O (1.2), DMAP (0.1). The modified HEMA-HA macromer was purified via overnight dialysis in DI H$_2$O at 4°C, acetone precipitation, another 5 days of dialysis in DI H$_2$O at 4°C, followed by lyophilization. ^{1}H NMR was used to determine the degree of modification and purity of the HEMA-HA.

SDF-1α electrostatics

Electrostatic surface potentials of SDF-1α were visualized with Adaptive Poisson-Boltzmann Solver (APBS) software[18]. The PDB file for SDF-1α (2KEC[19]) was first converted to a PQR file with PDB2PQR software[20] using a PARSE forcefield and PROPKA software[21] to assign protonation states at pH = 7.4. All calculations were performed on a web server hosted by the National Biomedical Computation Resource and surface potentials were visualized with Jmol[22].

Macromer binding affinity

Binding affinity between rSDF-1α and HEMA-HA was quantified using an intrinsic protein fluorescence quenching technique[23]. Fluorescence titration experiments were performed on a Tecan infinite m200 plate reader (Grödig, Austria) at 25°C. The fluorescence of a 2 μM rSDF-1α (460-SD, R&D Systems) solution in 100 mM HEPES buffer (pH 7.4) was recorded at 280/350nm excitation/emission. Fluorescence quenching was monitored by increasing the concentration of HEMA-HA in rSDF-1α solution in 13.5 μM increments. Dry macromer was dissolved in the rSDF-1α solution, mixed, and incubated for a 2 min equilibration period before measuring fluorescence. The normalized changes in fluorescence with each HEMA-HA titration were plotted against HEMA-HA concentration and resulting binding isotherms were fit by nonlinear regression (Mathematica, Wolfram Research, Inc.) to the equation describing

bimolecular association:

$$ F = F_i + F_f \left[\frac{K_d + [SDF] + [HA] - \sqrt{(K_d + [SDF] + [HA])^2 - 4[SDF][HA]}}{2[SDF]} \right] $$

where F is the change in fluorescence over initial fluorescence ($-\Delta F/F_o$), F_i is the initial value for ($-\Delta F/F_o$), F_f is the final value for ($-\Delta F/F_o$), and K_d is the dissociation constant [23].

Hydrogel formation

Hydrogels were formed upon visible light exposure using a previously established initiator system consisting of eosin Y, triethanolamine (TEOA), 1-vinyl-2-pyrrolidinone (VP), and a halogen curing light (Elipar 2500, 3M)[24]. 50 µL hydrogel precursor solutions were prepared by mixing HEMA-HA and initiators in PBS at final concentrations of: 6 wt% HEMA-HA, 0.02 wt% eosin Y, 225 mM TEOA, and 37 mM VP. 200 ng rSDF-1α was mixed into the 50 µL hydrogel precursor solution for HA Gel/rSDF-1α groups. Hydrogels were formed in cylindrical molds upon light exposure for 90 seconds. For release studies, gels were incubated in 1 mL of chemically defined (CD) media comprised of α-MEM media (Invitrogen) supplemented with 20 mM L-glutamine, 100 U/mL penicillin, 100 µg/mL streptomycin, and 0.1% bovine serum albumin (BSA). Gels were moved to fresh media at the indicated time points and media containing eluted molecules were stored at -20°C. rSDF-1α was quantified with ELISA (DY350, R&D Systems) and HA was quantified with a previously established uronic acid assay[25].

Enzyme-linked Immunosorbent Competition Assay

An ELISA kit (DY350, R&D Systems) was used to quantify rSDF-1α (460-SD, R&D Systems) as summarized in the General ELISA protocol from R&D Systems. Prior to loading samples, 0.5 ng/mL rSDF-1α was preincubated in

serial dilutions of a 5 mg/mL HEMA-HA solution in PBS for 90 min at 25°C. Percent inhibition of monoclonal antibody binding to rSDF-1α due to the added HEMA-HA was calculated after quantifying rSDF-1α in each sample.

BMC isolation

Adult BALB/CAnNHsd mice (10–12 weeks old, 22-26 g) were anesthetized with 100 mg/kg ketamine and 20 mg/kg xylazine. Unfractionated BMCs were obtained by removing the femurs, and flushing the marrow cavity with sterile PBS over a 40 µm filter. The cells were pelleted by centrifugation and resuspended in lysis buffer (BD Biosciences) for 1 min to lyse red blood cells. Cells were again pelleted and resuspended in 1 mL PBS to remove remaining lysis buffer. To visualize the cells *in vitro* and *in vivo*, PKH fluorescent linker kits were employed (Sigma).

In vitro BMC chemotaxis

The chemotactic activities of rSDF-1α and HEMA-HA were quantified using freshly isolated BMCs in microchemotaxis chambers (NeuroProbe) following a modified boyden chamber assay[26]. Briefly, BMCs ($2x10^6$ cells/mL) in CD media were separated from active molecules in CD media by a porous polycarbonate membrane (5 µm pores) coated with type 1 collagen (PureCol, Advanced BioMatrix). After 4 hrs at 37°C, non-migrated cells on the top side of the membrane were scraped away, while migrated cells on the bottom side were fixed in 4% formalin and imaged. PKH67GL fluorescence was used to visualize cells and Image J Particle Analysis software was used to quantify cells as follows. For each well containing fluorescently tagged cells, a circle was drawn to denote the well area using Image J. The same well area was used for all wells in each experiment. After converting fluorescent images to 8-bit, the images were threshold to eliminate background without excluding cells. Total cell counts in each well were quantified using the "Analyze Particles" function in Image J. Cells

were counted manually to validate threshold levels, and the same threshold was used for all wells in each experiment. For each experiment, the average number of migrated cells per well for each condition were normalized to the average number of migrated cells per well for control wells containing only CD media (n=6 wells per condition). A monoclonal antibody to CD44 (ab25064, abcam) was used for HA specific blocking at 3 µg/mL, while a CXCR4 antagonist (AMD3100, Calbiochem) was used for SDF-1α specific blocking at 0.5 µg/mL.

hMSC culture and chemotaxis

Human mesenchymal stem cells (hMSCs) were obtained from Lonza Corporation (Walkersville, MD) and expanded in growth media (α-MEM, 16.7% (v/v) fetal bovine serum, 20 mM L-glutamine, 100 U/mL penicillin, 100 µg/mL streptomycin). hMSCs were used at passage 4 after thawing from liquid N2 storage and culturing overnight on tissue culture polystyrene (TCPS) in growth media under anaerobic conditions (GasPak EZ, Becton Deckinson). hMSCs were removed from TCPS with TrypLE Express (Invitrogen), washed with CD media, and resuspended in CD media for chemotaxis experiments. Cells were seeded at 2x105 cells/mL in upper wells of chemotaxis chambers using collagen-coated membranes with 8 µm pores, and DAPI stained after formalin fixing to visualize cells. Recombinant human SDF-1α (350-NS, R&D systems), 3 µg/mL mouse monocolonal antibody for CD44 (ab6124, abcam) and 0.5 µg/mL AMD3100 (Calbiochem) were used for hMSC chemotaxis experiments.

Experimental MI

A cryoinjury model of MI was used to initiate MI remodeling[27]. Adult BALB/CAnNHsd mice (10–12 weeks old, 22-26 g) were anesthetized with 20 mg/kg ketamine and 4 mg/kg xylazine, shaved and disinfected with alcohol. The mice were kept under anesthesia (1.5% isoflurane), incubated and ventilated with 95% O_2 using a mechanical ventilator (MiniVent, Harvard Apparatus). The heart was exposed through a left lateral thoracotomy and cryoinjury was introduced by

applying a round 2 mm diameter stainless steel probe frozen with liquid nitrogen to the epicardial surface of the ventricle for 10 sec. After removing the probe, the cryoinjured area was confirmed by a white disk-shaped region. For mice receiving hydrogels, 25 µL of the liquid hydrogel precursor solutions were applied to the surface of the injured ventricle through a 27G syringe in the presence of curing lamp exposure. For mice receiving SDF-1α only, 10 µL of a 10 µg/mL rSDF-1α solution was injected into the ventricle wall using a 30G syringe. The order of therapeutic intervention was rotated from animal to animal. Following manipulations to the heart, the intercostal space and skin were closed with sutures. Mice received 100% oxygen until responding to interdigital pinch, after which the endotracheal tube was withdrawn. Mice were kept warm with a heating blanket during recovery. Meloxicam (5 mg/kg) was administered via intraperitoneal injection 1 hr after surgery and once a day for 1 week following surgery to minimize pain.

In vivo BMC homing

After a recovery period of 3 hrs following MI induction, mice were anesthetized with 20 mg/kg ketamine and 5 mg/kg xylazine. Freshly isolated BMCs from a donor mouse were fluorescently tagged with PKH linker kit, counted on a Vi-CELL (Beckman Coulter, Inc.), and 9×10^6 cells in 300 µL sterile PBS was injected into the femoral vein of the MI mouse. Blood samples were collected 1 day after BMC injection via retro orbital bleed, treated for RBC lysis, and analyzed for PKH+ cells using flow cytometry. Briefly, cells were gated for viability using 4',6-diamidino-2-phenylindole (DAPI, Invitrogen), size and granularity using characteristic BMC distributions of forward scatter (FSC) and size scatter (SSC), respectively, and fluorescent intensity using appropriate controls (Figure 4.1)[28]. PKH+ cells in the blood were reported as a percentage of total cells in the blood within the characteristic BMC size distribution. Mice were anesthetized 7 days after experimental MI with 100 mg/mL ketamine and xylazine, blood samples were collected from the abdomen, and hearts were

excised and either perfusion digested with collagenase (150 U/mL type 2 collagenase in Krebs buffer, Worthington) for PKH+ cell quantification using flow cytometry[28] or flash frozen in embedding medium for PKH+ cell visualization using histology. Quantified PKH+ cells in the blood were again reported as a percentage of total BMCs in the blood, while quantified PKH+ cells in the heart were reported as a total number of cells/heart. Embedded hearts were sectioned at a 12 µm thickness and imaged immediately upon thawing at room temperature.
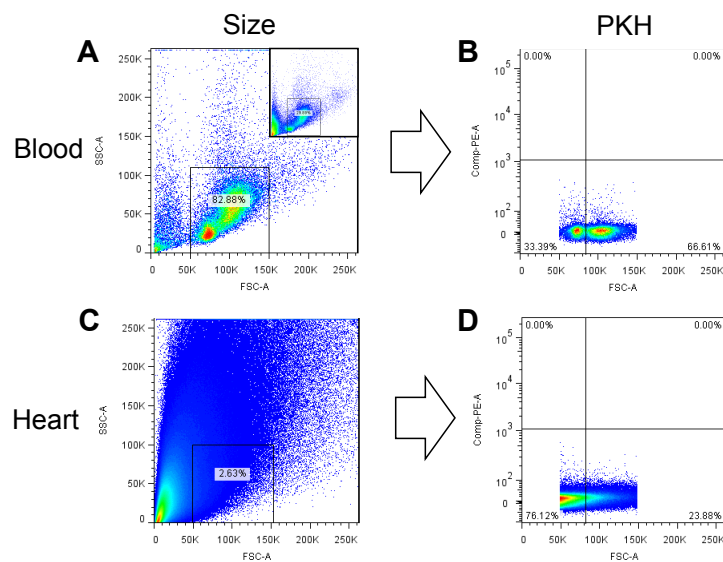
Figure 4.1. PKH- BMC negative controls for flow cytometry gating. After gating for viability with DAPI, BMCs in the blood (A) and the heart (C) were gated based on the typical size of freshly isolated BMCs (A, inset).   The cells within this size range were then analyzed for PKH fluorescence (C and D). This gating strategy minimized PKH false-positive counts in the blood and heart to less than 1 per 106 events (D). Abbreviations: SSC – side scatter, FSC – forward scatter.

Statistical analysis

Values are reported as mean ± standard error of the mean. Statistical differences between groups were determined using ANOVA in conjunction with a student's two-tailed t-test (Microsoft Excel), with $P <$ *0.05, **0.01, and ***0.001 considered as significant.

4.3. Results

HEMA-HA synthesis

HA macromers were synthesized to facilitate photoinitiated crosslinking into hydrogels through a terminal methacrylate group and degradation through hydrolysis of ester groups between the methacrylate and the HA backbone (Figure 4.2 A). The extent of HEMA modification was determined to be ~25% of disaccharide repeat units along the HA backbone via ^{1}H NMR (Figure 4.3). This percent can be easily tuned with the molar ratio of HEMA-COOH to BOC$_2$O in the coupling reaction[29].
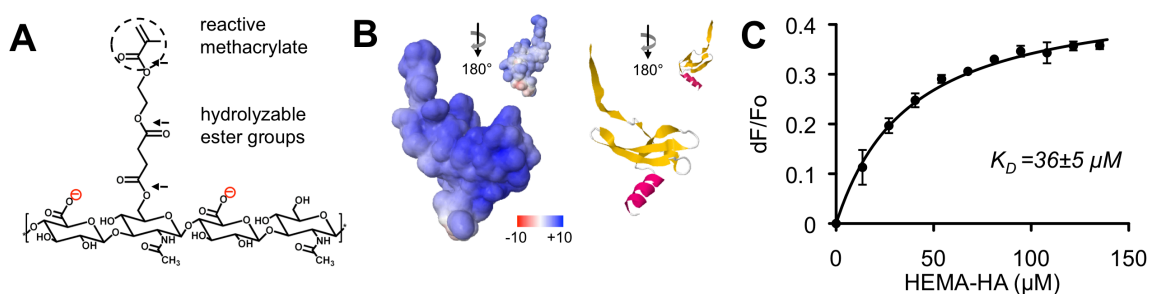

Figure 4.2. Electrostatic interactions between HEMA-HA and rSDF-1α. **(**A) Repeat unit of HEMA-HA macromer synthesized with reactive methacrylate group and hydrolyzable ester groups (black arrows) between the methacrylate functionality and HA backbone. The macromer carries a negative charge due to carboxylic acid groups along the HA backbone. (B) SDF-1α surface potentials visualized using APBS software package (left) that correspond to the beta sheet rich in basic amino acids (right). Scale for surface potentials is in units of kT/e where k is Boltzman's constant, T is temperature, and e is the charge of an electron. (C) Fluorescence quenching of rSDF-1α with HEMA-HA titration. Data fit to bimolecular association equation to calculate K$_D$ [23] (n = 3 independent experiments).
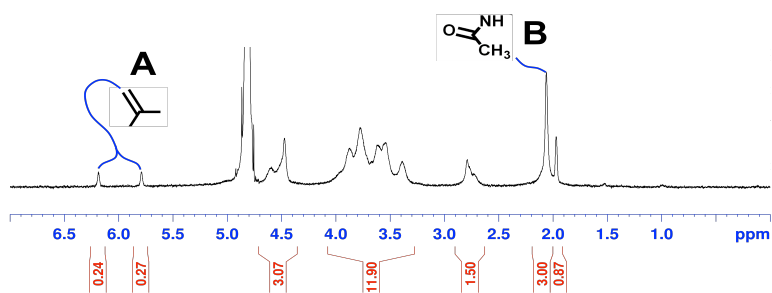

Figure 4.3. ^{1}H NMR of purified HEMA-HA macromer. Approximately 25% of the disaccharide repeat units were modified with HEMA. The ^{1}H peaks from the methacrylate group on HEMA (A) were normalized to the ^{1}H peaks from the methyl groups on *N*-acetylglucosamine (B) to determine percent modification.

HEMA-HA and SDF-1α binding

To investigate ionic interactions between the HEMA-HA macromer and rSDF-1α, the electrostatic surface potentials of SDF-1α were visualized and binding association constants were experimentally determined. Visualization of SDF-1α using APBS revealed an overall positive surface charge with the most positive charges of nearly +10 kT/e concentrated along the beta sheet of the protein structure (Figure 4.2 B). This charge distribution is attributed to an abundance of basic amino acids (i.e., arginine and lysine residues) in the beta sheet, which have important roles in SDF-1α binding to negatively charged GAGs[13]. Indeed, binding between rSDF-1α and the purified HEMA-HA macromer was observed with a dissociation constant (K_D) of 36 ± 5 µM (Figure 4.2 C). This interaction was significantly stronger than the measured interaction between HEMA-HA and BSA (K_D = 157 ± 4 µM, data not shown), illustrating the specificity of small, positively charged chemokines for negatively charged GAGs (i.e., HA) in the ECM.

BMC chemotaxis to rSDF-1α and HEMA-HA

In order to model endogenous BMC homing, unfractionated BMCs were isolated from mouse femurs, fluorescently tagged with PKH linker dyes, and used to assess the activity of rSDF-1α and HEMA-HA *in vitro* and *in vivo*. *In vitro,* both rSDF-1α and HEMA-HA stimulated chemotaxis of BMCs in a dose dependent manner, nearly 4-fold at the highest concentrations investigated (Figure 4.4, ****P* = 0.0001 and ****P* = 0.0008, respectively). The observed chemotaxis was specific to cell surface receptors for SDF-1α (CXCR4) and HA (CD44) as evidenced by antagonist and antibody blocking, respectively. Specifically, the introduction of the antagonist or antibody completely diminished any increased migration in response to the molecule and was indistinguishable from control groups. The chemotactic activity of rSDF-1α and HEMA-HA was also observed using a purified population of bone marrow derived stem cells, human

57

mesenchymal stem cells (hMSCs) (Figure 4.5). The hMSC response to rSDF-1α and HEMA-HA was also diminished in response to the introduction of a CXCR4 antagonist and CD44 antibody blocking, respectively.
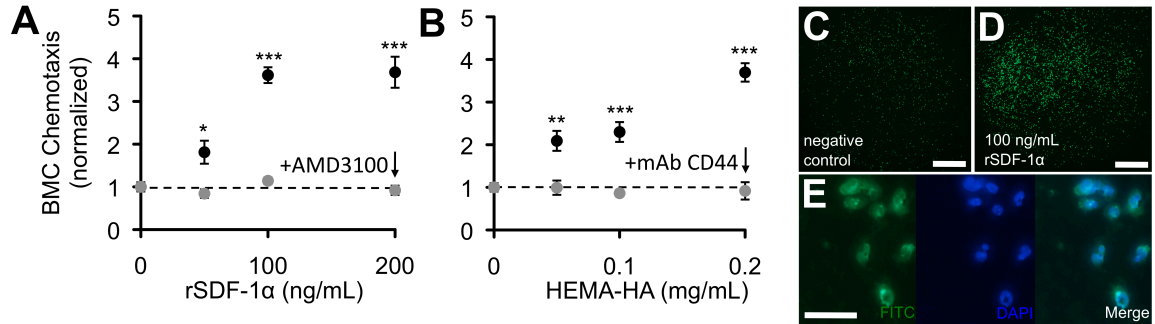

Figure 4.4. Chemotactic activity of rSDF-1α and HEMA-HA. (A) rSDF-1α stimulated significant dose-dependent chemotaxis of unfractionated BMCs and was blocked with a CXCR4 antagonist, AMD3100. (B) HEMA-HA stimulated similar dose-dependent chemotaxis of BMCs and was blocked with a monoclonal antibody to CD44. For each experiment, the average number of migrated cells per well for each condition was normalized to the average number of migrated cells per well for negative control wells containing only chemically defined media (mean ± SEM, n = 6 wells per condition). (C) Representative negative control well with migrated PKH+ BMCs. (D) Representative 100 ng/mL rSDF-1α well containing migrated PKH+ BMCs. E) Fluorescent visualization of migrated PKH+ BMCs. Scale bars: C-D = 500 µm; E = 50 µm.
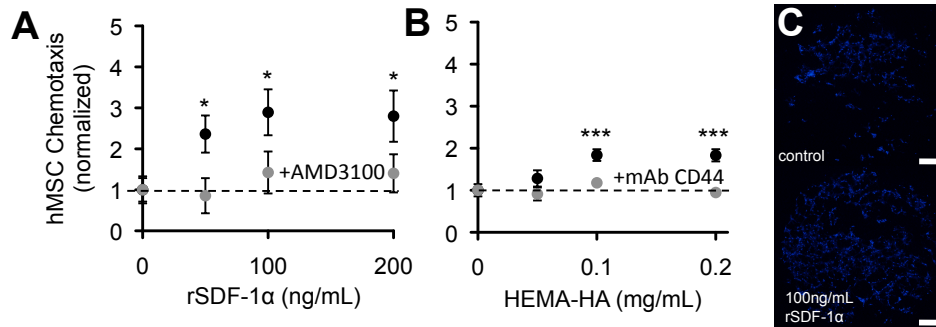
Figure 4.5. hMSC chemotaxis to rSDF-1α and HEMA-HA. (A) rSDF-1α stimulated chemotaxis of hMSCs in a dose-dependent manner and was blocked with a CXCR4 antagonist, AMD3100. (B) HEMA-HA stimulated chemotaxis of hMSCs in a dose dependent manner and was blocked with a monoclonal antibody to CD44. The average number of migrated cells per well for each condition was normalized to the average number of migrated cells per well for negative control wells containing only chemically defined media (n = 6 wells per condition). (C) Representative wells containing migrated cells for negative control (upper) and 100 ng/mL rSDF-1α (lower) conditions. Scale bars: C = 500 µm.

Molecule release from HEMA-HA hydrogels

To sustain release of rSDF-1α and HEMA-HA in the setting of MI*,* a visible light initiator system was used to crosslink the HEMA-HA macromer into hydrogels from a liquid precursor solution (containing rSDF-1α, HEMA-HA, and photoinitiator) upon blue light exposure.   Photocrosslinked   HEMA-HA

hydrogels sustained the release of rSDF-1α and HA, measured over 7 days *in vitro* (Figure 4.6 A-B). HEMA-HA hydrogels exhibit hydrolytic degradation of ester groups in the HEMA side groups, releasing HA,

Figure 4.6. Molecule release from photocrosslinked HA Gels. (A) Cumulative release of encapsulated rSDF-1α was sustained for 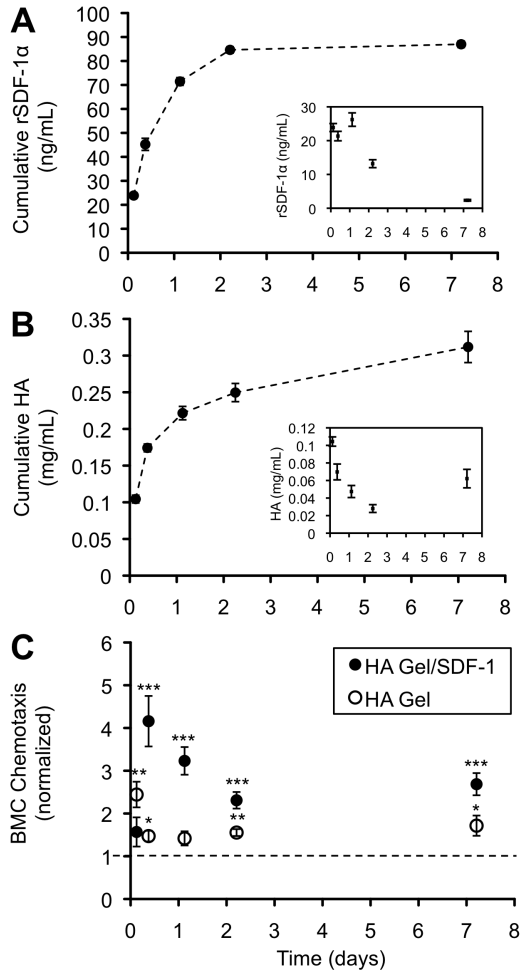7 days *in vitro* as determined by ELISA. (B) Cumulative release of uncrosslinked HEMA-HA and degradation products of the hydrogel was sustained for 7 days *in vitro* as determined by uronic acid analysis. Quantity of rSDF-1α and HA was measured from buffer collected and replaced at specified time points. Gels remained intact after the 7-day incubation. Insets indicate quantity of molecules in each sample (n = 3 gels, mean ± SEM). (C) The HA Gel significantly enhanced BMC chemotaxis for up to 7 days, which was further enhanced with release of encapsulated rSDF-1α. For each experiment, the average number of migrated cells per well for each condition was normalized to the average number of migrated cells per well for negative control wells containing only chemically defined media (mean ± SEM, n = 6 wells per condition).

entrapped rSDF-1α, and poly(methacrylic acid) kinetic chains with time. Generally, the release of rSDF-1α and HA was rapid in the first few days, due to diffusion of peripheral rSDF-1α and uncrosslinked HEMA-HA, and then slowed as release of encapsulated molecules was mediated by hydrogel degradation. Gels were still intact after 7 days in buffer at 37°C, while little additional rSDF-1α release was measured. While the ELISA kit provides a low limit of detection for rSDF-1α, this antibody "sandwich" technique was unable to detect rSDF-1α in the presence of soluble HEMA-HA, which acted as a binding competitor to the

monoclonal antibodies with 44% inhibition at 0.08 mg/mL HEMA-HA (Figure 4.7). Therefore, we suspect that reported concentrations of released rSDF-1α are for the free, unbound protein in solution, and that rSDF-1α/HEMA-HA complexes are also present in the release samples. Importantly, released molecules from HA hydrogels and HA hydrogels containing rSDF-1α both stimulated chemotaxis of BMCs over 7 days (Figure 4.6 C), indicating the influence of both HA and rSDF-1α components on BMC chemotaxis.
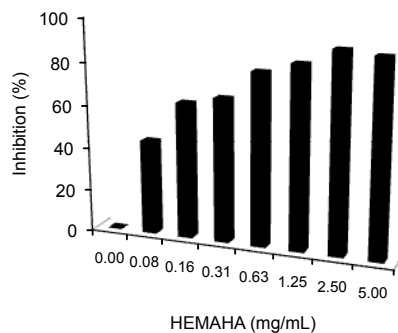
Figure 4.7. ELISA inhibition by soluble HEMA-HA. Incubating rSDF-1α in serial dilutions of HEMA-HA inhibited ELISA detection of rSDF-1α.

BMC homing to the remodeling heart

In order to quantify BMC homing *in vivo*, fluorescently tagged BMCs were infused into the circulation following experimental MI in mice and tracked in the blood and the heart using flow cytometry (Figure 4.8 A). Myocardial delivery of homing factors (HA and rSDF-1α) from hydrogels (formed on heart using blue light, Figure 4.8 B) was assessed for the ability to enhance BMC homing to the heart and compared to controls of MI only and MI with intramyocardial injection of rSDF-1α. Hydrogels were localized to the injury site and adhered to the myocardium for sustained delivery of homing molecules (Figure 4.8 C-D).

The circulating PKH+ BMCs were readily quantified in the blood and heart using flow cytometry (Figure 4.8 E). The fluorescence intensity of the cells varied over a wide range, so a PKH+/PKH- threshold was chosen to quantify PKH+ BMCs while minimizing PKH- false-positive events in the blood and the heart (Figure 4.1). Using this threshold, we observed a decrease in fluorescence intensity of the PKH+ BMCs in the blood from day 1 to day 7 (Figure 4.8 E).

60

Figure 4.8. *In vivo* model to quantify BMC homing. (A) HA Gels were applied to the heart immediately following experimental MI. Freshly isolated BMCs were fluorescently tagged with PKH linker dyes and infused into the circulation via a femoral vein injection 3 hrs after MI. Blood samples were collected 1 and 7 days followi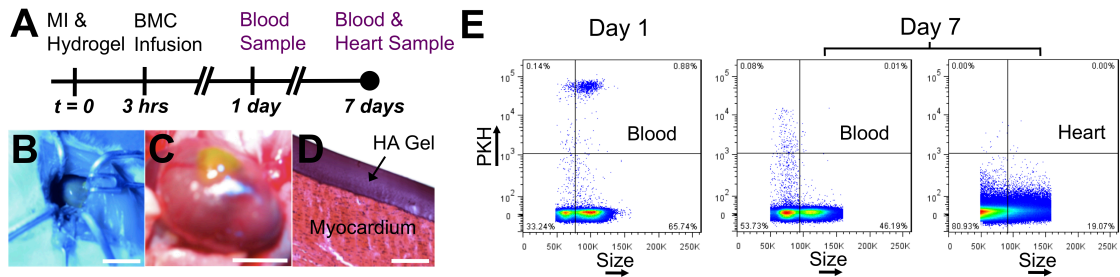ng MI and hearts were digested 7 days following MI to quantify PKH+ BMCs. (B) Hydrogels formed *in situ* by applying a liquid precursor solution to the epicardial surface of the ventricle upon blue light exposure. (C) This technique allowed the hydrogels to be localized on the injured myocardium for localized molecule delivery. (D) The hydrogels adhered to the myocardium while processing the tissue for histology and H&E staining. (E) Representative flow cytometry with constant threshold to quantify PKH+ BMCs in the blood and heart. Scale bars: B-10 mm; C-5 mm; D-100 μm.

Considering that the PKH linker dyes are stable *in vivo* for weeks, the decrease in fluorescent intensity could be due to cell proliferation, or simply due to preferential retaining of cell types in the blood that do not uptake PKH dyes as effectively as others[30]. Interestingly, BMCs quantified in the blood on day 1 were primarily larger cells around the size and granularity of granulocytes, while the BMCs quantified in the blood on day 7 were primarily smaller cells around the size and granularity of lymphocytes (Figure 4.9); however, both size phenotypes show similar ranges of PKH staining intensity immediately after exposure to the PKH linker dye.

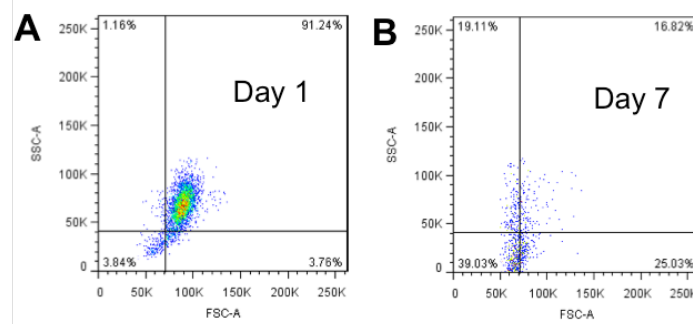**Figure 4.9.** Size of PKH+ BMCs in the blood. Circulating PKH+ BMCs exhibited a larger phenotype characteristic of granulocytes 1 day after infusion (A), while PKH+ BMCs exhibited a smaller phenotype characteristic of lymphocytes/monocytes 7 days after infusion (B). Both cell phenotypes were increased to the same extent in the blood after rSDF-1α delivery to the heart. Abbreviations: SSC – side scatter, FSC – forward scatter.

Delivery of the HA Gel with encapsulated rSDF-1α and delivery of rSDF-1α as a bolus injection significantly increased the number of infused BMCs circulating in the blood 1 day after infusion (Figure 4.10 A, ***P < 0.001 and *P = 0.01, respectively). Both rSDF-1α delivery groups more than doubled the number of circulating BMCs on day 1 from 1% to 2% of native BMCs; however, this effect was only apparent in the HA Gel/ rSDF-1α group on day 7, although not statistically significant (Figure 4.10 B). All intervention groups significantly increased the number of BMCs engrafted in the heart compared to MI only, and the HA Gel with encapsulated rSDF-1α significantly increased BMC engraftment compared to rSDF-1α alone and the HA Gel alone (Figure 4.10 C, #P = 0.01 and 0.047, respectively), indicating synergy between the released molecules.
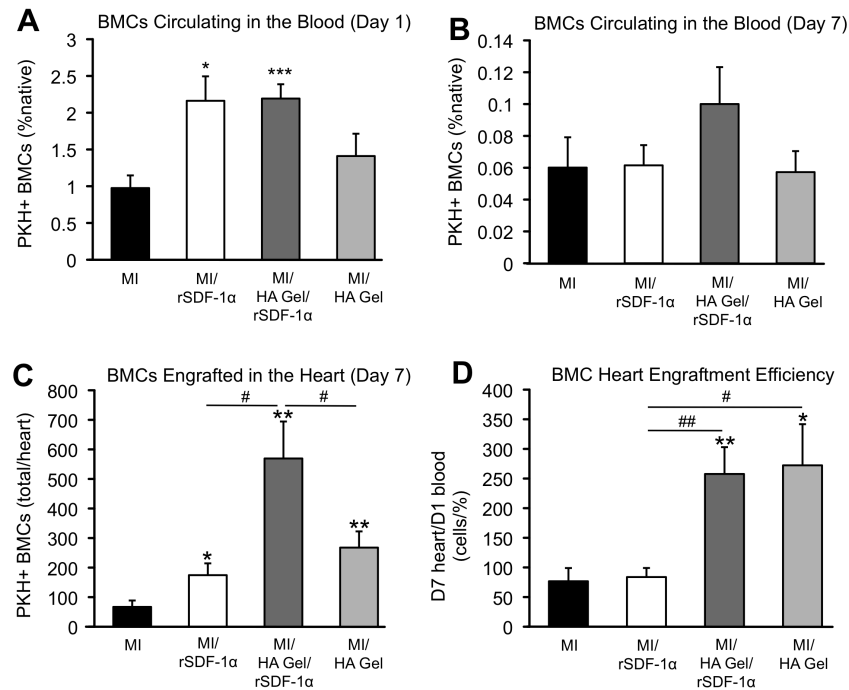
Figure 4.10. Quantification of BMC homing with molecule delivery to the heart. A) rSDF-1α delivery to the heart significantly increased the number of circulating PKH+ BMCs 1 day after infusion. B) This effect was sustained, although not statistically significant, 7 days after infusion when rSDF-1α was delivered from the HA Gel. PKH+ BMCs in the blood are reported as a percentage of total cells in the blood within the BMC size and granularity gating. C) Intramyocardial injection of rSDF-1α and application of the HA Gel alone following MI significantly enhanced the number of PKH+ BMCs in the heart compared to MI only 7 days after MI and cell infusion. Application of the HA Gel with encapsulated rSDF-1α further enhanced PKH+ BMC engraftment in the heart compared to delivering rSDF-1α or the HA gel individually. D) When normalized to the percent of PKH+ BMCs in the blood 1 day after infusion, the HA Gel enhances engraftment of circulating PKH+ BMC with a constant efficiency. (mean ± SEM, n = 7 animals for all groups except for MI only, n = 6).

When normalized to the percentage of BMCs circulating in the blood, the HA Gel (with and without rSDF-1α) enhanced myocardial engraftment of circulating BMCs at a significantly improved rate, over 3-fold greater than the bolus rSDF-1α injection and MI control, which showed the same engraftment rate (Figure 4.10 D). While both the HA Gel/rSDF-1α and bolus rSDF-1α injection groups had the same effect on circulating BMCs 1 day after infusion (2.2 ± 0.2 and 2.2 ± 0.3% native BMCs, respectively), they had significantly different effects on enhancing BMC engraftment in hearts 7 days after infusion, 570 ± 130 and 170 ± 40 BMCs per heart, respectively.

Engrafted BMCs localized to the infarct region (IR) and border region (BR) in the heart following MI (Figure 4.11), while PKH+ BMCs in other regions of the myocardium were very rare. The infarct region was characterized by dense collagen staining with Masson's Trichrome (Figure 4.11 A-B). This collagen scar tissue autofluoresced, allowing the infarct region to be easily identified for characterizing engrafted BMC locations within the heart, and PKH+ BMC fluorescence was bright enough to distinguish the BMCs against the tissue background as indicated by white arrows (Figure 4.11 C). PKH+ BMCs were identified in the infarct region in all groups, but were rare in the border region for all groups except for the HA Gel/rSDF-1α group. Border region BMCs in this group were commonly localized within and around vascular structures (Figure 4.11 D). Some cells also appeared to integrate into the tissue and align with the native tissue morphology (Figure 4.11 E).

4.4. Discussion

The objective of this study was to develop a biomaterial system to enhance BMC homing to the remodeling myocardium through exogenous delivery of the chemokine rSDF-1α. To accomplish this, we synthesized an *in situ* crosslinkable and degradable hydrogel system based on the molecule HA to encapsulate and sustain the local release of rSDF-1α to the myocardium.
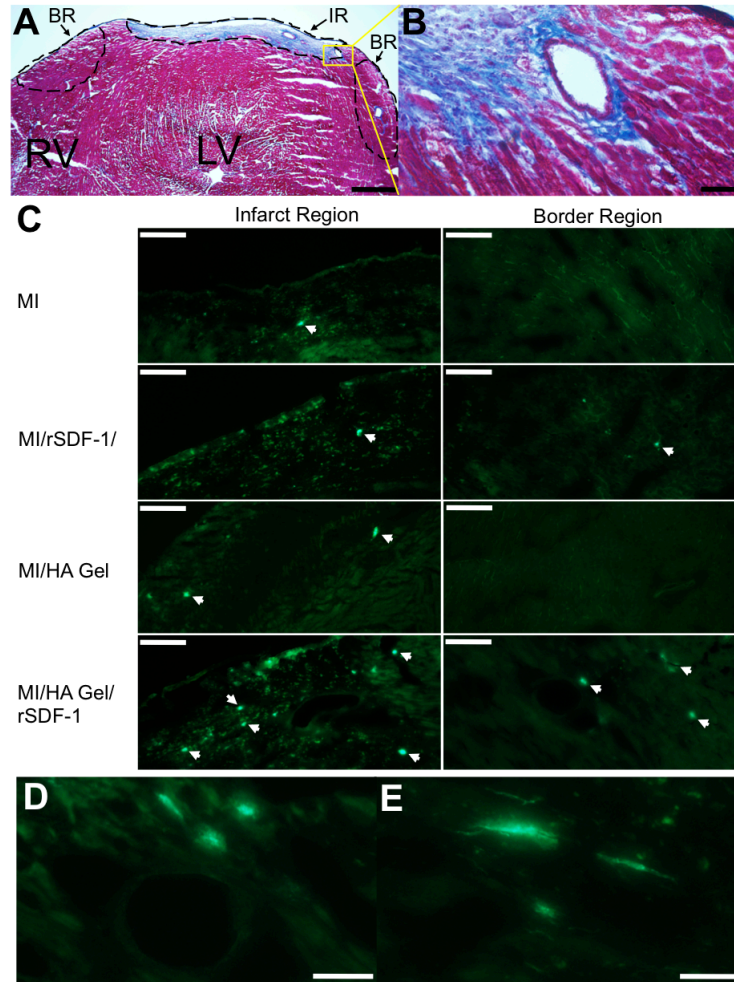
Figure 4.11. Visualization of PKH+ BMCs in the myocardium 7 days after systemic infusion. A) The cryoinjury resulted in the formation of a nontransmural collagen rich scar tissue (blue region) 7 days following MI as visualized with Masson's Trichrome. An infarct region (IR) and border region (BR) were defined to assess PKH+ BMC locations within the heart. B) Vasculature in the IR and BR remained intact following the cryoinjury. C) PKH+ BMCs were identified in the IR of all groups, while PKH+ BMCs in the BR were rare except in the HA Gel/rSDF-1α group. PKH+ BMCs were not found in remote regions of the myocardium for all groups. White arrowheads indicate PKH+ BMCs. D) PKH+ BMCs in the BR were often localized in and around vascular structures. E) In addition, cells in the BR appeared to align with the myocardial tissue structure. Scale bars: A-500 μm; B-50 μm; C-100 μm; D and E-50 μm.

Our rationale for choosing HA as our biomaterial was two-fold: (1) HA is a negatively charged GAG that naturally regulates chemokines in tissues, and (2) HA is the major ligand for CD44, which mediates cell motility processes that govern BMC homing.

GAGs are linear polysaccharides with an abundance of acidic groups that are negatively charged under physiologic conditions. Chemokines, on the

other hand, are characterized by an abundance of basic amino acid residues that are positively charged under the same conditions. These complimentary charges induce binding between GAGs and chemokines with an affinity that is dependent on the specific GAG chemistry, the size of the GAG molecule, and the net charge of the chemokine[12]. In particular, heparin sulfate (HS) has been shown to bind SDF-1α with high affinity (K_D~30 nM)[13]. Binding between SDF-1α and HS in the glycocalyx of the cell surface is important to localize SDF-1α and facilitate binding to CXCR4[13]; however, soluble HS has been shown to inhibit the chemotactic activity of SDF-1α in a dose dependent manner (0.1 to 100 μg/mL HS)[31]. Since the CXCR4 binding domain remains exposed after HS binding[13], the soluble HS is likely acting as a binding competitor to glycocalyx HS, preventing SDF-1α from achieving close contact with CXCR4 on the cell surface. Therefore, GAG chemistries with less affinity for SDF-1α may be optimal as a carrier matrix to allow glycocaylx sequestration of released SDF-1α in the presence of the degraded matrix. HA has 1 carboxylic acid per repeat unit compared to 3 sulfate groups per repeat unit of HS; therefore, we expected HA to bind SDF-1α with much less affinity (higher K_D) than HS. Indeed, we measured a K_D of 36 μM between our HA macromer and SDF-1α (Figure 4.2 C), which was selective to the positively charged SDF-1α ($K_{D,BSA}$=157 μM). This micromolar affinity was sufficient to slow SDF-1α diffusion within the HA Gels where the concentration of HA is very high (~100 mg/mL), without inhibiting cell chemotaxis to released SDF-1α in the presence of HA released from the gels (10 to 100 μg/mL HA) (Figure 4.6 B-C).

HA also interacts cooperatively with SDF-1α in directing cell motility through CD44 and CXCR4 receptor signaling crosstalk[17]. SDF-1α-CXCR4 binding on hematopoetic progenitor cells stimulated cell spreading on HA coated substrates through CD44 binding and CD44 polarized to the leading edge of cells migrating towards gradients of SDF-1α *in vitro*[17]. HA-CD44 binding initiates G-protein-dependent signal transduction that stimulates cell motility through Rho-ROCK signaling[32], as well as cell adhesion through integrin expression[33]. These

signaling pathways are important regulators of BMC homing processes in the bone marrow[17], as well as in peripheral tissues during inflammation[34]. For example, intravenously injected MSCs home to the injured kidney in a CD44 dependent process[35]. The role of HA in this process was corroborated *in vitro* as the MSCs exhibited CD44 dependent chemotaxis to HA.

In line with these studies, we showed that our modified HA macromer stimulates chemotaxis of BMCs through CD44 (Figures 4.4, 4.5). When delivered to the myocardium as an epicardial hydrogel immediately following experimental MI, the HA Gel enhanced engraftment of circulating BMCs in the myocardium (Figure 4.10 C). BMC engraftment was further enhanced by encapsulating rSDF-1α in the HA Gel (Figure 4.10 C). To form the hydrogels *in situ,* a photo-initiated crosslinking mechanism was utilized in order to localize molecule release to the myocardium while avoiding biomaterial injections that could cause further damage due to the small thickness of a mouse ventricle wall. In experimental models with larger ventricle wall thicknesses, a redox-initiated crosslinking mechanism can be used to form these hydrogels upon injection through a syringe[29].

Interestingly, delivering rSDF-1α to the heart had systemic effects in significantly increasing the number of PKH+ BMCs circulating in the blood, and sustained release of rSDF-1α from the HA Gel prolonged this effect (Figure 4.10 A-B). Separate studies have shown that an increase in circulating CXCR4+ cells coincides with the temporal expression of rSDF-1α in the heart following MI[8,9]. In addition, elevating SDF-1α concentrations in the blood has been shown to mobilize BMCs into the circulation[36]. Since we report the number of PKH+ BMCs in the blood as a percentage of total BMCs in the blood, an increase in this percentage may indicate that systemic concentrations of SDF-1α are high enough to prevent circulating PKH+ BMCs from homing to other organs, such as the bone marrow or spleen[37,38], but not high enough to mobilize native BMCs from SDF-1α gradients in the bone marrow. Indeed, mobilizing agents have been administered systemically following MI in order to mobilize CXCR4+ BMCs

into the circulation and therefore enhance the response to SDF-1α signals in the heart[39].

To model BMCs mobilized from the bone marrow, unfractionated BMCs were injected directly into the systemic circulation. These cells were used with minimal manipulations to include all CXCR4+ and CD44+ BMC populations that are present *in vivo*, and avoid culture conditions that are known to affect cell responsiveness to chemokines[40]. Using this model system, we were able to definitively quantify BMC homing with molecule delivery to the heart; however, investigation of how homed BMCs contribute to myocardial repair is beyond the scope of the model. Nevertheless, a growing body of literature suggests that delivery of SDF-1α and HA would promote a beneficial healing response following MI. For example, CXCR4 is expressed on selective populations of BMCs that have been implicated in myocardial tissue repair, including hematopoetic progenitor cells[41], mesenchymal stem cells[42], dendritic cells[43], T lymphocytes[44], and even committed tissue-specific stem cells[45]. Furthermore, SDF-1α delivery has been shown to largely promote neovascularization in ischemic tissues through BMC homing[9-11]. While enhancing CXCR4 positive cells in the heart has been shown to significantly attenuate post-MI remodeling, this approach seems to require complimentary growth factor and cell adhesion molecule expression that occurs in the early stages of post MI remodeling[46]. Therefore, early therapeutic intervention may be a limiting factor in translating SDF-1α-based therapies to the clinic.

Like SDF-1α/CXCR4, HA/CD44 interactions have important roles in regenerative processes during tissue remodeling including cell migration, proliferation, and differentiation[47]. In the setting of MI, CD44 expression is abundant on infiltrating leukocytes, myofibroblasts and endothelial cells that contribute to tissue repair[48]. CD44 knockout animals showed a prolonged maldaptive inflammatory response and diminished collagen synthesis, causing further ventricle dilation following MI[48]. Here, we report that dual delivery of SDF-1α and HA from *in situ* forming hydrogels enhances BMC homing to the

remodeling myocardium.   This finding highlights the importance of using materials that mimic components of the bone marrow niche to provide BMC specific cell adhesion ligands that act synergistically with SDF-1α/CXCR. However, applying these systems beyond the early stages of post MI remodeling remains to be investigated.

4.5. References

1. Roger VL, Go AS, Lloyd-Jones DM, Adams RJ, Berry JD, Brown TM, Carnethon MR, Dai S, de Simone G, Ford ES, Fox CS, Fullerton HJ, Gillespie C, Greenlund KJ, Hailpern SM, Heit JA, Ho PM, Howard VJ, Kissela BM, Kittner SJ, Lackland DT, Lichtman JH, Lisabeth LD, Makuc DM, Marcus GM, Marelli A, Matchar DB, McDermott MM, Meigs JB, Moy CS, Mozaffarian D, Mussolino ME, Nichol G, Paynter NP, Rosamond WD, Sorlie PD, Stafford RS, Turan TN, Turner MB, Wong ND, Wylie-Rosett J. Heart disease and stroke statistics--2011 update: A report from the american heart association. *Circulation*.123:e18-e209

2. Pfeffer MA, Braunwald E. Ventricular remodeling after myocardial-infarction: Experimental observations and clinical implications. *Circulation*. 1990;81:1161-1172

3. Abdel-Latif A, Bolli R, Tleyjeh IM, Montori VM, Perin EC, Hornung CA, Zuba-Surma EK, Al-Mallah M, Dawn B. Adult bone marrow-derived cells for cardiac repair: A systematic review and meta-analysis. *Arch Intern Med*. 2007;167:989-997

4. Seeger FH, Tonn T, Krzossok N, Zeiher AM, Dimmeler S. Cell isolation procedures matter: A comparison of different isolation protocols of bone marrow mononuclear cells used for cell therapy in patients with acute myocardial infarction. *Eur Heart J*. 2007;28:766-772

5. Zhang Y, Sievers RE, Prasad M, Mirsky R, Shih H, Wong ML, Angeli FS, Ye J, Takagawa J, Koskenvuo JW, Springer ML, Grossman W, Boyle AJ, Yeghiazarians Y. Timing of bone marrow cell therapy is more important than repeated injections after myocardial infarction. *Cardiovasc Pathol*.20:204-212

6. Penn MS, Ellis S, Gandhi S, Greenbaum A, Hodes Z, Mendelsohn FO, Strasser D, Ting AE, Sherman W. Adventitial delivery of an allogeneic bone marrow-derived adherent stem cell in acute myocardial infarction: Phase i clinical study. *Circ Res*.110:304-311

7. Dai SJ, Yuan FP, Mu JY, Li CX, Chen N, Guo SZ, Kingery J, Prabhu SD, Bolli R, Rokosh G. Chronic amd3100 antagonism of sdf-1 alpha-cxcr4 exacerbates cardiac dysfunction and remodeling after myocardial infarction. *J Mol Cell Cardiol*. 2010;49:587-597

8. Wojakowski W, Michalowska A, Majka M, Kucia M, Maslankievvicz K, Wyderka R, Ochala A, Ratajczak MZ, Tendera M. The mobilization of tissue-committed (cd34(+), cd117(+), cxcr4(+), c-met(+)) stem cells expressing early cardiac, muscle, and endothelial markers into peripheral blood in acute myocardial infarction: Regent study. *Circulation*. 2004;110:238-239

9. Askari AT, Unzek S, Popovic ZB, Goldman CK, Forudi F, Kiedrowski M, Rovner A, Ellis SG, Thomas JD, DiCorleto PE, Topol EJ, Penn MS. Effect of stromal-cell-derived factor 1 on stem-cell homing and tissue regeneration in ischaemic cardiomyopathy. *Lancet*. 2003;362:697-703

10. Zhang G, Nakamura Y, Wang XH, Hu QS, Suggs LJ, Zhang JY. Controlled release of stromal cell-derived factor-1alpha in situ increases c-kit(+) cell homing to the infarcted heart. *Tissue Eng*. 2007;13:2063-2071

11. Segers VF, Tokunou T, Higgins LJ, MacGillivray C, Gannon J, Lee RT. Local delivery of protease-resistant stromal cell derived factor-1 for stem cell recruitment after myocardial infarction. *Circulation*. 2007;116:1683-1692

12. Kuschert GSV, Coulin F, Power CA, Proudfoot AEI, Hubbard RE, Hoogewerf AJ, Wells TNC. Glycosaminoglycans interact selectively with chemokines and modulate receptor binding and cellular responses. *Biochemistry*. 1999;38:12959-12968

13. Amara A, Lorthioir O, Valenzuela A, Magerus A, Thelen M, Montes M, Virelizier JL, Delepierre M, Baleux F, Lortat-Jacob H, Arenzana-Seisdedos F. Stromal cell-derived factor-1 alpha associates with heparan sulfates through the first beta-strand of the chemokine. *J Biol Chem*. 1999;274:23916-23925

14. Ceradini DJ, Kulkarni AR, Callaghan MJ, Tepper OM, Bastidas N, Kleinman ME, Capla JM, Galiano RD, Levine JP, Gurtner GC. Progenitor cell trafficking is regulated by hypoxic gradients through hif-1 induction of sdf-1. *Nat Med*. 2004;10:858-864

15. Sadir R, Imberty A, Baleux F, Lortat-Jacob H. Heparan sulfate/heparin oligosaccharides protect stromal cell-derived factor-1 (sdf-1)/cxcl12 against proteolysis induced by

cd26/dipeptidyl peptidase iv. *J Biol Chem*. 2004;279:43854-43860

16. Fraser JR, Laurent TC, Laurent UB. Hyaluronan: Its nature, distribution, functions and turnover. *J Intern Med*. 1997;242:27-33

17. Avigdor A, Goichberg P, Shivtiel S, Dar A, Peled A, Samira S, Kollet O, Hershkoviz R, Alon R, Hardan I, Ben-Hur H, Naor D, Nagler A, Lapidot T. Cd44 and hyaluronic acid cooperate with sdf-1 in the trafficking of human cd34(+) stem/progenitor cells to bone marrow. *Blood*. 2004;103:2981-2989

18. Baker NA, Sept D, Joseph S, Holst MJ, McCammon JA. Electrostatics of nanosystems: Application to microtubules and the ribosome. *Proc Natl Acad Sci U S A*. 2001;98:10037-10041

19. Veldkamp CT, Ziarek JJ, Su JD, Basnet H, Lennertz R, Weiner JJ, Peterson FC, Baker JE, Volkman BF. Monomeric structure of the cardioprotective chemokine sdf-1/cxcl12. *Protein Sci* 2009;18:1359-1369

20. Dolinsky TJ, Nielsen JE, McCammon JA, Baker NA. Pdb2pqr: An automated pipeline for the setup of poisson-boltzmann electrostatics calculations. *Nucleic Acids Res*. 2004;32:W665-W667

21. Li H, Robertson AD, Jensen JH. Very fast empirical prediction and rationalization of protein pk(a) values. *Proteins*. 2005;61:704-721

22. Jmol: An open-source java viewer for chemical structures in 3d. Http://www.Jmol.Org/

23. Nomanbhoy TK, Cerione RA. Characterization of the interaction between rhogdi and cdc42hs using fluorescence spectroscopy. *J Biol Chem*. 1996;271:10004-10009

24. Pathak CP, Sawhney AS, Hubbell JA. Rapid photopolymerization of immunoprotective gels in contact with cells and tissue. *J Am Chem Soc*. 1992;114:8311-8312

25. Bitter TM, H. M. . A modified uronic acid carbazole reaction. *Anal Biochem*. 1962;4:330-334

26. Goncharova EA, Goncharov DA, Krymskaya VP. Assays for in vitro monitoring of human airway smooth muscle (asm) and human pulmonary arterial vascular smooth muscle (vsm) cell migration. *Nat Protoc*. 2006;1:2933-2939

27. van Amerongen MJ, Hamsen MC, Petersen AH, Popa ER, van Luyn MJA. Cryoinjury: A model of myocardial regeneration. *Cardiovasc Pathol*. 2008;17:23-31

28. Elser JA, Purcell BP, Allana IA, Burdick JA, Margulies KB. Ischemia induces p-selectin-mediated selective progenitor cell engraftment in the isolated-perfused heart. *J Mol Cell Cardiol*.52:105-112

29. Tous E, Ifkovits JL, Koomalsingh KJ, Shuto T, Soeda T, Kondo N, Gorman JH, Gorman RC, Burdick JA. Influence of injectable hyaluronic acid hydrogel degradation behavior on infarction-induced ventricular remodeling. *Biomacromolecules*. 2011;12:4127-4135

30. Kusumbe AP, Bapat SA. Cancer stem cells and aneuploid populations within developing tumors are the major determinants of tumor dormancy. *Cancer Res*. 2009;69:9245-9253

31. Murphy JW, Cho Y, Sachpatzidis A, Fan CP, Hodsdon ME, Lolis E. Structural and functional basis of cxcl12 (strornal cell-derived factor-1 alpha) binding to heparin. *J Biol Chem*. 2007;282:10018-10027

32. Tsuda M, Makino Y, Iwahara T, Nishihara H, Sawa H, Nagashima K, Hanafusa H, Tanaka S. Crk associates with erm proteins and promotes cell motility toward hyaluronic acid. *J Biol Chem*. 2004;279:46843-46850

33. Nandi A, Estess P, Siegelman M. Bimolecular complex between rolling and firm adhesion receptors required for cell arrest; cd44 association with vla-4 in t cell extravasation. *Immunity*. 2004;20:455-465

34. Mohamadzadeh M, DeGrendele H, Arizpe H, Estess P, Siegelman M. Proinflammatory stimuli regulate endothelial hyaluronan expression and cd44/ha-dependent primary adhesion. *J Clin Invest*. 1998;101:97-108

35. Herrera MB, Bussolati B, Bruno S, Morando L, Mauriello-Romanazzi G, Sanavio F, Stamenkovic I, Biancone L, Camussi G. Exogenous mesenchymal stem cells localize to the kidney by means of cd44 following acute tubular injury. *Kidney Int*. 2007;72:430-441

36. Kuraitis D, Zhang PC, McEwan K, Zhang J, Mckee D, Sofrenovic T, Griffith M, Cao XD, Ruel M, Suuronen EJ. Controlled release of stromal cell-derived factor-1 for enhanced

progenitor response in ischemia. *J Control Release*. 2011;152:E216-E218

37. Peled A, Petit I, Kollet O, Magid M, Ponomaryov T, Byk T, Nagler A, Ben-Hur H, Many A, Shultz L, Lider O, Alon R, Zipori D, Lapidot T. Dependence of human stem cell engraftment and repopulation of nod/scid mice on cxcr4. *Science*. 1999;283:845-848

38. Swirski FK, Nahrendorf M, Etzrodt M, Wildgruber M, Cortez-Retamozo V, Panizzi P, Figueiredo JL, Kohler RH, Chudnovskiy A, Waterman P, Aikawa E, Mempel TR, Libby P, Weissleder R, Pittet MJ. Identification of splenic reservoir monocytes and their deployment to inflammatory sites. *Science*. 2009;325:612-616

39. Misao Y, Takemura G, Arai M, Ohno T, Onogi H, Takahashi T, Minatoguchi S, Fujiwara T, Fujiwara H. Importance of recruitment of bone marrow-derived cxcr4+ cells in post-infarct cardiac repair mediated by g-csf. *Cardiovasc Res*. 2006;71:455-465

40. Honczarenko M, Le Y, Swierkowski M, Ghiran I, Glodek AM, Silberstein LE. Human bone marrow stromal cells express a distinct set of biologically functional chemokine receptors. *Stem Cells*. 2006;24:1030-1041

41. Mohle R, Bautz F, Rafii S, Moore MAS, Brugger W, Kanz L. The chemokine receptor cxcr-4 is expressed on cd34(+) hematopoietic progenitors and leukemic cells and mediates transendothelial migration induced by stromal cell-derived factor-1. *Blood*. 1998;91:4523-4530

42. Wynn RF, Hart CA, Corradi-Perini C, O'Neill L, Evans CA, Wraith JE, Fairbairn LJ, Bellantuono I. A small proportion of mesenchymal stem cells strongly expresses functionally active cxcr4 receptor capable of promoting migration to bone marrow. *Blood*. 2004;104:2643-2645

43. Anzai A, Anzai T, Nagai S, Maekawa Y, Naito K, Kaneko H, Sugano Y, Takahashi T, Abe H, Mochizuki S, Sano M, Yoshikawa T, Okada Y, Koyasu S, Ogawa S, Fukuda K. Regulatory role of dendritic cells in postinfarction healing and left ventricular remodeling. *Circulation*.125:1234-1245

44. Hofmann U, Beyersdorf N, Weirather J, Podolskaya A, Bauersachs J, Ertl G, Kerkau T, Frantz S. Activation of cd4+ t lymphocytes improves wound healing and survival after experimental myocardial infarction in mice. *Circulation*. 2012;125:1652-1663

45. Kucia M, Dawn B, Hunt G, Guo Y, Wysoczynski M, Majka M, Ratajczak J, Rezzoug F, Ildstad ST, Bolli R, Ratajczak MZ. Cells expressing early cardiac markers reside in the bone marrow and are mobilized into the peripheral blood after myocardial infarction. *Circ Res*. 2004;95:1191-1199

46. Abbott JD, Huang Y, Liu D, Hickey R, Krause DS, Giordano FJ. Stromal cell-derived factor-1alpha plays a critical role in stem cell recruitment to the heart after myocardial infarction but is not sufficient to induce homing in the absence of injury. *Circulation*. 2004;110:3300-3305

47. Jiang D, Liang J, Noble PW. Hyaluronan in tissue injury and repair. *Annu Rev Cell Dev Bi*. 2007;23:435-461

48. Huebener P, Abou-Khamis T, Zymek P, Bujak M, Ying X, Chatila K, Haudek S, Thakker G, Frangogiannis NG. Cd44 is critically involved in infarct healing by regulating the inflammatory and fibrotic response. *J Immunol*. 2008;180:2625-2633

CHAPTER 5

Sustained release of SDF-1α polypeptide analogue from injectable hyaluronic acid hydrogels attenuates post MI remodeling

(Adapted from: J.W. MacArthur Jr., B.P. Purcell, P.F. Hsiao, A.S. Fairman, E.C. Yang, A. Trubelja, W. Hiesinger, Y. Shudo, P. Atluri, J.A. Burdick, J.Y. Woo, *Circulation*, in press)

5.1. Introduction

Heart disease is the cause of significant morbidity and mortality in the US with estimates of nearly 800,000 new acute coronary events each year, a disease accounting for a substantial proportion of the national health care expenditure[1, 2]. On a cellular level, the events following a myocardial infarction include a change in composition of the extracellular matrix with a shift towards collagen deposition, hypocontractile scar formation, myocyte apoptosis, and progressive ventricular dilatation[3]. The deleterious remodeling that occurs over time leads to augmentation in the stress-strain relationship of ventricular myocytes, inefficient contractility, and ultimately heart failure. When current treatments for coronary artery disease fail, they usually do so because microvascular perfusion is not adequately restored – a critical, independent predictor of ventricular remodeling, reinfarction, heart failure, and death[4].

In an effort to restore microvascular perfusion, various cytokines have been used to stimulate angiogenesis, with moderate success. One such cytokine, stromal cell-derived factor 1-alpha (SDF-1), is a key regulator in hematopoietic stem cell trafficking between the bone marrow and peripheral circulation and effectively localizes endothelial progenitor cells to areas of ischemia[5, 6]. It has been shown by our group and others to increase vasculogenesis, decrease cardiac myocyte apoptosis, increase cardiac myocyte survival, and preserve ventricular geometry[7-10]. The functional and regenerative benefits of SDF-1 treatment are directly related to its ability to bind its receptor,

CXCR4. However, there is a temporal mismatch between peak expression of SDF-1 and upregulation of CXCR4 on bone marrow and cardiac stem cells. Within an hour of ischemia, cardiac SDF-1 expression is rapidly upregulated in the heart, while CXCR4 peaks at 96 hours, by which time SDF-1 is nearly absent[5, 11, 12]. Contributing to this mismatch is that SDF-1 is rapidly cleared from the circulation and cleaved by matrix metalloproteinase-2 and CD-26[13-16].

In order to address the temporal mismatch in the SDF-1:CXCR4 axis, SDF-1 concentration within cardiac tissue must be maintained over the course of several weeks to prolong its trophic effects on CXCR4+ cells, thereby optimizing angiogenesis, cardiac myocyte preservation, and ventricular performance. In the current study, we hypothesized that a hyaluronic acid based hydrogel could sustain the release of our previously reported engineered SDF-1 analog (ESA) over several weeks, resulting in the temporal realignment of the SDF:CXCR4 axis and consequently improved angiogenesis, limited ventricular remodeling, and preserved cardiac function in a rat model of myocardial infarction.

5.2. Methods

Custom Peptide Synthesis

We have previously reported on the design and synthesis of an engineered SDF-1α peptide analogue (ESA)[17, 18]. Briefly, the CXCR4 receptor binding N-terminus and the molecular stabilizing C-terminus were preserved while the central beta pleated sheet was deleted and replaced with 2 proline "linker" residues. Using mathematical modeling, this modified sequence was predicted to retain as similar a three-dimensional protein configuration to the native SDF-1α as possible. The designed protein was synthesized using solid phase peptide synthesis, where the N α-amino acids are incorporated into the peptide in a step-wise fashion while one end is attached to a solid support matrix. Additionally, we added HiLyte Fluor TR (AnaSpec, San Jose, California) during the synthesis process as a fluorophore tag for use in the in vitro studies, and HiLytefluor 750 (AnaSpec, San Jose, California) was added for the in vivo study.

Macromer Synthesis

Sodium hyaluronate (74kDa, Lifecore) was chemically modified with h

ydroxyethyl methacrylate (HEMA) to incorporate a terminal methacrylate group for free-radical initiated crosslinking and ester bonds to introduce hydrolytic degradation[19]. Briefly, HEMA was reacted with succinic anhydride via a ring opening polymerization in the presence of N-methylimidazole to obtain HEMA-COOH, which was then coupled to a tetrabutylammonium salt of HA in the presence of 4-dimethylaminopyridine. The resulting HA macromer with HEMA group modification (HEMA-HA) was purified via dialysis, lyophilized, and the percentage of HA disaccharides modified with a HEMA group was determined to be ~15% using ^{1}H NMR.

Hydrogel Crosslinking

To form hydrogels rapidly upon injection into the myocardium, a two-component redox initiator system consisting of ammonium persulfate (APS) and N,N,N′,N′-tetramethylethylenediamine (TEMED) was utilized. APS and TEMED were added to a final concentration of 10mM in a 4% (w/v) HEMA-HA solution and kept on ice. The kinetics of gel formation were characterized with rheometry at 37°C by monitoring the storage (G') and loss (G") modulus with time, while applying oscillatory strain (20mm 1° cone geometry, 1% strain, 1Hz, Texas Instruments AR 2000ex). For in vitro release kinetics, 25µg ESA was added per 50µL gel precursor solution, and 50uL gels were formed in cylindrical molds for 30 min at 37°C. Gels were incubated in 1mL PBS supplemented with 1% BSA at 37°C and buffers were refreshed every 2 days. Fluorescence of eluted ESA from each 2 day sample, extending over a 4 week period, was quantified on a microplate reader (TECAN, Austria), while HA content was quantified with a uronic acid assay[20]. After 28 days, hydrogels were enzymatically degraded with hyaluronidase (800 units/mL, Sigma) and evaluated for remaining ESA and HA.

Endothelial Progenitor Cell Chemotaxis

Bone marrow mononuclear cells were isolated from the long bones of syngeneic adult male Wistar rats (Charles River) by density centrifugation with Histopaque 1083 (Sigma-Aldrich), plated on vitronectin coated dishes, and cultured in endothelial basal medium-2 supplemented with EGM-2 SingleQuot (Lonza) containing human epidermal growth factor, FBS, vascular endothelial growth factor, basic human fibroblast growth factor, recombinant human long R3 insulin-like growth factor-1, ascorbic acid, heparin, gentamicin, and amphotericin-B. Media was changed on culture day 4 and non-adherent bone marrow mononuclear cells were discarded, enriching for the EPC phenotype.

A modified transwell migration assay (Neuro Probe, Gaithersburg, MD) was used to assess EPC migration. Briefly, 8-µm filters were loaded into control and experimental chambers. Seven-day EPCs cultured in endothelial-specific media on vitronectin-coated plates were trypsinized, counted, and brought to a concentration of 90 cells/µl in Dulbecco's phosphate buffered saline (DPBS). The bottom chamber was loaded with either DPBS or the eluted ESA from the hydrogel at each respective 2 day time point. DPBS from hydrogel without ESA served as a control. A 560µl cell suspension was added to the top chamber of each. All chambers were incubated at 37ºC, 5% CO_2 for 3.5 hours. The cells remaining in the top chamber were wiped clean with a cotton swab and the filter was removed, placed on a glass slide, and mounted with Vectashield w/ DAPI (Vector Laboratories). Slides were visualized on a DF5000B Leica fluorescent microscope and analyzed via LASAF version 2.0.2 (Leica) software. Boyden chamber analyses were performed in triplicate.

Animal Care and Biosafety

Male Wistar rats weighing 250-300g were obtained from Charles River Labs (Wilmington, Massachusetts). Food and water were provided ad lib. All experiments pertaining to this investigation conformed to the "Guide for the Care and Use of Laboratory Animals," published by the US National Institutes of

Health (Eighth Edition, 2011). The protocol was approved by the Institutional Animal Use and Care Committee of the University of Pennsylvania (protocol number 803394).

Animal Model

Myocardial infarction was induced in 33 male Wistar rats using an established and highly reproducible model. Briefly, the rats were anesthetized in a 2L induction chamber (VetEquip, Pleasantville, CA) and 3% isofluorane was continuously delivered. A 16-gauge angiocatheter was used for endotracheal intubation and connected to mechanical ventilation (Hallowedl EMC, Pittsfield Mass) where 1% isofluorane was maintained throughout the operation. A thoracotomy was performed through the left 4th intercostal space, the heart was exposed, and a 7-0 polypropylene suture was placed around the left anterior descending artery 2mm below the left atrium. The suture was briefly snared to verify the size and location of myocardial ischemia based on color change, and permanently tied down to produce a large anterolateral MI[8-10, 17, 18]. The animals were then randomized into 3 groups and received 4 separate peri-infarct intramyocardial injections of either saline (100μl, n=8) hydrogel alone (100μl, n=10), or hydrogel/25μg ESA (100μl, n=9). The thoracotomy was closed in multiple layers and tissue adhesive (VetBond, 3M, Minneapolis, MN) was applied over the incision. All rats were implanted with subcutaneous microchips (BioMedic Data Systems, Boise, ID), and recovered from anesthesia. Buprenorphine (0.5mg/kg) was administered for post-operative pain control.

Echocardiographic and Hemodynamic Assessment

LV geometry and function were evaluated pre-operatively and at 4 weeks in all animals[21]. A Phillips Sonos 5500 revD ultrasound system (Philips Medical Systems, Amsterdam ND) was used, utilizing a 12-MHz transducer at an image depth of 2cm. Left ventricular parasternal short axis 2D and M-mode images at the level of the papillary muscle were used to obtain echocardiographic data. All

analyses were performed by a single investigator who was blinded to the treatment groups.

Four weeks after LAD ligation, all three groups of animals underwent invasive hemodynamic measurements with a pressure-volume (P-V) conductance catheter (SPR-869; Millar Instruments, Inc.). The catheter was calibrated via 5 point cuvette linear interpolation with parallel conductance subtraction by the hypertonic saline method. Rats were anesthetized as above, and the catheter was introduced into the LV utilizing a closed-chest approach via the right carotid artery. Measurements were obtained before and during inferior vena cava occlusion to produce static and dynamic P-V loops under varying load conditions. Data were recorded and analyzed with LabChart version 6 software (AD instruments) and ARIA Pressure Volume Analysis software (Millar Instruments, Inc). Finally, cardiac output was assessed by placing a 2.5mm peri-aortic Doppler flow probe (Transonic Systems, Ithaca, NY) around the ascending aorta.

In-vivo ESA release

In a subset of 6 animals from the hydrogel/ESA group, in vivo fluorescence of ESA was quantified using a Pearl Impulse small animal imaging system (LI-COR) on post injection day 1, and every 4 days thereafter through the 4 week time point in order to visualize intramyocardial ESA. Animals were anesthetized with 1% isoflurane via nose cone, the left chest was shaved, and the animals were placed in the right lateral decubitus position on the imaging platform with the left chest closest to the camera. Dynamic images were obtained using the 800nm channel of the instrument (785/820nm excitation/emission), with standardized parameter settings scaled to the same maximum values. Estimates of the fluorescence of ESA were determined by fixed regions of interest (ROI) over the heart, and signal intensity was calculated using the manufacturer's software. Signal intensity for each time point was normalized to the peak signal observed for each animal, and the ratio for each

time point was averaged for all 6 animals. Animals from the saline group (n=3) served as negative controls.

Histologic Analysis and Immunohistochemistry

In order to assess ventricular geometry, infarct size, and microvascular angiogenesis, hearts were explanted in a subset of 11 animals after the invasive hemodynamic assessment was performed (saline, n=3; hydrogel, n=4; hydrogel/ESA, n=4) and flushed with PBS, then injected retrograde with Tissue Tek OCT compound (Sekura, Netherlands) through the aorta and pulmonary artery. Hearts were submerged in OCT, frozen, and stored in a -80ºC freezer. Orientation of hearts during freezing was standardized so as to result in consistent positioning during the sectioning process. Eight, 10µm thick sections were prepared from each heart at the level of the papillary muscles and stained with hematoxylin and eosin or Masson's Trichrome. Standardized digital photographs were taken with a Nikon D5100 SLR camera (Nikon, Tokyo, Japan). Photographs were uploaded to ImageJ (v1.46b) and the size of the infarct assessed with digital planimetry.

Two, 10µm thick sections from each animal were co-stained with antibodies directed against von Willebrand Factor (vWF) in order to quantify capillary density. Sections were fixed with HistoChoice (Amresco, Solon, OH), blocked in 10% FBS, and incubated with sheep anti-VWF (conjugated to FITC, 1:100 dilution, Abcam) for 2 hours. Slides were washed and mounted with Vectashield (Vector Laboratories). Quantitative analysis of capillary density within the borderzone was conducted under the 20x objective of a Zeiss LSM 710 confocal microscope (Zeiss, Germany). Group blinded counts were averaged over 4 fields per specimen. Sections were also stained with antibodies directed towards CXCR4. Sections were fixed with ice cold acetone, blocked in 10% FBS, and incubated with goat anti-CXCR4 (Abcam 1671, 1:300) for 2 hours. Donkey anti-goat antibody-FITC (Abcam 7121, 1:1000) was used as a secondary reagent, and sections were counterstained with DAPI to visualize nuclei.

Immunofluorescent images were acquired and analyzed as above.

Statistical Analysis

Continuous variables were reported as means ± standard deviation. The Student's t-test was used to compare continuous variables. Statistical significance was set at $p < 0.05$. Analyses were preformed with STATA (StataCorp, College Station, TX) statistical software package, version 12.1.

5.3. Results

Hydrogel Formation

HEMA-HA gels formed rapidly through the mixing of two solutions that each contain components of the APS/TEMED free-radical initiator system (Figure 5.1). Gelation occurred within 1 minute and the crosslinking reaction reached a plateau within 30 minutes. By using this crosslinking route, we are able to inject the liquid precursor solution through a syringe and form solid gels under physiologic conditions.
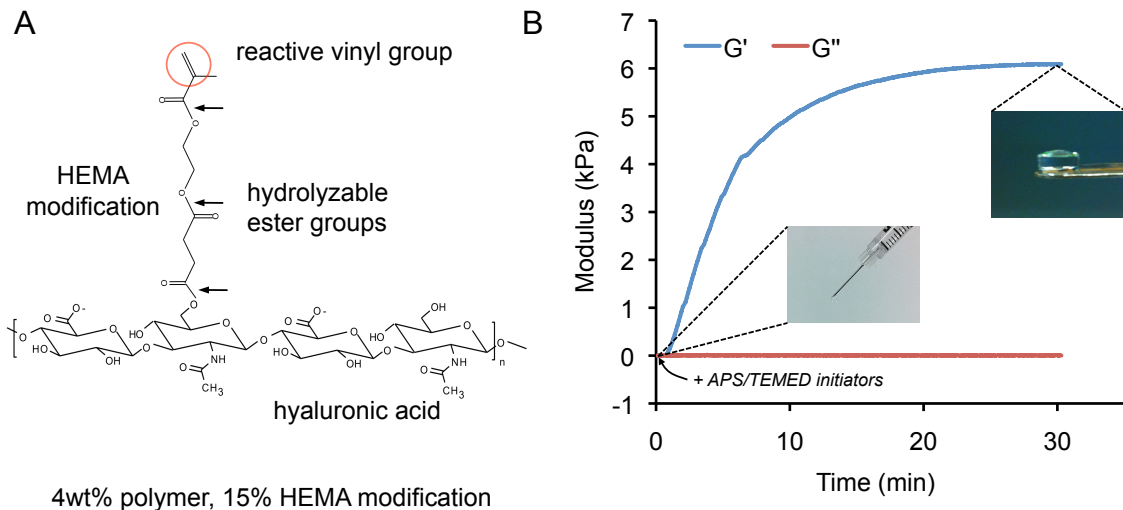
Figure 5.1. Hydrogel formation. (A) HEMA modified HA macromers synthesized with terminal vinyl double bonds for free-radical initiated crosslinking into gels and ester groups to introduce hydrolytic degradation of the gels. (B) Monitoring storage (G', elastic component) and loss (G'', viscous component) moduli over time with rheometry shows that solid gels form from an injectable liquid solution within minutes upon addition of APS/TEMED initiators.

Hydrogel Degradation and ESA Release Kinetics

ESA release was sustained for over 28 days in vitro when encapsulated in degradable HEMA-HA hydrogels (Figure 5.2 A). An initial burst release of ESA was observed during the first few days due to ESA that was not encapsulated during gel formation or encapsulated in the periphery of the gels. Similarly, an initial burst release of HA was observed due to HEMA-HA polymers that were not incorporated into the gels during the crosslinking reaction. After this initial period, ESA release was steady for approximately 20 days while the gels remained intact. The retention of ESA within the hydrogels was surprising considering the small size of ESA (~4kDa). Upon closer examination, microscale ESA aggregates were observed within the gel (purple due to the fluorescent tag) which would account for the reduced diffusion of the peptide within the hydrated gel (Figure 5.2 C). As the gels began to hydrolyze and HA was released, the rate of ESA release increased due to less restricted diffusion of the particles within the gels (Figure 5.2 D).

Hydrogel Release of ESA Remains Functional

Using a transwell migration assay, EPCs showed significant chemotaxis towards ESA released from the gels, indicating that the peptide remains active after gel encapsulation and release (Figure 5.2 B). Importantly, the ESA remained active throughout the entire 28 day in vitro study. Significant increases in EPC chemotaxis were also observed in samples from the hydrogel alone when compared to PBS, which is attributed to the HA degradation products being released from the material.
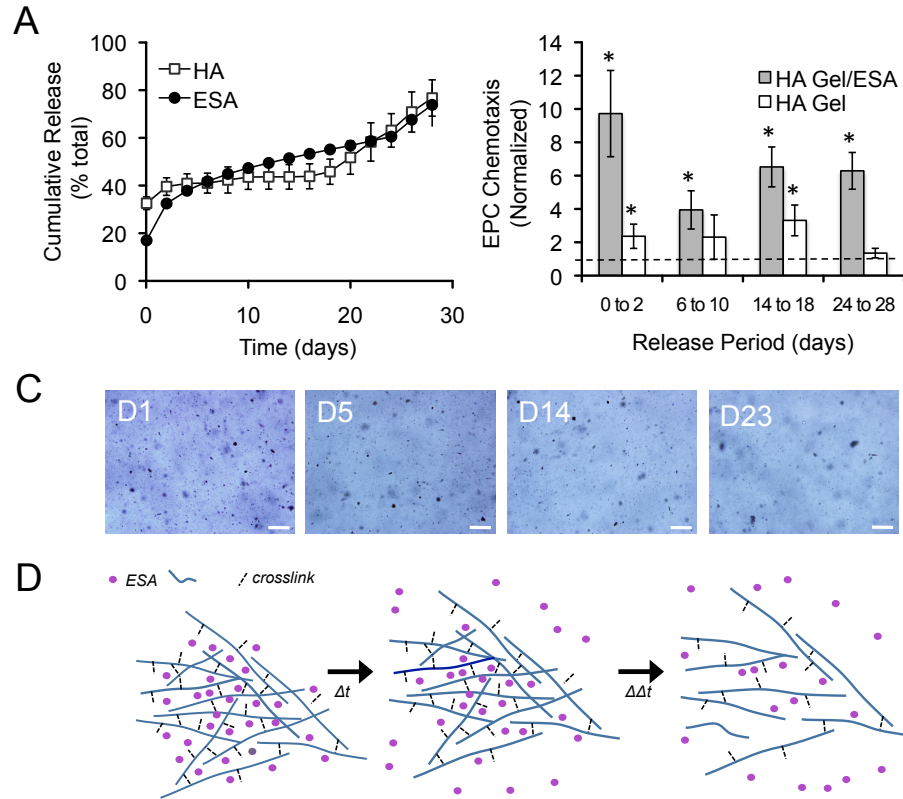
Figure 5.2. Molecule release from hydrogels. (A) ESA release from the gels was sustained for 28 days in vitro and correlated with gel stability (n=3 gels, mean±SD). (B) Released ESA and HA stimulated EPC chemotaxis throughout the 28 day study (n=5-6 wells/condition, mean±SD, *p<0.05 compared to saline control. Dotted line represents saline control). (C) Representative bright field images of ESA aggregates (purple due to fluorescent tag) encapsulated in the hydrogel at Days 1, 5, 14, and 23 (scale bar = 200 µm). (D) Schematic of diffusion controlled release of encapsulated ESA from degradable HA gels.

Tracking ESA within the Heart post MI

By utilizing ESA that had been conjugated with a near IR wavelength fluorophore (i.e., HiLyte Fluor 750, 753/778nm excitation/emission), we were able to image ESA in the heart to quantify the dynamics of ESA release from hydrogels. Rats treated with the fluorescently tagged ESA encapsulated in hydrogels manifested a strong fluorescent signal for the first 10 days, followed by a steady decline in signal until a plateau at day 24, when there was no difference in signal compared to the saline control group (Figure 5.3). The quantitative data for ESA localized to the heart is shown in Figure 5.3 and demonstrates that ESA is released over a 24 day time period in-vivo.
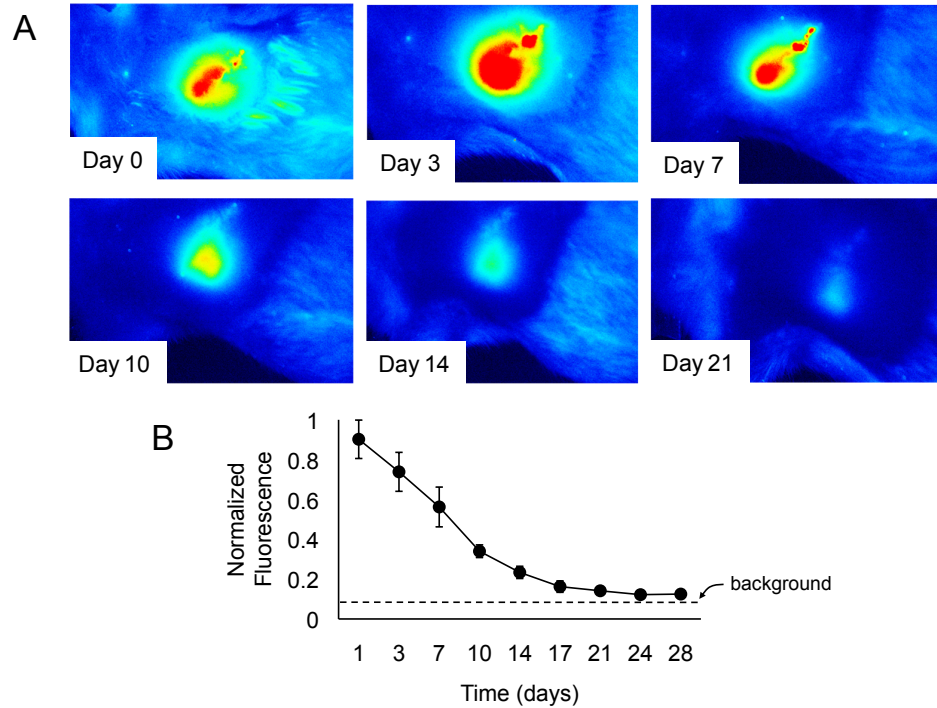
Figure 5.3. *In vivo* **ESA tracking.** After undergoing LAD ligation and injection with hydrogel/ESA, animals underwent *in vivo* imaging to visualize ESA fluorescence. Animals receiving saline injections served as a negative control. (A) Representative images of hydrogel/ESA injection group. (B) Quantitative analysis of fluorescent images showed a fluorescent ESA signal in the heart out to day 24, after which fluorescence was not different than background (dotted line denotes fluorescence of saline control) (Saline n=3; hydrogel/ESA, n=6; mean±SD).

Hydrogel + ESA Improves Hemodynamics post-MI

Echocardiographic assessment of cardiac structure and function revealed significant benefits with hydrogel injection and ESA delivery (Figure 5.4 A-B). At 4 weeks post MI, LV inner diameter at end diastole (LVIDd) was reduced in the hydrogel groups compared to the saline control group; however, there was no statistical difference between hydrogel and hydrogel/ESA groups (Figure 5.4 A). LV ejection fraction was preserved and significantly greater in the hydrogel/ESA group compared to the saline and hydrogel alone groups (Figure 5.4 B). Additionally, hemodynamic assessment of LV function revealed significant improvements with hydrogel injection and ESA delivery (Figure 5.4 C-D). Cardiac output was significantly greater in the hydrogel/ESA group compared to

82

saline and hydrogel alone groups (Figure 5.4 C). In addition, there was a significant increase in the LV end systolic pressure-volume relationship (ESPVR) in the hydrogel/ESA group compared to the saline and hydrogel alone groups (Figure 5.4 D).
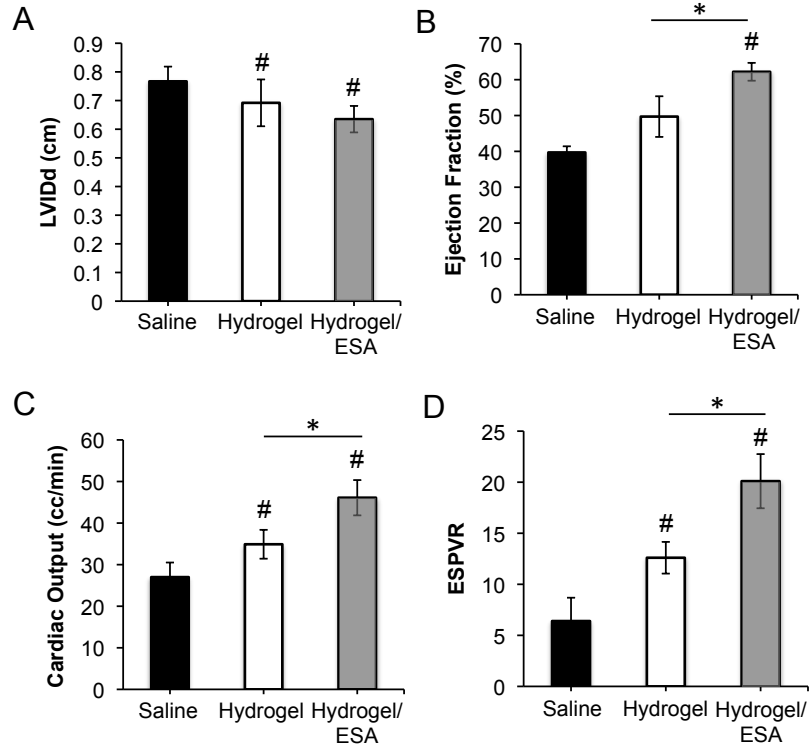
Figure 5.4. LV functional assessment. LV function was quantified using echocardiography (A-B) and hemodynamic analysis (C-D) 28 days following experimental MI and injections in rats. (A) Injection of hydrogels significantly reduced LV dilation as indicated by LV internal diameter and diastole (LVIDd). (B) A significant improvement in LV ejection fraction was observed with hydrogel delivery of ESA. (C) Significant improvements in cardiac output were observed with hydrogel injections, and further improvement was observed with encapsulation of ESA. (D) Significant improvements in LV end systolic pressure-volume relationship (ESPVR) were observed with gels injection, and further improvement was observed with encapsulation of ESA. (Saline, n=8; HA Gel, n=10; HA Gel/ESA, n=9; mean±SD; #p<0.025 versus control, *p<0.025 between groups, student's t-test with Bonferonni correction).

Hydrogel + ESA Results in Preservation of Ventricular Geometry, Smaller Infarcts, Greater Borderzone Capillary Density, and Upregulation of CXCR4+ Cells

Histologic analyses showed smaller LV areas in the hydrogel/ESA group when compared to saline control, but was statistically similar to the hydrogel

alone group, while the infarct fraction of theLV was significantly smaller in the hydrogel/ESA group compared to controls. Representative images are shown in Figure 5.5. Analysis of immunofluorescently labeled vWF showed a significant increase in capillary density in the hydrogel/ESA group and hydrogel alone group when compared to the saline group (Figure 5.6 A). Additionally, there were significantly more CXCR4+ cells in the hydrogel /ESA group compared to hydrogel and saline groups (Figure 5.6 B).
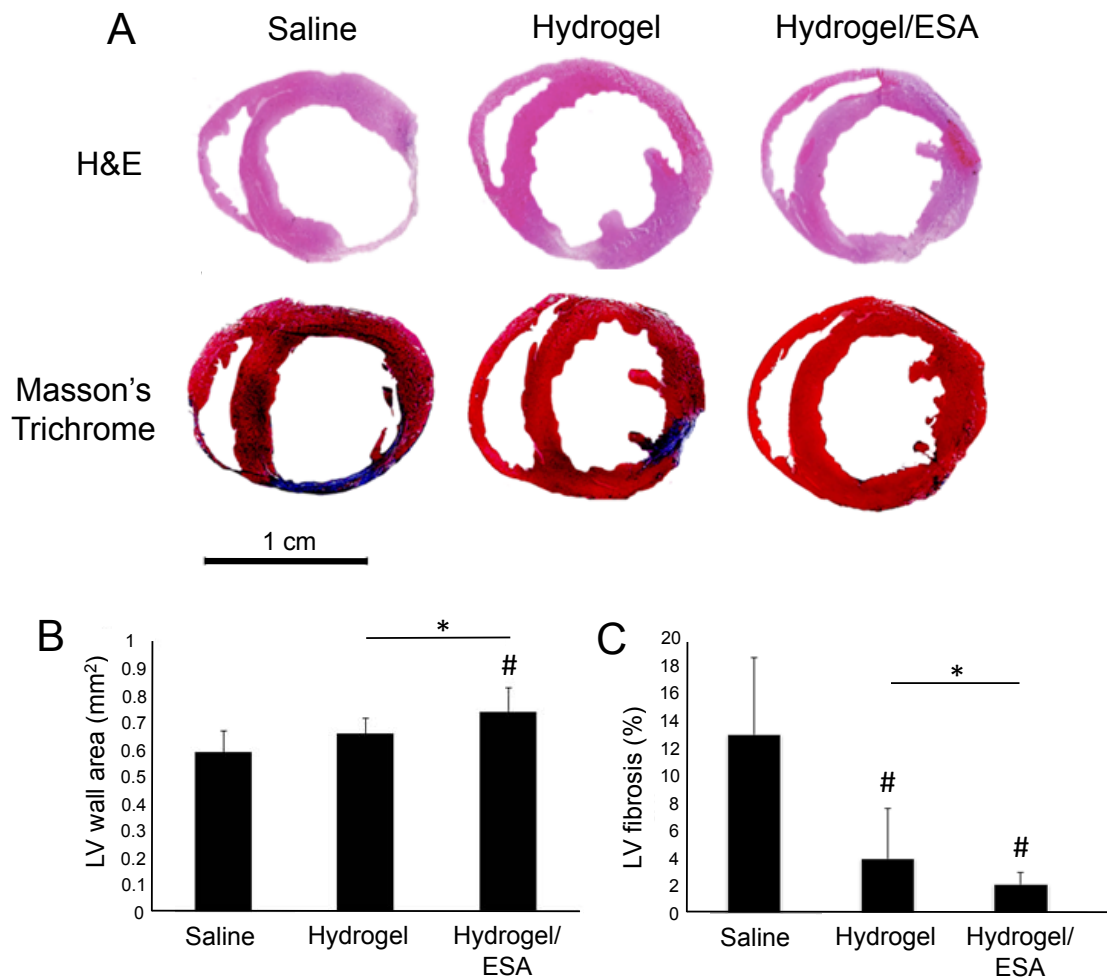
Figure 5.5. Histologic assessment of LV geometry and structure. (A) Representative sections from rat hearts 28 days post MI after haematoxylin and eosin (H&E) or Masson's Trichrome staining. (B) ESA delivery from injected hydrogels significantly increased LV wall area (C) and reduced fibrosis compared to hydrogel alone and saline control groups (saline, n=3; hydrogel, n=4; hydrogel/ESA, n=4; mean±SD, #p<0.025 versus control, *p<0.025 between groups, student's t-test with Bonferroni correction)
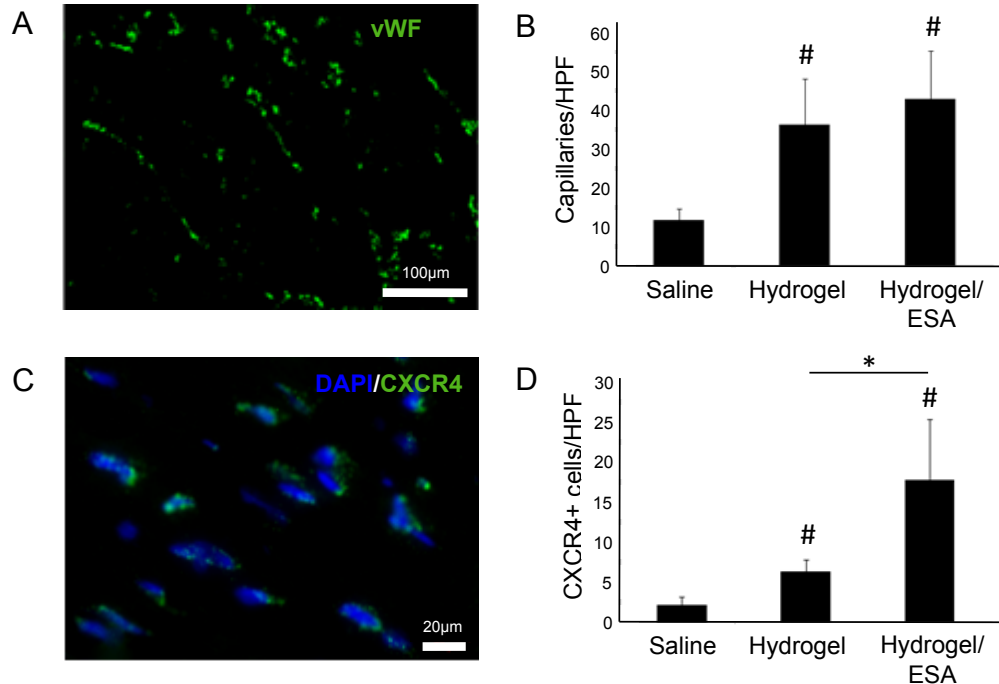
Figure 5.6. Immunohistochemistry of the border zone myocardium 28 days post MI. (A) Representative von Willebrand factor (vWF) staining. (B) Quantitative analysis of vWF expression showed a significant increase in capillary density with hydrogel injections. (C) Representative CXCR4 staining (SDF-1α receptor). (D) Quantitative analysis of CXCR4 showed a significant increase in the number of CXCR4+ cells with hydrogel injection, and a further increase with ESA encapsulation. (mean±SD, #p<0.025 versus control, *p<0.025 between groups, student's t-test with Bonferroni correction)

5.4. Discussion

Over the past five years, investigations into intramyocardial injection of bioengineered, chemically modified materials after MI have showed promising results, causing thicker, stiffer infarcts, limiting infarct expansion and preserving LV geometry[22-26]. Although promising, it may be very useful to improve on these techniques through further biological targets, such as stimulating a robust angiogenic response and localizing progenitor cells to the site of infarction. HA based hydrogels offer an intriguing benefit as they are able to provide both support to the infarcted myocardium during the acute phase and a platform for the delivery of potent chemokines, where release is controlled with diffusion and hydrolytic degradation.

In the present study we utilized a HA based hydrogel to encapsulate an engineered SDF-1 analog (ESA) to sustain release of this polypeptide over 28 days. The hydrogel was chemically engineered to degrade in about 28 days, which was confirmed *in vitro* by a uronic acid assay. We were able to show that functional ESA can be released from the hydrogels over the entire 28 days study, recruiting EPCs in a transwell migration assay across all time points. Interestingly, the hydrogel alone group also stimulated migration of EPCs, albeit to a lesser extent than hydrogel/ESA, a finding that is supported by prior studies and likely due to the interaction of HA with the membrane protein CD44 on EPCs[19, 27, 28].

Our in vivo studies demonstrated that treatment with hydrogel/ESA resulted in smaller infarcts, stimulated angiogenesis at the borderzone, and preserved LV geometry and function. Again, we observed that treatment with hydrogel alone stimulated a moderate amount of angiogenesis at the borderzone and maintained LV geometry, findings which are consistent with previous literature showing that injectable hydrogels can limit infarct expansion by providing structural support to the myocardium, resulting in improved hemodynamic functioning[24, 25]. Lastly, we were able to successfully track ESA in the heart over 24 days using fluorescent imaging, confirming that our hydrogels sustained release of ESA *in vivo* as we originally proposed.

It is noteworthy the degree to which the hydrogel alone group derived structural and functional benefit in this study. Although this is not a new finding, it is interesting that HA hydrogels can limit infarct expansion and preserve ventricular geometry, causing improved hemodynamics. It is likely that these benefits are multifactorial in nature, resulting from the structural properties of the gel itself as well as HA interaction with CD44 on bone marrow progenitor cells. Ultimately, however, we have shown that hydrogel/ESA has a synergistic effect on the heart following MI, resulting in improved structure and function of the myocardium and upregulation of CXCR4+ cells. Despite the similarities in angiogenesis between the hydrogel and hydrogel/ESA groups, improved

hemodynamic function was observed in the hydrogel/ESA group. This is most likely due to the fact that the role of ESA is not merely to attract bone marrow progenitor cells, but also recruit endogenous cardiac progenitor cells to the infarct borderzone. Through its interaction with CXCR4+ cardiomyocytes, ESA may lead to preservation of cardiac cells through reduced apoptosis via CXCR4 pathways, leading to improved hemodynamics. In a very eloquent knockout model, Dong and colleges were able to show that the SDF-1:CXCR4 axis is vitally important for preservation of cardiac function following MI, specifically showing SDF-1 binding to CXCR4+ cardiac cells leads to retention of cardiomyocytes, reduction in infarct size and localization of cardiac stem cells at the borderzone – and all without altering vascular density[29].

One limitation of this study is that it was performed in an acute model of MI, where the treatment was given immediately after coronary artery ligation. Although this satisfies our scientific search for how hydrogel encapsulated ESA interacts with ischemic myocardium, the positive findings reported here may not be generally applied to clinical situations where treatment modalities must be effective in the setting of chronic heart failure. Chronic post-ischemic changes offer a complex problem to the investigator, where deleterious remodeling and a diminutive stem cell supply must be overcome. However, as a proof of principle study and a starting point, we have effectively shown that sustained release of ESA by injectable hydrogels is possible in the heart.

5.5. References

1. Lloyd-Jones D, Adams R, Carnethon M, De Simone G, Ferguson TB, Flegal K, Ford E, Furie K, Go A, Greenlund K, Haase N, Hailpern S, Ho M, Howard V, Kissela B, Kittner S, Lackland D, Lisabeth L, Marelli A, McDermott M, Meigs J, Mozaffarian D, Nichol G, O'Donnell C, Roger V, Rosamond W, Sacco R, Sorlie P, Stafford R, Steinberger J, Thom T, Wasserthiel-Smoller S, Wong N, Wylie-Rosett J, Hong Y, American Heart Association Statistics C, Stroke Statistics S. Heart disease and stroke statistics--2009 update: A report from the american heart association statistics committee and stroke statistics subcommittee. *Circulation*. 2009;119:e21-181

2. Heidenreich PA, Trogdon JG, Khavjou OA, Butler J, Dracup K, Ezekowitz MD, Finkelstein EA, Hong Y, Johnston SC, Khera A, Lloyd-Jones DM, Nelson SA, Nichol G, Orenstein D, Wilson PW, Woo YJ, American Heart Association Advocacy Coordinating C, Stroke C, Council on Cardiovascular R, Intervention, Council on Clinical C, Council on E, Prevention, Council on A, Thrombosis, Vascular B, Council on C, Critical C, Perioperative, Resuscitation, Council on Cardiovascular N, Council on the Kidney in Cardiovascular D, Council on Cardiovascular S, Anesthesia, Interdisciplinary Council on Quality of C, Outcomes R. Forecasting the future of cardiovascular disease in the united states: A policy statement from the american heart association. *Circulation*. 2011;123:933-944

3. Yankey GK, Li T, Kilic A, Cheng G, Satpute A, Savai K, Li S, Moainie SL, Prastein D, DeFillipi C, Wu ZJ, Griffith BP. Regional remodeling strain and its association with myocardial apoptosis after myocardial infarction in an ovine model. *The Journal of thoracic and cardiovascular surgery*. 2008;135:991-998, 998 e991-992

4. Araszkiewicz A, Grajek S, Lesiak M, Prech M, Pyda M, Janus M, Cieslinski A. Effect of impaired myocardial reperfusion on left ventricular remodeling in patients with anterior wall acute myocardial infarction treated with primary coronary intervention. *The American journal of cardiology*. 2006;98:725-728

5. Askari AT, Unzek S, Popovic ZB, Goldman CK, Forudi F, Kiedrowski M, Rovner A, Ellis SG, Thomas JD, DiCorleto PE, Topol EJ, Penn MS. Effect of stromal-cell-derived factor 1 on stem-cell homing and tissue regeneration in ischaemic cardiomyopathy. *Lancet*. 2003;362:697-703

6. Yamaguchi J, Kusano KF, Masuo O, Kawamoto A, Silver M, Murasawa S, Bosch-Marce M, Masuda H, Losordo DW, Isner JM, Asahara T. Stromal cell-derived factor-1 effects on ex vivo expanded endothelial progenitor cell recruitment for ischemic neovascularization. *Circulation*. 2003;107:1322-1328

7. Unzek S, Zhang M, Mal N, Mills WR, Laurita KR, Penn MS. Sdf-1 recruits cardiac stem cell-like cells that depolarize in vivo. *Cell transplantation*. 2007;16:879-886

8. Woo YJ, Grand TJ, Berry MF, Atluri P, Moise MA, Hsu VM, Cohen J, Fisher O, Burdick J, Taylor M, Zentko S, Liao G, Smith M, Kolakowski S, Jayasankar V, Gardner TJ, Sweeney HL. Stromal cell-derived factor and granulocyte-monocyte colony-stimulating factor form a combined neovasculogenic therapy for ischemic cardiomyopathy. *The Journal of thoracic and cardiovascular surgery*. 2005;130:321-329

9. Atluri P, Liao GP, Panlilio CM, Hsu VM, Leskowitz MJ, Morine KJ, Cohen JE, Berry MF, Suarez EE, Murphy DA, Lee WM, Gardner TJ, Sweeney HL, Woo YJ. Neovasculogenic therapy to augment perfusion and preserve viability in ischemic cardiomyopathy. *The Annals of thoracic surgery*. 2006;81:1728-1736

10. Atluri P, Panlilio CM, Liao GP, Hiesinger W, Harris DA, McCormick RC, Cohen JE, Jin T, Feng W, Levit RD, Dong N, Woo YJ. Acute myocardial rescue with endogenous endothelial progenitor cell therapy. *Heart, lung & circulation*. 2010;19:644-654

11. Tang YL, Zhu W, Cheng M, Chen L, Zhang J, Sun T, Kishore R, Phillips MI, Losordo DW, Qin G. Hypoxic preconditioning enhances the benefit of cardiac progenitor cell therapy for treatment of myocardial infarction by inducing cxcr4 expression. *Circulation research*. 2009;104:1209-1216

12. Penn MS. Importance of the sdf-1:Cxcr4 axis in myocardial repair. *Circulation research*. 2009;104:1133-1135

13. De La Luz Sierra M, Yang F, Narazaki M, Salvucci O, Davis D, Yarchoan R, Zhang HH, Fales H, Tosato G. Differential processing of stromal-derived factor-1alpha and stromal-derived factor-1beta explains functional diversity. *Blood*. 2004;103:2452-2459

14. Davis DA, Singer KE, De La Luz Sierra M, Narazaki M, Yang F, Fales HM, Yarchoan R, Tosato G. Identification of carboxypeptidase n as an enzyme responsible for c-terminal cleavage of stromal cell-derived factor-1alpha in the circulation. *Blood*. 2005;105:4561-4568

15. Segers VF, Tokunou T, Higgins LJ, MacGillivray C, Gannon J, Lee RT. Local delivery of protease-resistant stromal cell derived factor-1 for stem cell recruitment after myocardial infarction. *Circulation*. 2007;116:1683-1692

16. Kanki S, Segers VF, Wu W, Kakkar R, Gannon J, Sys SU, Sandrasagra A, Lee RT. Stromal cell-derived factor-1 retention and cardioprotection for ischemic myocardium. *Circulation. Heart failure*. 2011;4:509-518

17. Hiesinger W, Frederick JR, Atluri P, McCormick RC, Marotta N, Muenzer JR, Woo YJ. Spliced stromal cell-derived factor-1alpha analog stimulates endothelial progenitor cell migration and improves cardiac function in a dose-dependent manner after myocardial infarction. *The Journal of thoracic and cardiovascular surgery*. 2010;140:1174-1180

18. Hiesinger W, Perez-Aguilar JM, Atluri P, Marotta NA, Frederick JR, Fitzpatrick JR, 3rd, McCormick RC, Muenzer JR, Yang EC, Levit RD, Yuan LJ, Macarthur JW, Saven JG, Woo YJ. Computational protein design to reengineer stromal cell-derived factor-1alpha generates an effective and translatable angiogenic polypeptide analog. *Circulation*. 2011;124:S18-26

19. Purcell BP, Elser JA, Mu A, Margulies KB, Burdick JA. Synergistic effects of sdf-1alpha chemokine and hyaluronic acid release from degradable hydrogels on directing bone marrow derived cell homing to the myocardium. *Biomaterials*. 2012;33:7849-7857

20. Bitter T, Muir HM. A modified uronic acid carbazole reaction. *Analytical biochemistry*. 1962;4:330-334

21. Brown L, Fenning A, Chan V, Loch D, Wilson K, Anderson B, Burstow D. Echocardiographic assessment of cardiac structure and function in rats. *Heart, lung & circulation*. 2002;11:167-173

22. Zhang G, Nakamura Y, Wang X, Hu Q, Suggs LJ, Zhang J. Controlled release of stromal cell-derived factor-1 alpha in situ increases c-kit+ cell homing to the infarcted heart. *Tissue engineering*. 2007;13:2063-2071

23. Ryan LP, Matsuzaki K, Noma M, Jackson BM, Eperjesi TJ, Plappert TJ, St John-Sutton MG, Gorman JH, 3rd, Gorman RC. Dermal filler injection: A novel approach for limiting infarct expansion. *The Annals of thoracic surgery*. 2009;87:148-155

24. Ifkovits JL, Tous E, Minakawa M, Morita M, Robb JD, Koomalsingh KJ, Gorman JH, 3rd, Gorman RC, Burdick JA. Injectable hydrogel properties influence infarct expansion and extent of postinfarction left ventricular remodeling in an ovine model. *Proceedings of the National Academy of Sciences of the United States of America*. 2010;107:11507-11512

25. Morita M, Eckert CE, Matsuzaki K, Noma M, Ryan LP, Burdick JA, Jackson BM, Gorman JH, 3rd, Sacks MS, Gorman RC. Modification of infarct material properties limits adverse ventricular remodeling. *The Annals of thoracic surgery*. 2011;92:617-624

26. Tous E, Ifkovits JL, Koomalsingh KJ, Shuto T, Soeda T, Kondo N, Gorman JH, 3rd, Gorman RC, Burdick JA. Influence of injectable hyaluronic acid hydrogel degradation behavior on infarction-induced ventricular remodeling. *Biomacromolecules*. 2011;12:4127-4135

27. Avigdor A, Goichberg P, Shivtiel S, Dar A, Peled A, Samira S, Kollet O, Hershkoviz R, Alon R, Hardan I, Ben-Hur H, Naor D, Nagler A, Lapidot T. Cd44 and hyaluronic acid cooperate with sdf-1 in the trafficking of human cd34+ stem/progenitor cells to bone marrow. *Blood*. 2004;103:2981-2989

28. Huebener P, Abou-Khamis T, Zymek P, Bujak M, Ying X, Chatila K, Haudek S, Thakker

G, Frangogiannis NG. Cd44 is critically involved in infarct healing by regulating the inflammatory and fibrotic response. *Journal of immunology*. 2008;180:2625-2633

29.   Dong F, Harvey J, Finan A, Weber K, Agarwal U, Penn MS. Myocardial cxcr4 expression is required for mesenchymal stem cell mediated repair following acute myocardial infarction. *Circulation*. 2012;126:314-324

CHAPTER 6

Local hydrogel delivery of recombinant tissue inhibitor of metalloproteinase-3 attenuates adverse left ventricular remodeling after myocardial infarction

(Adapted from: S.R. Eckhouse, B.P. Purcell, J.M. Oelsen, C.B. Logdon, W.F. Rawls, R.K. Patel, K.N. Zellars, R.E. Stroud, J.A. Jones, R. Mukherjee, R.C. Gorman, R.A. Black, J.A. Burdick, F.G. Spinale, *Sci Trans Med*, in revision)

6.1. Introduction

A structural milestone in the progression of heart failure following a myocardial infarction (MI) is left ventricular (LV) remodeling, defined as changes in LV geometry and structure[1-10]. While post MI remodeling is a multifactorial process, one ubiquitous event is infarct expansion[4-10]. Specifically, infarct expansion is the regional process by which continuous turnover of the extracellular matrix (ECM) results in the LV wall thinning and the loss of structural support[8-13]. One biological system that is active in the post MI context is a family of ECM proteases, the matrix metalloproteinases (MMPs)[13-25]. MMPs are a family of enzymes involved in proteolytic processing of interstitial structural proteins, signaling molecules and growth factors[13,26,27]. The induction and release of MMPs have been demonstrated in patients post MI, and were associated with adverse LV remodeling and the development of heart failure[22-25]. Moreover, direct measurement of interstitial MMP activity through microdialysis techniques have established that MMP activation occurs within the ischemic myocardium[21,28]. Thus, localized control of MMP activity within the MI region is a potential therapeutic target for the purposes of interrupting the maladaptive process of infarct expansion.

The cause-effect relationship between MMP activity and adverse LV remodeling has been established in experimental models through pharmacological MMP inhibition, as well as transgenic constructs[13-20]. For

example, continuous, systemic adminstration of pharmacologic MMP inhibitors reduced the extent of infarct expansion and LV dilation following experimental MI in adult pigs[14]. However, translation of systemic pharmacologic MMP inhibition to clinical application has encountered problematic issues, including concerns surrounding dosing and potential side-effects[29-32]. Under ambient physiologic states, endogenous MMP inhibition is achieved through the synthesis and release of the tissue inhibitors of MMPs (TIMPs)[13,33-35]. In contradistinction to the induction of MMPs in the early post-MI period, a concomitant increase in relative TIMP levels does not occur, causing an imbalance between endogenous proteolytic activity and inhibition, which in turn would facilitate early adverse LV remodeling and infarct expansion[13-15,22-25]. It is now becoming recognized that the biological effects of TIMPs may not be uniform, and studies have identified unique functionality[34-38]. Of particular relevance, TIMP-3 levels are reduced in patients post MI[22], and transgenic deletion of TIMP-3 causes adverse remodeling and acceleration to heart failure[39-41]. Unique biological features of TIMP-3 include a high affinity to bind to the ECM through interactions with glycoasaminoglycans[34,42,43], influences on cytokine processing[41,44], and alterations in fibroblast phenotype *in-vitro*[36,45]. However, localized augmentation of TIMP-3 in the context of post-MI remodeling has not been examined.

Accordingly, the central hypothesis of this study was that local delivery of exogenous TIMP-3 within the MI region would reduce infarct expansion and alter the course of post-MI remodeling. Polymers that form solid water-swollen hydrogel matrices from liquid precursor solutions upon injection through a syringe have been applied in order to localize and sustain the release of macromolecules to the MI region[46]. Past studies have demonstrated that composite materials such as hydrogels containing hydroxyapatite or fibrin-alginate can be safely injected into the MI region[47-51]. Moreover, injectable hydrogels based on hyaluronic acid (HA), a glycosaminoglycan found abundantly in the ECM, have been deployed in large animal models of MI[47]. Thus, the first aim of the present study was to develop a method by which to incorporate a recombinant TIMP-3

(rTIMP-3) within a degradable HA hydrogel construct for localized myocardial delivery in a large animal model of MI. The second aim of the present study was to locally place the Hydrogel/rTIMP-3 system within the MI region and quantify the effects on regional interstitial MMP activity, infarct expansion, and LV geometry and structure within the early post MI period.

6.2. Methods

Animals

All animals were treated and cared for in accordance with the National Institutes of Health *Guide for the Care and Use of Laboratory Animals* (*Eighth Edition*. Washington, DC: 2011), and all protocols were approved by the Medical University of South Carolina's Institutional Animal Care and Use Committee.

rTIMP-3 Synthesis

A stable human TIMP-3 poly-His (rTIMP-3) expressing Chinese hamster ovary cell line was established using a vector with a Cytomegalovirus promoter, whereby 60 L of conditioned medium were concentrated to 8 L via Tangential Flow Filtration (TFF) (Millipore, 10kD MWCO). The full length human TIMP-3 sequence was utilized[52]. The concentrated supernatant was filtered and applied to Fractogel EMD SO3 (Merck KGaA, Darmstadt, Germany), and protein was eluted with a 0.1 M sodium chloride (NaCl) gradient. The TIMP-3 containing fractions were applied to Ni-NTA resin (Qiagen, Valencia, CA), and poly-His tagged protein was eluted with 300 mM Imidizol. To further remove contaminants, the protein was then subjected to size-exclusion chromatography. TIMP-3 containing fractions were concentrated by TFF and buffer exchanged to 10 mM Na Acetate pH 5.2, 9% Sucrose. The material was then lyophilized for later reconstitution. Using a previously validated global MMP fluorogenic peptide assay, 10 µM of the MMP substrate (Cat no. ES001, R&D Systems) and 4 nM of a recombinant active MMP-2 (Cat no. 902-MP R&D Systems) were incubated in the presence and absence of increasing concentrations of rTIMP-3.

Fluorescence of the cleaved substrate was measured at an emission/excitation wavelength of 320/405 nm. An exponential decay in MMP activity occurred with increasing concentrations of rTIMP-3, with a computed half maximal inhibitory concentration of approximately 26 ng/mL (Figure 6.1 A).

Hydrogel Synthesis

A degradable hydrogel was fabricated by synthesizing HA macromers as described previously[48-49]. Briefly, HA (74kDa, Lifecore) was modified with hydroxyethyl methacrylate (HEMA) to incorporate a terminal methacrylate group for free-radical initiated crosslinking as well as ester bonds to introduce hydrolytic degradation (Figure 6.1 B). Briefly, HEMA was reacted with succinic anhydride via a ring opening polymerization in the presence of N-methylimidazole to obtain HEMA-COOH, which was then coupled to a tetrabutylammonium salt of HA in the presence of 4-dimethylaminopyridine. The resulting HA macromer with HEMA group modification (HEMA-HA) was purified with dialysis, lyophilized and characterized by ^{1}H NMR. For hydrogel formation upon injection, a redox initiator system consisting of ammonium persulfate (APS) and N,N,N′,N′-tetramethylethylenediamine (TEMED) was utilized. 10 mM APS and 10 mM TEMED were mixed with a 4 wt% (w/v) HEMA-HA solution in phosphate buffered saline (PBS) to form hydrogels. Kinetics of hydrogel formation were characterized with rheometry by monitoring the storage (G') and loss (G") with time (20mm 1° cone geometry, 1% strain, 1Hz, Texas Instruments AR 2000ex).

rTIMP-3 Binding Affinity to HEMA-HA

Binding affinity between rTIMP-3 and HEMA-HA was quantified using an intrinsic protein fluorescence quenching technique. Fluorescence titration experiments were performed on a Tecan infinite m200 plate reader (Grödig, Austria) at 25°C. The fluorescence of a 2 μM rTIMP-3 solution in 100 mM HEPES buffer (pH 7.4) was recorded at 280/350nm excitation/emission. Fluorescence quenching was monitored by increasing the concentration of

HEMA-HA in rTIMP-3 solution in 0.64 µM increments. 2 µL of concentrated polymer solution in HEPES was added to 1 mL rTIMP-3 solution for each titration, mixed, equilibrated for 2 min and fluorescence was measured. The normalized changes in fluorescence with each HEMA-HA titration were plotted against HEMA-HA concentration and resulting binding isotherms were fit by nonlinear regression to the equation describing bimolecular association:

$$F = F_i + F_f \left[\frac{K_d + [SDF] + [HA] - \sqrt{(K_d + [SDF] + [HA])^2 - 4[SDF][HA]}}{2[SDF]} \right]$$

where F is the change in fluorescence over initial fluorescence (-$\Delta F/F_o$), F_i is the initial value for (-$\Delta F/F_o$), F_f is the final value for (-$\Delta F/F_o$), and K_d is the dissociation constant.

Hydrogel Encapsulation of rTIMP-3 and in vitro Release Kinetics

rTIMP-3 was mixed with a 4 wt% HEMA-HA macromer solution in PBS, and hydrogels were formed upon mixing 10mM APS/TEMED initiators as described above. 50 µL hydrogels containing 10 µg rTIMP-3 were crosslinked in cylindrical molds for 30 minutes at 37°C and then transferred to eppendorf tubes containing 1mL PBS supplemented with 1% (w/v) bovine serum albumin (BSA). Hydrogels were incubated in buffer at 37°C, and samples were collected for up to 14 days. At each time point, buffer was collected and replaced and analyzed for released molecules. rTIMP-3 was quantified with a His ELISA (QUAexpress, Ni-NTA HisSorb, Quiagen Inc) using rTIMP-3 standards (0.7-25 ng) and HA degradation products were quantified using a uronic acid assay[47,48]. After 14 days, hydrogels were enzymatically degraded by overnight incubation with hyaluronidase (800 units/mL, Sigma Aldrich), and evaluated for remaining rTIMP-3 and HA.

In vivo Validation of rTIMP-3 Releasing Hydrogel

Hydrogel/rTIMP-3 injections were performed within the LV free wall of Yorkshire pigs (n=3, 25 kg, Hambone Farms, Orangeburg, SC). The pigs were

anesthetized with isoflurane (2%), and through a left thoracotomy, the LV free wall was exposed. A 2 cm square calibrated grid was sutured below the origin of the first two obtuse marginal arteries of the circumflex artery (OM1 and OM2)[14,50], which provided for a total of 9 distinct injection sites within a targeted 2X2 cm region of myocardium (Figure 6.1 E). The hydrogel precursors containing initiators and rTIMP-3 (20 µg rTIMP-3/100 µL hydrogel) were mixed in a sterile fashion, drawn into micro-syringes, and injected into the mid-myocardium of each target site. This volume of hydrogel and concentration of rTIMP-3 was determined during initial titration studies, which provided the optimal ratio of volume and concentration. The duration of time from final polymer mixing to completion of the 9 injections was 3 minutes. Successful injections were confirmed by visualization of an opacification of the epicardial surface at the point of myocardial injection. The perimeter of the injection grid was marked at each corner with radiopaque markers (1.6mm diameter, VNUS Medical Systems, Sunnyvale, CA) and the grid removed[14]. At 7 days post injection, the pigs were again anesthetized, the LV harvested, the myocardial tissue isolated and sectioned into 9 regions, and immediately processed. The LV samples were prepared in an ice cold extraction/homogenization buffer (QUAexpress, Ni-NTA HisSorb, Quiagen Inc) and subjected to the His ELISA technique described in the previous section.

MI Induction and Hydrogel Injection Protocol

Pigs were randomized to one of three different groups: MI and no injections (MI only, n=6), MI and hydrogel injections (MI/Hydrogel, n=8), and MI and hydrogel with rTIMP-3 injections (MI/Hydrogel/rTIMP-3, n=8). Non-instrumented pigs were used as referent, non-MI controls (n=8). The pigs were anesthetized and markers placed as described in the previous section. OM1 and OM2 were ligated to induce an MI, and characteristic ECG changes occurred, but electrical cardioversion and/or defibrillation were not required, and past studies demonstrated that this technique creates a uniform and consistent MI involving

22% of the LV free wall[14,50]. For pigs assigned to either hydrogel groups, nine injections were performed as described in the previous section.

Measurements of Infarct Expansion, LV Geometry and Function, In-vivo MMP Activity

Two weeks after chronic instrumentation, the animals were sedated and two-dimensional echocardiographic studies (ATL Ultramark VI, 2.25MHz transducer, Bothell, WA) were performed to calculate LV volume and dimensions[14,22,50]. In addition, LV short-axis images gated to end-diastole were digitized and used to compute regional wall stress as previously described[14,50]. Following which, fluoroscopic images of the myocardial markers were recorded with a high-speed cinefluoroscopy (Philips Cardiac-Diagnostic) and were digitized (ATI Radeon). Using projections of the markers from two orthogonal planes, intermarker distances were computed in three-dimensional spaces and used to determine the area circumscribed by the markers[14].

Following imaging studies, the pigs were anesthetized with sufentanyl (2 µg/kg IV, Baxter Healthcare), morphine sulfate (3 mg/kg/h IV, Elkin-Sinn), and isoflurane (1%, 3 L/min O_2, Baxter Healthcare), and mechanically ventilated. The LV was exposed through a sternotomy, a microdialysis probe (20 kDA, outer diameter of probe shaft 0.77 mm; CMA/Microdialysis, North Chelmsford, MA) placed within the MI region, and infused with the MMP fluorescent substrate (5 µL/min) described in the previous section and validated previously[21,28]. The dialysate was then subjected to fluorometry which reflected interstitial MMP activity. Following these measurements, the LV was harvested, separated into MI and remote regions (area served by left anterior descending artery), and prepared for biochemical and histological measurements.

Ex vivo Measurements of TIMP-3, LV Histology, and Cytokine Assay

Immunoblotting. Immunoblotting was performed for total myocardial TIMP-3 levels using approaches described in detail previously[14,15,28,50,51]. LV extracts

97

(80 µg of total protein) underwent electrophoretic separation, transferred to a nitrocellulose, incubated with anti-TIMP-3 (1:2000, Cat#AB6000, Millipore, Billerica, MA, overnight 4°C), the immune-positive signal detected by chemiluminescence (Western Lighting, Perkin Elmer), and digitally quantified (Gel-Pro Analyzer, v3.1.14, Media Cybernetics Inc., Silver Spring, MD). In order to confirm the presence and absence of rTIMP-3 within the LV targeted regions, immunoblotting was performed using anti-polyHis (1:1000, Cat#ab27025, Abcam, Cambridge, MA, overnight 4°C).

Histomorphometry. The formalin fixed full thickness LV samples were embedded, sectioned (7 µm), and stained with picrosirius red for fibrillar collagen, and the percent area of collagen within the remote and MI regions were computed using computer assisted morphometry[14-16,51,53]. Immunostaining was used to colocalize with cells that stained positive for α-smooth muscle actin (1:100; α-smooth muscle actin: Sigma A5228), a marker for actin present in vascular smooth muscle cells as well as myofibroblasts, using approaches described previously[53]. Additional LV sections were stained with hematoxylin and eosin, and histopathological examination was performed.

Cytokine Assay. LV myocardial homogenates were subjected to cytokine analysis using a 2-laser flow cytometric detection system (Bio-Plex 200, BioRad Laboratories) and a previously validated platform (Cat. no. MPXHCYT060KPMX39, Millipore, Billerica, MA)[21]. Using pre-calibrated standards and regression modeling, the fluorescence emission was converted to an absolute cytokine concentration.

Computation and Data Analysis

Statistical analyses were performed using STATA statistical software (STATA Corp, College Station, TX). LV geometry, function, and area within the markers were compared between the control and MI groups using a one-way analysis of variance (ANOVA). Post-hoc separation following ANOVA was performed using pairwise comparisons with a Bonferroni analysis (prcomp

module, STATA). The interstitial global MMP activity was evaluated by ANOVA and subsequently compared against the control values of 100% by a Student's t-test. For TIMP-3 levels and myocardial cytokine concentrations, values from each group were first evaluated by ANOVA, and then a post-hoc separation following ANOVA was performed using pairwise comparisons with a Bonferroni analysis. For morphometric measurements, a multi-way ANOVA (MANOVA) was performed, evaluating for treatment dependent, MI dependent, and region dependent effects. Post-hoc separation following MANOVA was performed using pairwise comparisons with a Bonferroni analysis. Results are presented as a mean ± standard error of the mean (SEM), and values of p<0.05 were considered to be statistically significant.

6.3. Results

Hydrogel Formation and rTIMP-3 Release

HEMA-HA macromers were synthesized with a modification of ~20% as determined by ^{1}H NMR analysis. The negatively charged HEMA-HA macromers bound rTIMP-3 with a dissociation constant (K_D) of 3.8±0.03μM (Figure 6.1 B). Solutions of the HEMA-HA macromer and APS/TEMED initiators (4 wt% HEMA-HA, 10 mM APS/TEMED) were mixed together for hydrogel formation, with gelation occurring approximately 1 minute after mixing, and a plateau of crosslinking reached within 30 minutes (Figure 6.1 C). Upon mixing APS and TEMED, a free-radical is generated, which initiates the growth of kinetic chains between methacrylate groups on the HEMA-HA macromers, covalently crosslinking the hydrogel. The crosslinked hydrogels steadily degraded in aqueous solution throughout the 14 day period, as determined by release of uronic acid, although the gels remained intact at day 14 (Figure 6.1 D). rTIMP-3 was successfully encapsulated in the hydrogel and released at a nearly uniform rate throughout the 14 day period (Figure 6.1 D). A significant amount of rTIMP-3 remained in the hydrogels after the 14 day study. When injected into the myocardium, the hydrogels maintained the levels of rTIMP-3 above remote

background levels over a 7 day period. Specifically, a consistent signal for rTIMP-3 was detected at each of the targeted injection sites, but no signal was obtained in non-targeted injection sites (Figure 6.1 F).

LV Geometry, Infarct Expansion, and Wall Stress

LV end-diastolic volume, ejection fraction, and regional infarct expansion, defined as the area of myocardium within the markers (MI marker area), are summarized in Figure 6.2. At 14 days post MI, LV volumes increased in all three MI groups but were reduced in the MI/rTIMP-3/Hydrogel group. LV ejection fraction fell in all MI groups but was higher in the MI/rTIMP-3/Hydrogel group when compared to the MI only group. Regional infarct expansion increased in the MI only and MI/Hydrogel groups at 14 days post-MI, whereas this index of MI expansion was significantly attenuated in the MI /Hydrogel/rTIMP-3 group. In light of the changes in LV global geometry and MI expansion, LV regional wall stress was computed in all groups (Figure 6.3 A). LV regional wall stress increased in all MI groups when compared to referent controls but was reduced in both the MI/Hydrogel and the MI/Hydrogel/rTIMP-3 groups when compared to MI only values. However, the greatest reduction in LV regional wall stress occurred in the MI/Hydrogel/rTIMP-3 group.

In vivo interstitial MMP activity and ex-vivo TIMP-3 levels

Myocardial interstitial MMP activity was quantified within the MI region at 14 days post-MI using a validated microdialysis-fluorogenic approach[21,28,53], and the results are summarized in Figure 6.3. Interstitial MMP activity was higher in the MI only and the MI/Hydrogel groups, and was significantly reduced in the MI/Hydrogel/rTIMP-3 group. LV myocardial extracts were subjected to anti-polyHis immunoblotting, whereby only apositive signal corresponding to rTIMP-3 could be identified within the MI region at 14 days post-MI (Figure 6.4 A).
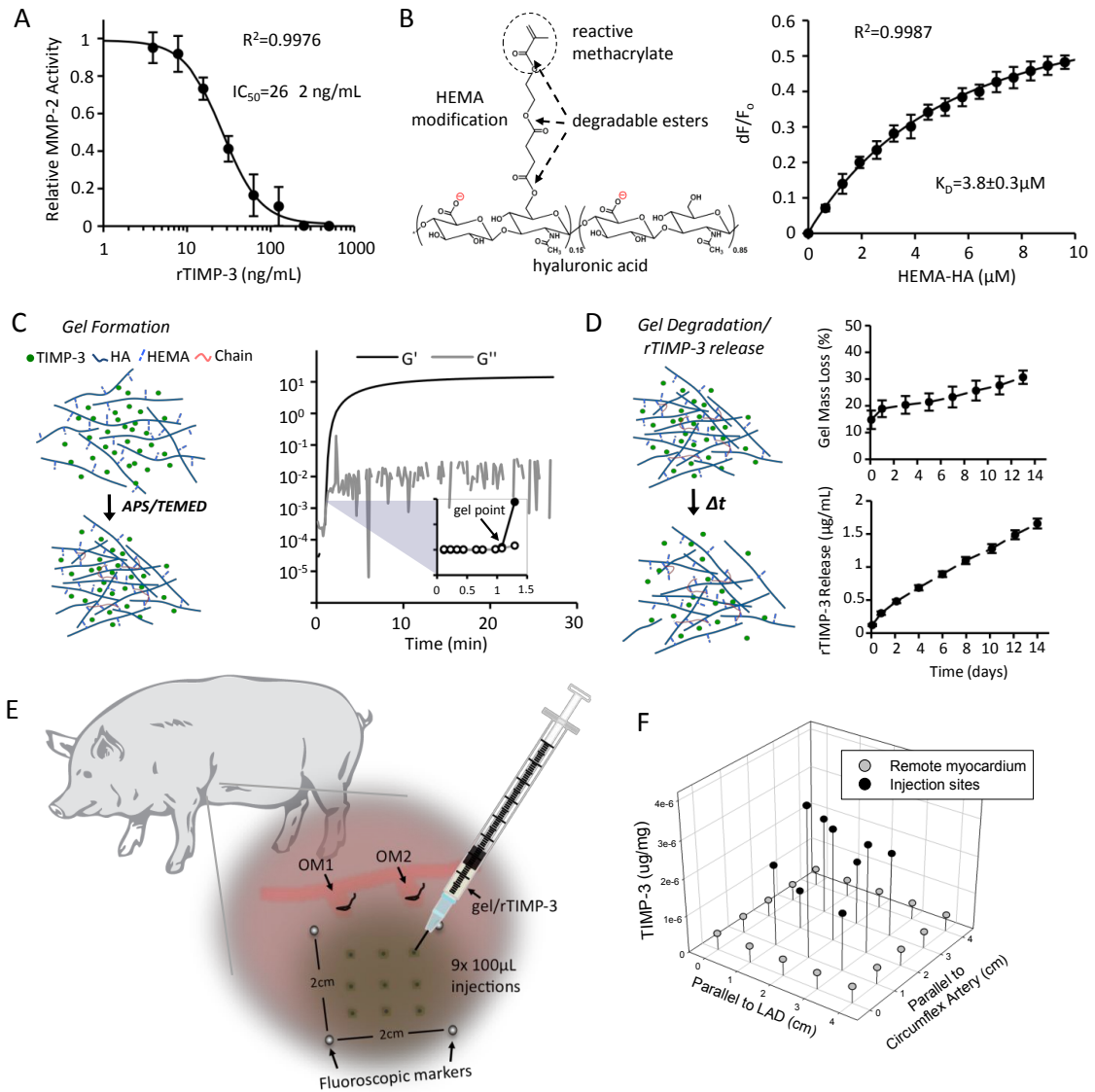
Figure 6.1. Hydrogel fabrication for targeted rTIMP-3 delivery. (A) rTIMP-3 inhibits rMMP-2 activity in a dose-dependent manner with a half maximal inhibitory concentration, $IC_{50}=26\pm2$ ng/mL. (B) Synthesized HA macromer with reactive methacrylate group for gel crosslinking and hydrolytically unstable ester groups for gel degradation. This negatively charged macromer binds to rTIMP-3 with a $K_D=3.8\pm0.3\mu M$ through electrostatic interaction. (C) Gel crosslinking was quantified with rheometry by measuring the storage (G') and loss (G'') moduli over time. Crosslinking of 4wt% macromer (20% HEMA modification) reaches a gel point within 1 min after adding 10mM APS/TEMED free-radical initiators and plateaus by 30 min. (D) Encapsulated rTIMP-3 (10μg/gel) diffuses from the gels in a steady fashion for 14 days as the gels degrade in aqueous buffer. A significant amount of rTIMP-3 remained in the gels after the 14-day study. (E) Gels containing rTIMP-3 (20μg/100μL gel) were delivered to the MI region through a syringe immediately following ligation of obtuse marginal arteries 1 and 2 (OM1 and OM2) in pigs. (F) rTIMP-3 was quantified locally at the 9 injections sites 1 week after MI with no spillover to remote sites.
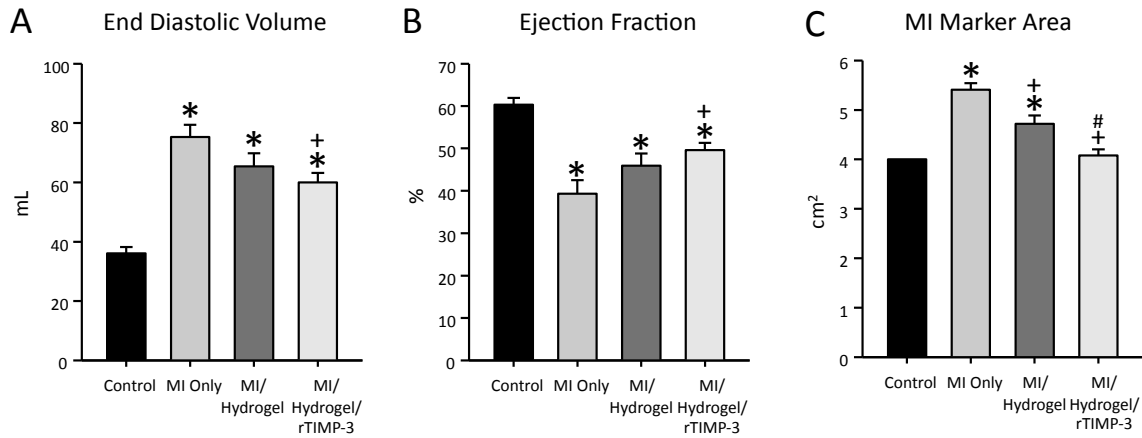
Figure 6.2. LV end-diastolic volumes and ejection fraction were computed by echocardiography and the area within the radiopaque markers (MI marker area) by fluoroscopy at 14 days post MI. LV dilation, as measured by LV end-diastolic volume, increased in all 3 groups post MI when compared to referent control values. However, the degree of LV dilation was significantly reduced in the MI/Hydrogel/rTIMP-3 group. LV ejection fraction significantly fell in all 3 groups at 14 days post-MI. However, LV ejection fraction was significantly higher in the MI/Hydrogel/rTIMP-3 group when compared to the MI only group. MI marker area, indicative of infarct expansion, increased in the MI only and MI/Hydrogel groups, but was significantly reduced to control values in the MI/Hydrogel/rTIMP-3 group. (*p<0.05 vs referent control, +p<0.05 vs MI only, #p<0.05 vs MI/Hydrogel).
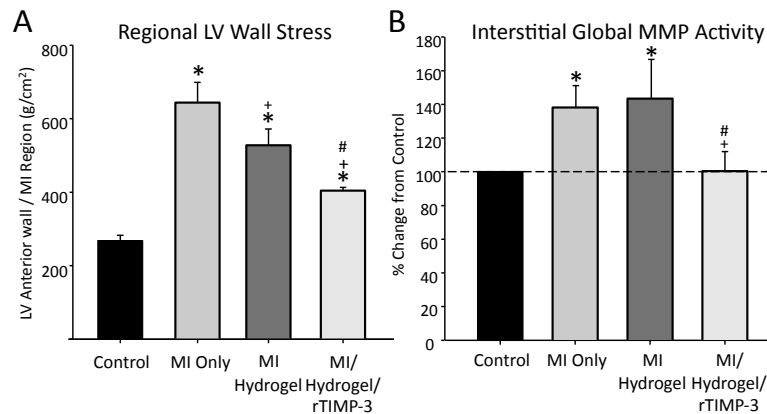

Figure 6.3. (A) Regional peak systolic wall stress at the LV anterior wall (targeted MI region) was computed using LV short axis dimensions, and wall thickness measurements as described in the Methods section. LV regional wall stress increased within the targeted MI region in all 3 groups at 14 days post-MI when compared to referent controls. However, LV regional wall stress was reduced in the MI/Hydrogel group when compared to MI only values. Moreover, LV regional wall stress was reduced even further in the MI/Hydrogel/rTIMP-3 group. (B) Interstitial MMP activity within the MI region was determined using microdialysis and a fluorogenic peptide, as described in the Methods section, and normalized to referent control values (dashed line). Interstitial MMP activity increased in the MI only and MI/Hydrogel groups at 14 days post MI and was reduced in the MI/rTIMP-3/Hydrogel group. (*p<0.05 versus referent control, +p<0.05 versus MI only, #p<0.05 versus MI/Hydrogel)

Using anti-TIMP-3 targeted against both native TIMP-3 and rTIMP-3, quantitative immunoblotting was performed and summarized in Figure 6.4 B. Total TIMP-3 levels fell within the MI region in both the MI only and MI/Hydrogel groups, but increased in a robust fashion within the MI region of M/Hydrogel/rTIMP-3 group. Total myocardial TIMP-3 levels were similar across groups in the LV remote region.
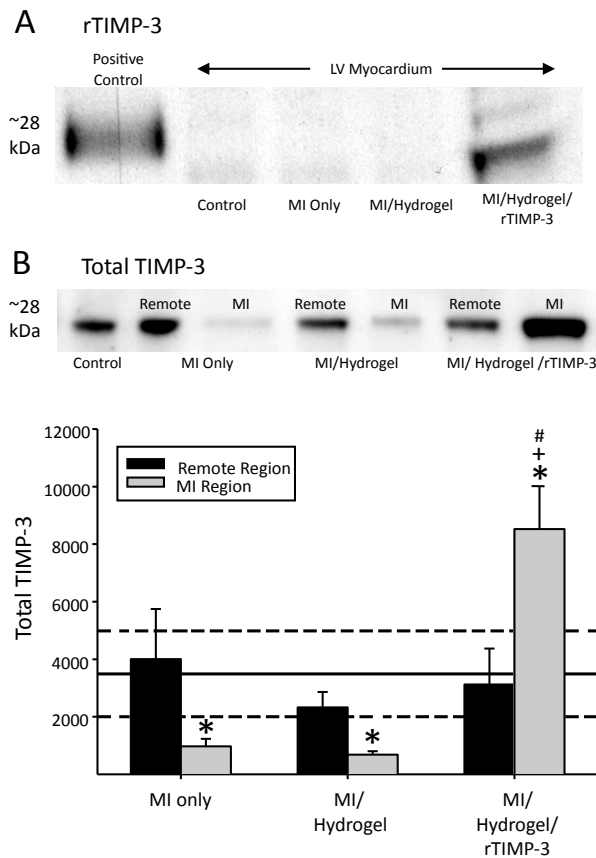

Figure 6.4. (A) Representative immunoblot for the His-tagged rTIMP-3 within the targeted MI region at 14 days post MI. A strong positive signal was identified within the MI/rTIMP-3/Hydrogel samples and was absent in the referent control, MI only, and MI/Hydgrogel groups. (B-Top Panel) A representative immunoblot for TIMP-3, using an antibody which reacted against both rTIMP-3 and native TIMP-3. The signal for total TIMP-3 was reduced within the MI region in the MI only and MI/Hydrogel groups. (B-Bottom Panel) Quantitative immunoblotting for total LV myocardial TIMP-3 levels within the MI and remote regions was performed at 14 days post MI as well as in referent control samples (the mean is represented by the solid line, and the SEM is represented by the dashed lines). Within the MI region, total TIMP-3 was reduced in the MI only and MI/Hydrogel groups, and was significantly increased from both MI groups and referent control values in the MI/Hydrogel/rTIMP-3 group. (*p<0.05 versus referent control, +p<0.05 versus MI only, #p<0.05 versus MI/Hydrogel)

Cytokine levels relative to referent control values are summarized in Figure 6.5. LV myocardial levels of interleukin-6, -9, and -12 increased in both the MI only group and the MI/Hydrogel group. Interestingly, the myocardial concentrations of IL-6, -9, -12 were significantly reduced in the MI/Hydrogel/rTIMP-3 group. Monocyte chemoattractant protein-1 (MCP-1) concentrations were similar in

the MI only and MI//Hydrogel groups, and actually fell below referent control values in the MI/Hydrogel/rTIMP-3 group.
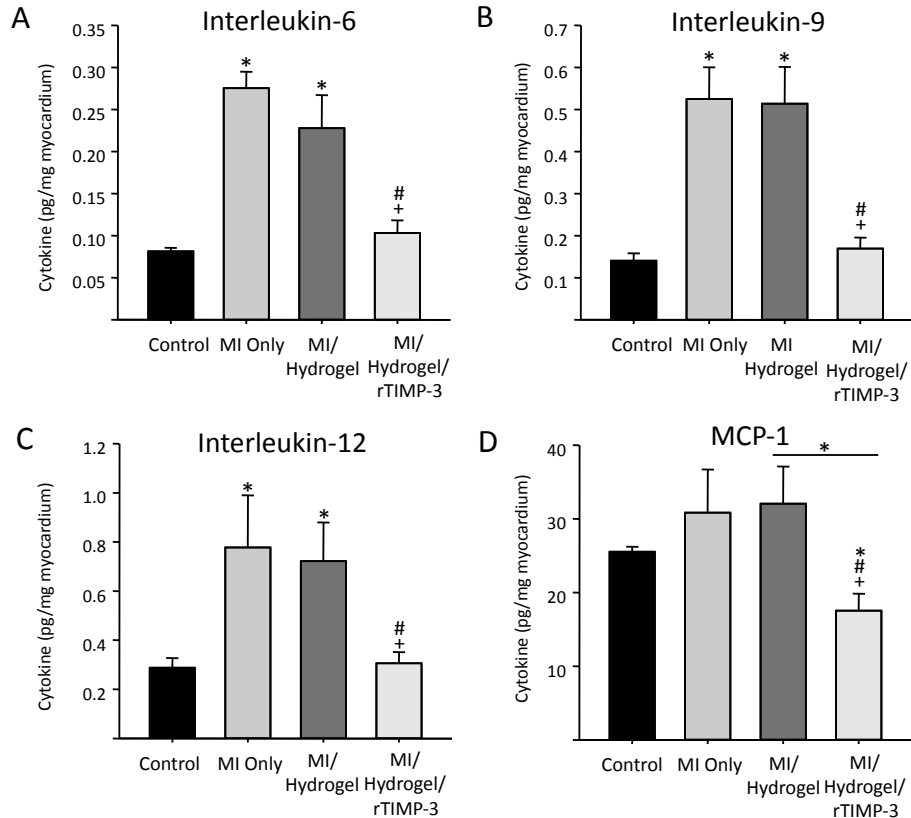

Figure 6.5. Significant changes in specific inflammatory cytokines were detected within the MI region at 14 days post MI, which included interleukin-6,-9,-12, and monocyte chemoattractant protein-1 (MCP-1) when compared to referent control values. Interleukin-6, -9, and -12 increased significantly in the MI only and MI/Hydrogel groups, whereas these cytokine levels were significantly reduced in the MI/Hydrogel/ rTIMP-3 group. MCP-1 were similarly increased in the MI and MI/Hydrogel groups and actually fell below referent control values in MI/Hydrogel/rTIMP-3 group. (*p<0.05 versus referent control, +p<0.05 versus MI only, #p<0.05 versus MI/Hydrogel)

Myocardial Histology and Fibrillar Collagen Content

Histological examination of LV sections taken from the referent control and MI region revealed significant myofibrillar loss and an influx of inflammatory cells (Figure 6.6 B-D). The presence of remnant hydrogel was observed within the MI/Hydrogel and MI/Hydrogel/rTIMP-3 groups. Collagen content increased in all MI groups when compared to controls (Figure 6.6 E). Collagen content was further increased in the MI/Hydrogel and MI/Hydrogel/rTIMP-3 groups when

compared to the MI only group. LV mid-myocardial sections devoid of large blood vessels were examined with respect to immunolocalization for smooth muscle actin (SMA), and representative photomicrographs are shown in Figure 6.6 F. While in the referent control and remote regions, SMA staining predominated around arterioles and venules. The predominant staining pattern within the MI region was that of interstitial cells, consistent with myofibroblasts. This myofibroblast positive staining was increased in the MI/Hydrogel group and increased further in the MI/Hydrogel/rTIMP-3 group (Figure 6.6 F).

6.4. Discussion

Targeting Myocardial Infarct Expansion

While a number of pathophysiological events contribute to adverse remodeling following MI, the myocardial process generically termed as infarct expansion is a significant contributing factor[5-10]. In the early post MI period (hours-days), an influx of inflammatory cells, cytokine release, and activation of multiple signaling pathways occurs, and results in heightened MMP activation and matrix degradation[12,13]. While this early MMP induction may be an adaptive biological response to myocardial injury, the persistently elevated MMP activation which can occur in the later post MI period (days-weeks) can result in matrix instability and abnormalities in stress-strain patterns, which in turn cause thinning of the MI region as well as jeopardize the cellular and extracellular structure and function of the viable border zone[9-13]. In contrast to the robust MMP induction and activation in the post MI period, animal and clinical studies have demonstrated that there is not a parallel increase in TIMPs, which in turn would further potentiate interstitial MMP proteolytic activity[14,15,22,24,25,51,53]. Moreover, transgenic models have underscored the importance of TIMPs in terms of the adverse LV remodeling process[16]. Thus, targeting MMPs remains an area of active therapeutic investigation and development[29-32] and would be particularly relevant in terms of the infarct expansion process.
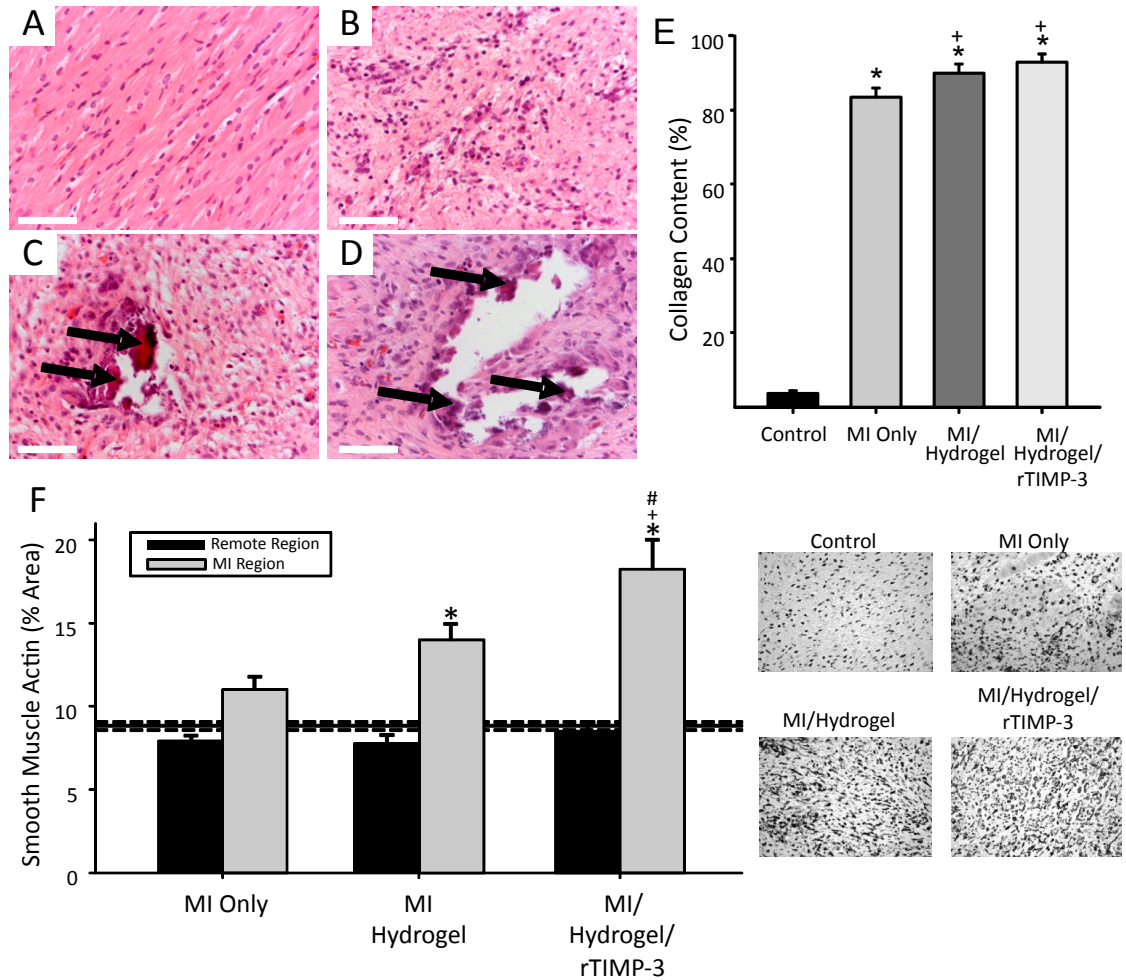
Figure 6.6. (A-D) Representative photomicrographs of LV sections taken from the MI region stained with hematoxylin and eosin: (A) a referent control and 14 days post-MI for (B) MI only, (C) MI/Hydrogel, and (D) MI/Hydrogel/rTIMP-3. In contrast to the organized distribution of myofibrils within the referent control LV myocardium, an influx of inflammatory cells and myofibril disruption could be appreciated within the MI region, but to a lesser extent in the MI/Hydrogel/rTIMP-3 sections. Histological features consistent with islands of remnant Hydrogel were observed within the MI region of the MI/Hydrogel group and the MI /Hydrogel/rTIMP-3 (black arrows). Scale bars are 50 µm. (E) Computer assisted morphometric measurements of picro-sirius stained sections from referent controls and the MI region were used to compute relative fibrillar collagen content. Collagen content was increased in all MI groups when compared to referent control values (F=3.07, p=0.04). Collagen content was further increased in the MI/Hydrogel group and the MI/Hydrogel/rTIMP-3 group when compared to the MI only group. (F) Top Panels- Representative smooth muscle actin staining within the referent control and MI sections. In the referent control as well as the remote sections, smooth muscle actin staining was primarily associated with small vascular structures (arterioles/venules), whereas in the MI region the staining pattern was primarily associated with interstitial cells – i.e. myofibroblasts. Quantification using densitometry revealed a substantial increase in this pattern of smooth muscle actin staining within the MI region of the MI/ Hydrogel/rTIMP-3 group. (*p<0.05 versus control group, +p<0.05 versus MI only group, #p<0.05 versus MI/Hydrogel)

The present study was built upon these past clinical observational studies, transgenic model systems, and broad based systemic pharmacological inhibitors, through directly targeting the region of the LV myocardium where a clear imbalance exists between MMPs and TIMPs. Using a clinically relevant model of post MI remodeling[54], the present study demonstrated that targeted TIMP delivery is feasible and effective in interrupting the infarct expansion process. These findings underscore the importance of developing therapeutic strategies focused upon restoring the balance between MMP/TIMPs following MI. Specifically, the new and unique findings from the present study were three-fold: (1) regional Hydrogel/rTIMP-3 injections abrogates infarct expansion, reduces LV dilation and regional wall stress, and improves systolic function in the early post-MI period; (2) local Hydrogel/rTIMP-3 delivery augments total TIMP-3 levels within the MI region and reduces myocardial interstitial MMP activity without causing significant collagen accumulation over and above that of hydrogel delivery alone; and (3) rTIMP-3 delivery within the MI region reduces local pro-inflammatory cytokine levels and increases myofibroblast density. This unique translational study provides the first proof of concept that local and sustained delivery of a recombinant TIMP effectively interrupts infarct expansion and improves LV geometry, likely through modifying biological mediators of the adverse post MI remodeling process.

LV Remodeling and Function: Effects of rTIMP-3

LV remodeling following MI invariably includes LV dilation, whereby the progression and extent of post MI LV dilation is an independent risk factor for morbidity and mortality[1-7]. In the present study, regional injection of rTIMP-3 into the MI region reduced the degree of LV dilation when compared to MI only values as well as to that of Hydrogel injection alone. It is important to note that a range of hydrogels have been investigated to alter local tissue bulking and to reduce stress profiles in the myocardium, leading to changes in LV dilation, without the delivery of biological molecules[47]. Here, there is a clear improvement

in outcomes with the addition of rTIMP-3. Also, LV ejection fraction increased in the rTIMP-3 group in the post MI period. LV ejection fraction, as with any index of LV pump function, is influenced by loading conditions and intrinsic contractile performance.

In the present study, rTIMP-3 injection resulted in increased MI thickness, and when considered in conjunction with the changes in chamber radius, caused a net reduction in regional LV peak wall stress. Since LV peak wall stress is a fundamental measure of LV afterload and is inversely related to LV ejection performance, one likely mechanism for the improved LV ejection fraction with rTIMP-3 injection was favorable effects on regional LV afterload. However, it must be recognized that these measures of LV global and regional geometry were taken at only one time point post MI, and whether these improvements with rTIMP-3 are due to changes in the trajectory of adverse post-MI remodeling, or actually represent a complete cessation of this process, will require future serial studies. Significantly increased collagen accumulation within the LV myocardium can contribute to increased myocardial stiffness properties[13]. One critical observation was that while rTIMP-3 release into the MI region, while significantly reducing interstitial MMP activity, was not associated with excessive collagen accumulation. These findings would suggest that localized rTIMP-3 augmentation did not disproportionally alter ECM turnover and accelerate fibrosis.

Potential Biological Effects and Mechanisms of rTIMP-3 Delivery Post-MI

In the present study, interstitial MMP activity was reduced within the MI region with rTIMP-3 delivery, demonstrating a localized MMP inhibitory effect, and therefore, the hydrogel mediated delivery strategy released an active protein. However, multiple substrates and biological pathways are influenced by MMPs[58,59], and therefore, it would be an oversimplification to assume that rTIMP-3 delivery merely inhibited matrix proteolysis. In addition, it has been demonstrated that TIMP-3 can induce direct biological effects, which include influencing fibroblast growth and function, cell survival, and cytokine

processing[36,42,44]. The present study provides evidence to suggest that the reduction in MI wall thinning and infarct expansion that occurred with rTIMP-3 delivery was likely due to a summation of these biological effects.

One unique finding from the present study was that rTIMP-3 delivery resulted in a significant reduction in pro-inflammatory cytokines within the MI region. This effect may have been due to several factors, which include interference of MMP matrix proteolysis and egress of inflammatory cells, MMP mediated cytokine processing, and/or direct effects of TIMP-3 on cytokine induction. Nevertheless, it is likely that the attenuation of cytokine signaling within the MI region with rTIMP-3 delivery influenced the post MI remodeling process. Another observation from the present study was that rTIMP-3 caused a significant increase in α-smooth muscle actin, predominantly in interstitial cells (i.e. myofibroblasts)[58,59]. Since myofibroblasts are critical in the wound healing context and provide significant contractile force across the ECM[13,58,59], it is likely that the increase in this fibroblast phenotype with rTIMP-3 delivery influenced regional tissue geometry and structure within the MI region. While this potential contributory mechanism for the effects of rTIMP-3 remains associative, what is clear from the present study is that regional TIMP-3 delivery within the MI region likely altered biological signaling pathways as well as fibroblast phenotype.

6.5. References

1. Pfeffer MA, and Braunwald E. Ventricular remodeling after myocardial infarction. Experimental observations and clinical implications. Circulation 81: 1161-1172, 1990.
2. Weisman HF, Bush DE, Mannisi JA, Weisfeldt ML, and Healy B. Cellular mechanisms of myocardial infarct expansion. Circulation 78: 186-201, 1988.
3. White HD, Norris RM, Brown MA, Brandt PW, Whitlock RM, and Wild CJ. Left ventricular end-systolic volume as the major determinant of survival after recovery from myocardial infarction. Circulation 76: 44-51, 1987.
4. Weir RA, McMurray JJ, and Velazquez EJ. Epidemiology of heart failure and left ventricular systolic dysfunction after acute myocardial infarction: prevalence, clinical characteristics, and prognostic importance. Am J Cardiol 97: 13F-25F, 2006.
5. Erlebacher JA, Weiss JL, Weisfeldt ML, and Bulkley BH. Early dilation of the infarcted segment in acute transmural myocardial infarction: role of infarct expansion in acute left ventricular enlargement. J Am Coll Cardiol 4: 201-208, 1984.
6. Chareonthaitawee P, Christian TF, Hirose K, Gibbons RJ, and Rumberger JA. Relation of initial infarct size to extent of left ventricular remodeling in the year after acute myocardial infarction. J Am Coll Cardiol 25: 567-573, 1995.
7. Cannon RO 3rd. Mechanisms, management and future directions for reperfusion injury after acute myocardial infarction. Nat Clin Pract Cardiovasc Med. 2005 Feb;2(2):88-94.
8. Moens AL, Claeys MJ, Timmermans JP, Vrints CJ. Myocardial ischemia/reperfusion-injury, a clinical view on a complex pathophysiological process. Int J Cardiol. 2005 Apr 20;100(2):179-90.
9. Ertl G, Frantz S. Healing after myocardial infarction. Cardiovasc Res. 2005 Apr 1;66(1):22-32.
10. Sutton MG, and Sharpe N. Left ventricular remodeling after myocardial infarction: pathophysiology and therapy. Circulation 101: 2981-2988, 2000.
11. Olivetti G, Capasso JM, Sonnenblick EH, and Anversa P. Side-to-side slippage of myocytes participates in ventricular wall remodeling acutely after myocardial infarction in rats. Circ Res 67: 23-34, 1990.
12. Cleutjens JP, Kandala JC, Guarda E, Guntaka RV, and Weber KT. Regulation of collagen degradation in the rat myocardium after infarction. J Mol Cell Cardiol 27: 1281-1292, 1995.
13. Spinale FG. Matrix remodeling and the matrix metalloproteinases: Influence on cardiac form and function. Physiol Rev. 2007 Oct;87(4):1285-342.
14. Mukherjee R, Brinsa TA, Dowdy KB, Scott AA, Baskin JM, Deschamps AM, Lowry AS, Escobar GP, Lucas DG, Yarbrough WM, Zile MR, Spinale FG. Myocardial infarct expansion and matrix metalloproteinase inhibition. Circulation 2003 Feb 4; 107(4): 618-25
15. Wilson EM, Moainie SL, Baskin JM, Lowry AS, Deschamps AM, Mukherjee R, Guy TS, St, John-Sutton MG, Gorman JH, Edmunds LH, Gorman RC, Spinale FG. Region and species specific induction of matrix metalloproteinases occurs with post-myocardial infarction remodeling. Circulation, 2003 Jun 10;107(22):2857-63
16. Ikonomidis JS, Hendrick JW, Parkhurst AM, Herron AR, Escobar PG, Dowdy KB, Hapke E, Zile MR, Spinale FG. Accelerated LV remodeling post MI in mice deficient of TIMP-1: effects of exogenous matrix metalloproteinase inhibition. Am J Physiol, 2005 Jan;288 (1):H149-58
17. Matsumura S, Iwanaga S, Mochizuki S, Okamoto H, Ogawa S, and Okada Y. Targeted deletion or pharmacological inhibition of MMP-2 prevents cardiac rupture after myocardial infarction in mice. J Clin Invest 115: 599-609, 2005.
18. Ducharme A, Frantz S, Aikawa M, Rabkin E, Lindsey M, Rohde LE, Schoen FJ, Kelly RA, Werb Z, Libby P, and Lee RT. Targeted deletion of matrix metalloproteinase-9 attenuates left ventricular enlargement and collagen accumulation after experimental myocardial infarction. J Clin Invest 106: 55-62, 2000.

19. Heymans S, Luttun A, Nuyens D, Theilmeier G, Creemers E, Moons L, Dyspersin GD, Cleutjens JP, Shipley M, Angellilo A, Levi M, Nube O, Baker A, Keshet E, Lupu F, Herbert JM, Smits JF, Shapiro SD, Baes M, Borgers M, Collen D, Daemen MJ, and Carmeliet P. Inhibition of plasminogen activators or matrix metalloproteinases prevents cardiac rupture but impairs therapeutic angiogenesis and causes cardiac failure. Nat Med 5: 1135-1142, 1999.

20. Rohde LE, Ducharme A, Arroyo LH, Aikawa M, Sukhova GH, Lopez-Anaya A, McClure KF, Mitchell PG, Libby P, and Lee RT. Matrix metalloproteinase inhibition attenuates early left ventricular enlargement after experimental myocardial infarction in mice. Circulation 99: 3063-3070, 1999.

21. Spinale FG, Koval CN, Deschamps AM, Stroud RE, Ikonomidis JS. Dynamic changes in matrix metalloproteinase activity within the human myocardial interstitium during ischemia reperfusion. Circulation. 2008 Sep 30;118:S16-23. PMCID: PMC2663795.

22. Webb CS, Bonnema DD, Ahmed SH, Leonardi AH, McClure CD, Clark LL, Stroud RE, Corn WC, Finklea L, Zile MR, Spinale FG. Specific temporal profile of matrix metalloproteinase release occurs in patients following myocardial infarction: relation to left ventricular remodeling. Circulation, 2006 Sept 5; 114(10):1020-7

23. Kai H, Ikeda H, Yasukawa H, Kai M, Seki Y, Kuwahara F, Ueno T, Sugi K, and Imaizumi T. Peripheral blood levels of matrix metalloproteases-2 and -9 are elevated in patients with acute coronary syndromes. J Am Coll Cardiol 32: 368-372, 1998.

24. Inoue T, Kato T, Takayanagi K, Uchida T, Yaguchi I, Kamishirado H, Morooka S, and Yoshimoto N. Circulating matrix metalloproteinase-1 and -3 in patients with an acute coronary syndrome. Am J Cardiol 92: 1461-1464, 2003.

25. Squire IB, Evans J, Ng LL, Loftus IM, and Thompson MM. Plasma MMP-9 and MMP-2 following acute myocardial infarction in man: correlation with echocardiographic and neurohumoral parameters of left ventricular dysfunction. J Card Fail 10: 328-333, 2004.

26. Overall CM, Tam EM, Kappelhoff R, Connor A, Ewart T, Morrison CJ, Puente X, Lopez-Otin C, and Seth A. Protease degradomics: mass spectrometry discovery of protease substrates and the CLIP-CHIP, a dedicated DNA microarray of all human proteases and inhibitors. Biol Chem 385: 493-504, 2004.

27. Woessner JF, Jr., and Nagase H. Protein substrates of the MMPs. In: Matrix Metalloproteinases and TIMPs. 87-97, 2000.

28. Deschamps AM, Yarbrough WM, Squires CE, Allen RA, Dowdy KB, McLean JE, Mingoia JT, Sample, JA, Mukherjee R, Spinale FG. Trafficking of the membrane type-1 matrix metalloproteinase (MT1-MMP) in ischemia and reperfusion: relation to interstitial MT1-MMP activity. Circulation, 2005 Mar 8;111(9):1166-74.

29. Fingleton B. Matrix metalloproteinases as valid clinical targets. Curr Pharm Des. 2007;13(3):333-46.

30. Dormán G, Cseh S, Hajdú I, Barna L, Kónya D, Kupai K, Kovács L, Ferdinandy P. Matrix metalloproteinase inhibitors: a critical appraisal of design principles and proposed therapeutic utility. Drugs. 2010 May 28;70(8):949-64.

31. Dormán G, Kocsis-Szommer K, Spadoni C, Ferdinandy P. MMP inhibitors in cardiac diseases: an update. Recent Pat Cardiovasc Drug Discov. 2007 Nov;2(3):186-94.

32. Peterson JT. Matrix metalloproteinase inhibitor development and the remodeling of drug discovery. Heart Fail Rev. 2004 Jan;9(1):63-79.

33. Brew K, Dinakarpandian D, and Nagase H. Tissue inhibitors of metalloproteinases: evolution, structure and function. Biochim Biophys Acta 1477: 267-283, 2000.

34. Chirco R, Liu XW, Jung KK, and Kim HR. Novel functions of TIMPs in cell signaling. Cancer Metastasis Rev 25: 99-113, 2006.

35. Gomis-Ruth FX, Maskos K, Betz M, Bergner A, Huber R, Suzuki K, Yoshida N, Nagase H, Brew K, Bourenkov GP, Bartunik H, and Bode W. Mechanism of inhibition of the human matrix metalloproteinase stromelysin-1 by TIMP-1. Nature 389: 77-81, 1997.

36. Lovelock JD, Baker AH, Gao F, Dong JF, Bergeron AL, McPheat W, Sivasubramanian N, and Mann DL. Heterogeneous effects of tissue inhibitors of matrix metalloproteinases on cardiac fibroblasts. Am J Physiol Heart Circ Physiol 288: H461-468, 2005.
37. Zhao H, Bernardo MM, Osenkowski P, Sohail A, Pei D, Nagase H, Kashiwagi M, Soloway PD, DeClerck YA, and Fridman R. Differential inhibition of membrane type 3 (MT3)-matrix metalloproteinase (MMP) and MT1-MMP by tissue inhibitor of metalloproteinase (TIMP)-2 and TIMP-3 regulates pro-MMP-2 activation. J Biol Chem 279: 8592-8601, 2004.
38. Oelmann E, Herbst H, Zuhlsdorf M, Albrecht O, Nolte A, Schmitmann C, Manzke O, Diehl V, Stein H, and Berdel WE. Tissue inhibitor of metalloproteinases 1 is an autocrine and paracrine survival factor, with additional immune-regulatory functions, expressed by Hodgkin/Reed-Sternberg cells. Blood 99: 258-267, 2002.
39. Tian H, Cimini M, Fedak PW, Altamentova S, Fazel S, Huang ML, Weisel RD, Li RK. TIMP-3 deficiency accelerates cardiac remodeling after myocardial infarction. J Mol Cell Cardiol. 2007 Dec;43(6):733-43.
40. Fedak PW, Smookler DS, Kassiri Z, Ohno N, Leco KJ, Verma S, Mickle DA, Watson KL, Hojilla CV, Cruz W, Weisel RD, Li RK, Khokha R. TIMP-3 deficiency leads to dilated cardiomyopathy. Circulation. 2004 Oct 19;110(16):2401-9.
41. Kassiri Z, Defamie V, Hariri M, Oudit GY, Anthwal S, Dawood F, Liu P, Khokha R. Simultaneous transforming growth factor beta-tumor necrosis factor activation and cross-talk cause aberrant remodeling response and myocardial fibrosis in Timp3-deficient heart. J Biol Chem. 2009 Oct 23;284(43):29893-904.
42. Leco KJ, Khokha R, Pavloff N, Hawkes SP, and Edwards DR. Tissue inhibitor of metalloproteinases-3 (TIMP-3) is an extracellular matrix-associated protein with a distinctive pattern of expression in mouse cells and tissues. J Biol Chem 269: 9352-9360, 1994.
43. Yu WH, Yu S, Meng Q, Brew K, Woessner JF Jr. TIMP-3 binds to sulfated glycosaminoglycans of the extracellular matrix. J Biol Chem. 2000 Oct 6;275(40):31226-32. PMID: 10900194.
44. Amour A, Slocombe PM, Webster A, Butler M, Knight CG, Smith BJ, Stephens PE, Shelley C, Hutton M, Knauper V, Docherty AJ, and Murphy G. TNF-alpha converting enzyme (TACE) is inhibited by TIMP-3. FEBS Lett 435: 39-44, 1998.
45. Yang TT, and Hawkes SP. Role of the 21-kDa protein TIMP-3 in oncogenic transformation of cultured chicken embryo fibroblasts. Proc Natl Acad Sci U S A 89: 10676-10680, 1992.
46. Tous E, Purcell BP, Ifkovits JL, Burdick JA, Injectable Acellular Hydrogels for Cardiac Repair, *Journal of Cardiovascular Translational Research,* 4:528-542, 2011.
47. Ifkovits JL, Tous E, Minakawa M, Morita M, Robb JD, Koomalsingh KJ, Gorman JH 3rd, Gorman RC, Burdick JA. Injectable hydrogel properties influence infarct expansion and extent of postinfarction left ventricular remodeling in an ovine model. Proc Natl Acad Sci U S A. 2010 Jun 22;107(25):11507-12.
48. Tous E, Ifkovits JL, Koomalsingh KJ, Shuto T, Soeda T, Kondo N, Gorman JH, Gorman RC, Burdick JA, Influence of Injectable Hyaluronic Acid Hydrogel Degradation Behavior on Infarction Induced Ventricular Remodeling, *Biomacromolecules*, 12:4127-4135, 2011.
49. Burdick JA and Prestwich G, Hyaluronic Acid Hydrogels for Biomedical Applications, *Advanced Materials*, 23:H41-H56, 2011.
50. Mukherjee R, Zavadzkas JA, Saunders SM, McLean JE, Jeffords LB, Stroud RE, Leone AM, Koval CN, Rivers WT, Basu S, Sheehy A, Michal G, Spinale FG. Targeted myocardial microinjections of a biocomposite material reduces infarct expansion in pigs. Ann Thorac Surg. 2008 Oct;86(4):1268-76. PMCID: PMC2664621.
51. Dixon JA, Gorman RC, Stroud RE, Mukherjee R, Meyer EC, Baker NL, Morita M, Hamamoto H, Ryan LP, Gorman JH 3rd, Spinale FG. Targeted regional injection of biocomposite microspheres alters post-myocardial infarction remodeling and matrix proteolytic pathways. Circulation. 2011 Sep 13;124(11 Suppl):S35-45. PMID: 21911817
52. Pavloff N, Staskus PW, Kishnani NS, Hawkes SP. A new inhibitor of metalloproteinases

from chicken: ChIMP-3. A third member of the TIMP family. J Biol Chem. 1992 Aug 25;267(24):17321-6. PMID: 1512267.

53. Mukherjee R, Rivers WT, Ruddy JM, Matthews RG, Koval CN, Plyler RA, Chang EI, Patel RK, Kern CB, Stroud RE, Spinale FG. Long-term localized high frequency electrical stimulation within the myocardial infarct: effects on matrix metalloproteinases and regional remodeling. Circulation, 2010 July 6;122(1):20-32. PMCID: PMC2946370.

54. Dixon JA, Spinale FG. Large animal models of heart failure: a critical link in the translation of basic science to clinical practice. Circ Heart Fail. 2009 May;2(3):262-71. PMID: 19808348.

55. Spinale FG, Coker ML, Heung LJ, Bond BR, Gunasinghe HR, Etoh T, Goldberg AT, Zellner JL, Crumbley AJ. A matrix metalloproteinase induction/activation system exists in the human left ventricular myocardium and is upregulated in heart failure. Circulation. 2000 Oct 17;102(16):1944-9. PMID: 11034943.

56. Kleiner DE Jr, Unsworth EJ, Krutzsch HC, Stetler-Stevenson WG. Higher-order complex formation between the 72-kilodalton type IV collagenase and tissue inhibitor of metalloproteinases-2. Biochemistry. 1992 Feb 18;31(6):1665-72. PMID: 1310615.

57. Liu YE, Wang M, Greene J, Su J, Ullrich S, Li H, Sheng S, Alexander P, Sang QA, Shi YE. Preparation and characterization of recombinant tissue inhibitor of metalloproteinase 4 (TIMP-4). J Biol Chem. 1997 Aug 15;272(33):20479-83. PMID: 9252358.

58. Hinz B, Gabbiani G. Cell-matrix and cell-cell contacts of myofibroblasts: role in connective tissue remodeling. Thromb Haemost. 2003 Dec;90(6):993-1002. PMID: 14652629.

59. Eyden B. The myofibroblast: an assessment of controversial issues and a definition useful in diagnosis and research. Ultrastruct Pathol. 2001 Jan-Feb;25(1):39-50. PMID: 11297318.

60. Lee DC, Oz MC, Weinberg AD, Ting W. Appropriate timing of surgical intervention after transmural acute myocardial infarction. J Thorac Cardiovasc Surg. 2003 Jan;125(1):115-9; discussion 119-20. PMID: 12538993.

CHAPTER 7

Incorporation of sulfated hyaluronic acid macromers into degradable hydrogels for controlled presentation of proteins through electrostatic interactions

7.1. Introduction

Hyaluronic acid (HA) based hydrogels have been used widely in recent years for applications in drug delivery and tissue engineering[1]. HA is a ubiquitous biological polymer composed of repeating D-glucuronic acid [β-1-3] and N-acetyl-D-glucosamine [β-1-4] disaccharides and is found abundantly in the extracellular matrix (ECM) of tissues. During endogenous tissue remodeling, HA plays a critical role in regulating cell motility through CD44 receptor interactions and provides a hydrated microenvironment for growth factor and cytokine stability and diffusion[2].

HA is unique among glycosaminoglycans (GAGs) in that it is produced and secreted from cells as a linear polymer unattached to a polypeptide. This feature makes HA production amendable to typical genetic engineering approaches using microbial fermentation[3]. These recombinant HAs are nonimmunogenic, available in a wide range of well-defined molecular weights, and have been used in numerous biomedical applications. Further, due to the abundance of hydroxyl and carboxylic acid groups, HA is readily modified with reactive groups to form hydrogels[1]. In particular, modification of HA with vinyl groups permits gel formation through free-radical initiated crosslinking. This approach has allowed spatiotemporal control of network architectures to direct stem cell differentiation *in vitro*[4,5], as well as *in situ* gelation to localize therapeutic protein delivery *in vivo*[6].

While protein binding to vinyl modified HA macromers has been observed[6], HA lacks the sulfate groups typically associated with high protein-

ECM binding affinities. For example, heparin has been shown to bind, stabilize, and in some cases enhance the activity of hundreds of heparin binding proteins (HBPs) through electrostatic interaction between sulfates and basic amino acid residues[7]. These interactions are critical to regulating tissue remodeling processes by localizing HBP activity in a temporally controlled fashion (i.e., HBP presentation)[8,9]. A variety of conjugation techniques have been developed to covalently incorporate heparin into scaffolds, and these systems have been used to control HBP presentation and subsequent cellular processes[10-12]. However, since heparin is normally present in tissues attached to a core protein (i.e., proteoglycan), production of heparin is limited to crude isolation from animal tissues. As a result, commercially available heparin is a heterogeneous distribution of polysaccharides with diverse protein binding specificities and some polysaccharide contaminants found in heparin have caused a sudden increase of severe side effects in patients undergoing antithrombotic treatment[13].

To minimize contaminants and provide a higher level of HBP specificity, there has been a growing interest in producing well-defined heparin mimetics through synthetic routes[14]. Heparin mimetics are highly sulfated polymers that are structurally distinct from naturally occurring GAGs, but perform some of the same functions as heparin (e.g., HBP binding)[7]. These sulfated polymers have been shown to bind HBPs with high affinity and when delivered *in vivo* they significantly enhance tissue repair, presumably by replacing degraded heparin and increasing the bioavailability of HBPs[15]. While HA is unique among GAGs in that it lacks sulfate groups, researchers have demonstrated synthetic sulfation of HA through nucleophilic substitution of primary hydroxyl hydrogens on HA with SO_3 by simply reacting SO_3 complexes with HA in an organic solvent[16-18]. Reaction of an SO_3/DMF complex with HA results in a specific sulfation pattern that binds HBPs with a high affinity[17,19]. Further, sulfated HA polymers exhibit good cytocompatibility and enhance HBP presentation to cells *in vitro*[20]. Also, sulfated HA polymers themselves have been shown to influence cell activity *in vitro* including stimulating Wnt and Notch signaling[16], as well as increasing cell-

cell junctions[18]. However, sulfated HA has not previously been modified for covalent incorporation into hydrogels to alter features such as protein interactions and diffusion.

Here, we synthesized sulfated and vinyl modified HA macromers to incorporate protein-binding features into radically crosslinked HA hydrogels. Further, we incorporated hydrolytically unstable ester groups between the reactive vinyl group and the sulfated HA backbone to liberate bound proteins in a controlled fashion. We show that these macromers bind a HBP with an affinity comparable to heparin, can be readily incorporated into unsulfated HA hydrogels without significantly altering hydrogel crosslinking, and therefore can be used to control the presentation of HBPs for drug delivery and tissue engineering applications.

7.2. Methods

Materials.

Sodium hyaluronate (NaHy) was purchased from Lifecore (100 and 440 kDa, as measured with GPC). ELISA kit and reagents were purchased from R&D Systems. Recombinant human TIMP-3 with a 6x His tag was provided as a gift from Amgen, Inc. Anti-6x His antibodies were purchased from Abcam. Heparin binding plates were purchased from BD Biosciences. Polyethylene glycol standards were purchased from Waters. All other materials and chemicals were purchased from Sigma Aldrich.

Macromer Synthesis.

NaHy (100kDa) was chemically modified with a hydroxyethyl methacrylate (HEMA) group to incorporate methacrylate reactivity for free-radical initiated crosslinking, as well as hydrolytic degradation through ester group hydrolysis as previously described[6]. Briefly, HEMA was reacted with succinic anhydride via a ring opening polymerization in the presence of N-methylimidazole to obtain HEMA-COOH, which was then coupled to a tetrabutylammonium (TBA) salt of

116

HA in the presence of 4-dimethylaminopyridine (DMAP) and di-tert-butyl dicarbonate (BOC$_2$O). The resulting HA macromer with HEMA group modification (HEMA-HA) was purified with dialysis and characterized by ^{1}H NMR.

For HEMA-SHA synthesis, a 440kDa NaHy was first synthesized to HEMA-HA as described above and then converted to a TBA salt through resin exchange (Dowex 50x8w hydrogen form) and TBA-OH titration to pH 7.02 to permit polymer solubility in DMF for the sulfation reaction. HEMA-HA TBA was then frozen and lyophilized. Dry HEMA-HA TBA was dissolved in N,N-dimethylformimide (DMF) at 0.25% (w/v) under N$_2$ at room temperature (RT). SO$_3$/DMF complex in DMF solution (10% (w/v)) was added to the reaction at a 20:1 (mol/mol) SO$_3$/DMF:HA repeat unit ratio and reacted for 1 hr at RT under N$_2$. The reaction solution was then dialyzed against DI H$_2$O for 14 days at 4°C to remove solvent and TBA salts, frozen and lyophilized.

Gel Permeation Chromatography.

Molecular weights were determined with gel permeation chromatography (GPC) analysis using a Waters 1525 Binary HPLC Pump, Waters 2414 Refractive Index (RI) Detector, and Waters Ultrahydrogel 1000 columns. The eluent was PBS buffer and the flow rate was 0.5 mL/min. Size calibrations for molecule weight determination were made with polyethylene glycol standards (Polymer Standard Services USA, Inc).

Zeta Potential Measurements.

Polymers were dissolved in MilliQ H$_2$O at 3.5wt% for HEMA-HA and 4wt% for HEMA-SHA and loaded into folded capillary cells (Malvern). Zeta Potential measurements were made on a ZetaSizer Nano ZS (Malvern).

Dimethylmethylene Blue Assay.

Serial dilutions of each polymer were prepared in MilliQ H$_2$O (50µg/mL→0µg/mL) and assayed for the presence of sulfate groups using a

previously developed dimethylmethylene blue (DMMB) assay[21]. Absorbance at 520 nm was measured using a cuvette reader (Tecan). To visualize sulfate groups, 50µL hydrogels were formed (see subsequent methods), washed for 2 days in PBS, incubated in DMMB solution overnight at 37°C, rinsed and photographed.

Solid-phase Binding Assay.

HEMA-HA, HEMA-SHA and heparin at 2.5µM in PBS were coated overnight at 25°C onto heparin binding plates (BD Life Sciences)[22]. Wells were washed in TNC buffer (50 mM Tris/HCl, 150 mM NaCl, 10 mM $CaCl_2$, 0.05 % Brij-35 and 0.02 % sodium azide) containing 0.1 % Tween 20 between each subsequent incubation. Wells were blocked with 0.2% gelatin in TNC buffer and then incubated with rTIMP-3-His (0.02-3µg/mL in blocking solution for 3 h at 37°C). Bound rTIMP-3-His was detected using a biotin labeled antibody against the 6xHis tag on rTIMP-3 (Abcam, ab27025, 3 hr incubation at 37∘C), followed by streptavidin coupled to horseradish peroxidase (R&D Systems) for 1h at 37°C. Hydrolysis of a 1:1 mixture of H_2O_2 and tetramethylbenzidine (R&D Systems) was measured at 450 nm using a microplate reader (Tecan infinite m200).

Hydrogel Formation.

For crosslinking, a redox initiator system consisting of ammonium persulfate (APS) and N,N,N′,N′-tetramethylethylenediamine (TEMED) was utilized. APS and TEMED were mixed with polymers dissolved in phosphate buffered saline (PBS) to initiate crosslinking at final concentrations of 10mM APS, 10mM TEMED, and 4wt% (w/v) polymer. HEMA-HA/HEMA-SHA blends were formed by mixing different volumetric ratios of the respective polymers dissolved at the same concentrations in PBS. Kinetics of the crosslinking reaction were characterized with rheometry by monitoring the storage (G') and loss (G") moduli with time (20mm 1° cone geometry, 1% strain, 1Hz, TA Instruments AR 2000ex).

Hydrogel Swelling.

50µL hydrogels (4wt% polymer, 10mM APS/TEMED) were formed in cylindrical molds at 37°C for 30 min after mixing APS/TEMED initiators. Hydrogels were then incubated in PBS for 2 days at 37°C. Gel diameters were measured after 30 min crosslinking and again after 2 days in PBS. Swelling ratios were reported as a percent change in diameter after 2 days in PBS.

Protein Release Studies.

rTIMP-3 or FITC-BSA were dissolved in the polymer solutions at 10µg of protein/50µL gel. 50µL hydrogels (4wt% polymer, 10mM APS/TEMED) were formed in cylindrical molds at 37°C for 30 min after mixing APS/TEMED initiators. After a wash in PBS, hydrogels were incubated in PBS supplemented with 1% BSA (R&D Systems) at 37°C. Hydrogels were moved to fresh buffer every 2 days and samples were stored at -20°C until the end of the study. After the final time point, hydrogels were degraded in 0.3 mg/mL hyaluronidase to release remaining protein. FITC-BSA was quantified using fluorescence while rTIMP-3 was quantified using ELISA (R&D Systems).

Statistical Analysis.

Statistical comparisons between groups were performed with a two-tailed student's t-test, followed by a Bonferroni correction for multiple comparisons; $p<0.05$ were considered statistically significant for comparison between two groups, while $p<0.025$ were considered statistically significant for comparison between three groups. The results are reported as mean values ± standard deviations.

7.3. Results and Discussion

Sulfation of HEMA Modified HA.

HA has been previously modified with sulfate groups through nucleophilic substitution of primary hydroxyls along the HA backbone[17]. When the reaction

was performed with the SO_3/DMF complex at a 20:1 SO_3/DMF:HA ratio, a high degree of sulfation was observed, estimated at 2.8 sulfate groups per HA disaccharide, in a specific pattern that resulted in high protein binding affinities. We applied this sulfation reaction to our previously developed hydroxyethylmethacrylate (HEMA) modified HA (HEMA-HA) in order to incorporate protein-binding features into a degradable, radically crosslinked hydrogel. Using this strategy, sulfated HEMA-HA macromers (HEMA-SHA) could be blended with non-sulfated HEMA-HA macromers at any desired ratio and crosslinked using a variety of free-radical initiator systems (Figure 7.1). Further, the degradation kinetics of the system can be controlled through HEMA group modification to release bound proteins in a temporally controlled fashion.

HEMA-HA was synthesized as previously reported by first converting sodium hyaluronate (NaHy, 100kDa) to a tetrabutylammonium (TBA) salt and then coupling HEMA succinate to primary hydroxyls on HA through an esterification reaction[6] (Figure 7.2 A). The modification process decreased the number average molecular weight (M_n) of the HA polymer by 20% and slightly increased the HA polydispersity, as determined by GPC (Figure 7.2 B). The decrease in M_n is likely due to acid hydrolysis
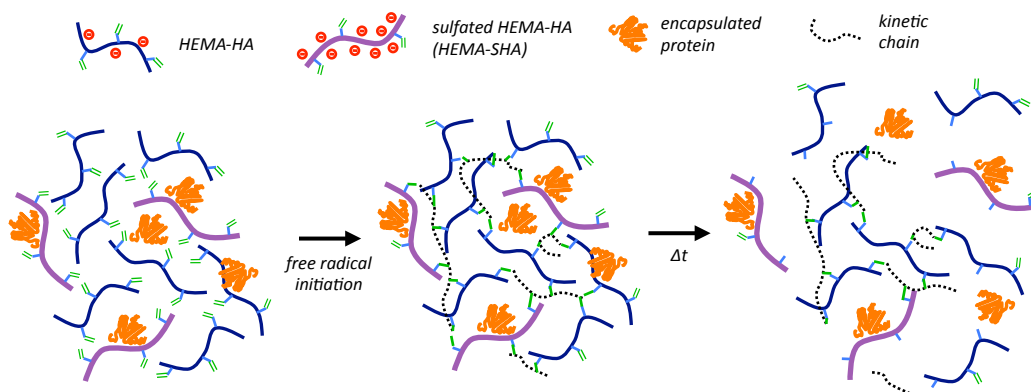

Figure 7.1. Incorporation of sulfated hyaluronic acid (HA) macromers into hydrogels through free-radical initiated crosslinking. Hydroxyethylmethacrylate (HEMA) modified HA macromers were synthesized with or without sulfate groups to control sulfated polymer concentration in hydrogels by simply blending the two macromers together and crosslinking with free-radical initiators. Release of encapsulated proteins in these networks is controlled by electrostatic interactions with the negatively charged polymers and by gel degradation through ester group hydrolysis of the HEMA crosslinks.

of the polysaccharide backbone during HA-TBA synthesis as a proton-rich exchange resin was used for protonation of NaHy. The final HEMA-HA had a M_n of ~80kDa and a HEMA modification of ~16%.

To synthesize HEMA-SHA, HEMA-HA was synthesized starting with NaHy of 440kDa and converted to a TBA salt through a protonated resin exchange. This step did not affect the HEMA modification as indicated by peak integration of vinyl protons on the methacrylate group (approximately 5.8 and 6.2 ppm) via ^{1}H NMR (Figure 7.3 A). Next, the TBA salt of HEMA-HA was reacted with SO_3 in DMF, which also did not affect HEMA modification as indicated by the vinyl proton integrations before and after the reaction (Figure 7.3 A). Also, there was an obvious shift in hydroxyl proton peaks along the HA backbone (approximately 3 to 4 ppm) following the sulfation reaction as expected due to substitution of these protons with sulfate groups (Figure 7.3 A).
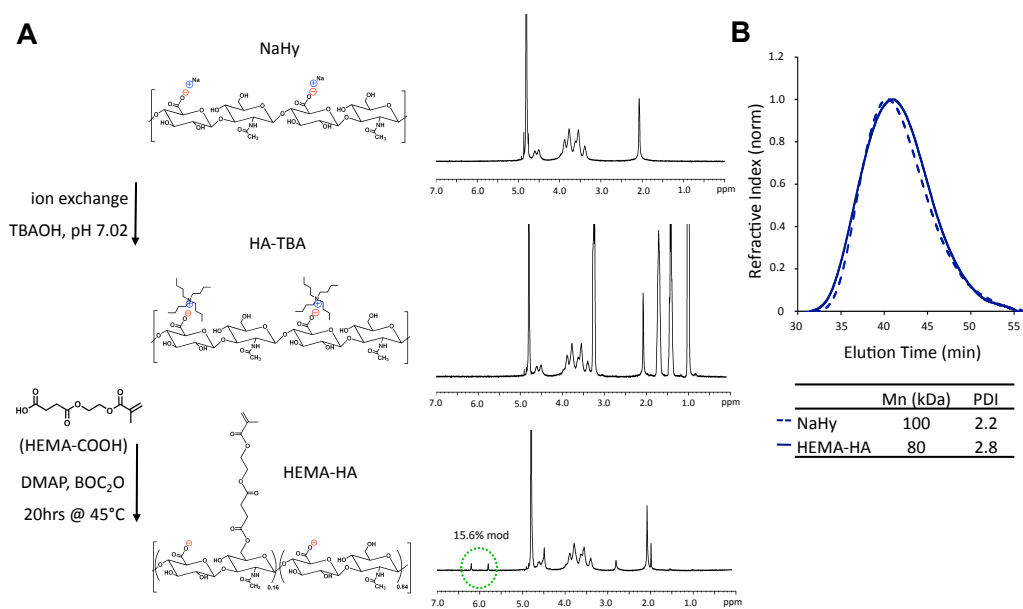

Figure 7.2. Synthesis of HEMA modified HA. (A) Sodium hyaluronate (NaHy) was converted to a tertbutylammonium (TBA) salt and reacted with HEMA-succinate in dimethyl sulfoxide using dimethylaminopyridine (DMAP)/di-tert-butyl dicarbonate (BOC$_2$O) catalyzed esterification. HEMA modification was quantified by methacrylate group ^{1}H NMR peaks (green circle). (B) This modification slightly reduced the number average molecular weight (M_n) and increased the polydispersity index (PDI) as measured with GPC when compared to unmodified NaHy.
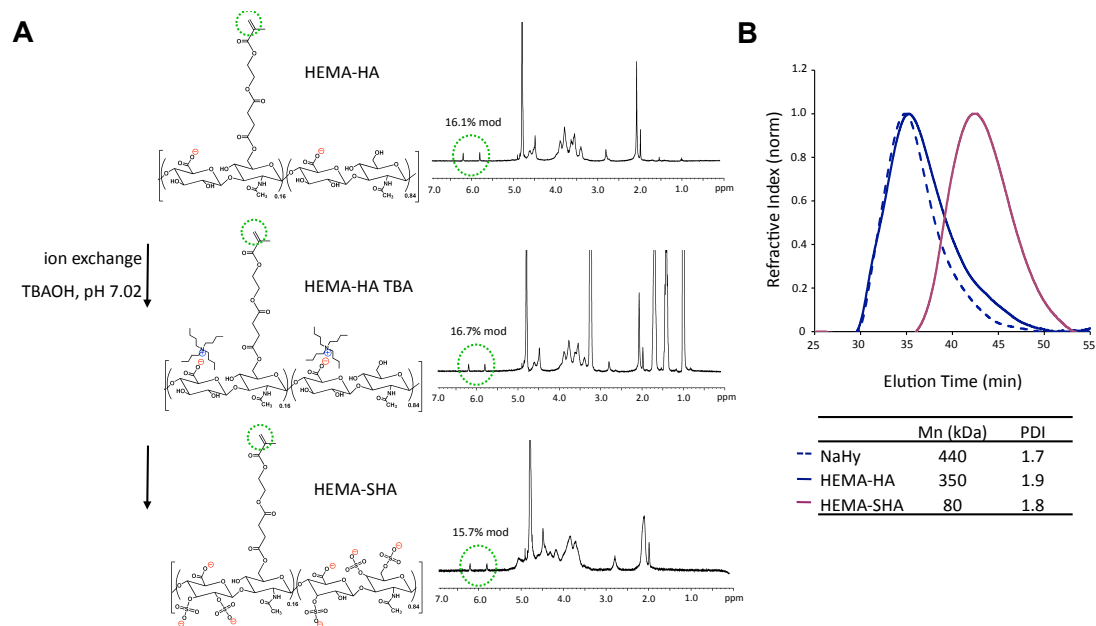
Figure 7.3. Synthesis of sulfated HEMA-HA. (A) HEMA-HA was converted to a TBA salt and reacted with SO_3/dimethylformamide (DMF) complex in DMF. This reaction altered hydroxyl group ^{1}H NMR peaks as expected, but did not affect methacrylate ^{1}H NMR peaks (green circles). (B) Sulfation reduced the M_n of HEMA-HA by almost 80% as measured by GPC, so a larger 440kDa NaHy was used to generate HEMA-SHA macromers with comparable M_n to HEMA-HA macromers (80kDa).

Although there was no change in HEMA modification (~16%) there was an expected and significant reduction of the macromer M_n following the sulfation reaction, which is likely due to acid hydrolysis of HA from H_2SO_4 formed from reaction of SO_3/DMF and water vapor, or from non-specific nucleophilic substitution (Figure 7.3 B). By starting with a 440kDa NaHy, the final M_n of HEMA-SHA was maintained at ~80kDa so that HEMA-HA and HEMA-SHA could be blended at approximately the same molecular weight and modification. Naturally sulfated GAGs are typically much smaller than 80kDa; therefore, our approach allows generation of sulfated and crosslinkable polymers with larger molecular weights for covalent incorporation into hydrogels. Using this approach, the sulfate group content within hydrogels can be easily controlled by blending sulfated and non-sulfated polymers at the desired ratios.

Sulfating HEMA-HA Alters Polymer Charge and Increases Binding to a HBP.

Heparin has been shown to bind hundreds of proteins through electrostatic interaction between negatively charged sulfate groups on heparin and positively charged amino acid residues on proteins[7]. While intermolecular forces such as hydrogen bonding and van der Waals interactions involving other chemistries on heparin have been shown to contribute to some highly specific binding events[23], charge interactions from sulfate groups are the major force driving heparin-protein binding[24]. Similarly, the addition of sulfate groups to HA has been shown to dramatically increase binding of proteins that are rich in basic amino acid residues[17,19]. While the degree of sulfation of HA was shown to directly correlate with protein binding affinity, oversulfation of polysaccharides can inhibit protein binding [25] and the distribution of sulfate groups along the polysaccharide is important in protein binding affinity[17,19].

The sulfate content on HEMA-SHA macromers was compared to HEMA-HA and heparin using a modified dimethylmethylene blue (DMMB) assay[21]. Using this assay, a significant increase in sulfate content was observed on HEMA-SHA compared to HEMA-HA, confirming success of the sulfation reaction (Figure 7.3 A). Further, the sulfate content on HEMA-SHA was comparable to that of heparin. To quantify the effect of the sulfate groups on polymer charge, an important contributor to protein binding affinity, zeta potentials of the polymers were measured from pH 2 to 10. HEMA-SHA polymers possessed a more negative charge when compared to HEMA-HA polymers across all pHs (Figure 7.3 B). Further, a clear difference was observed in the protonation states characteristic of sulfate groups on HEMA-SHA polymers compared to carboxylate groups on HEMA-HA polymers. The sulfate groups remained deprotonated across all pHs, while the carboxylate groups were protonated at lower pH.
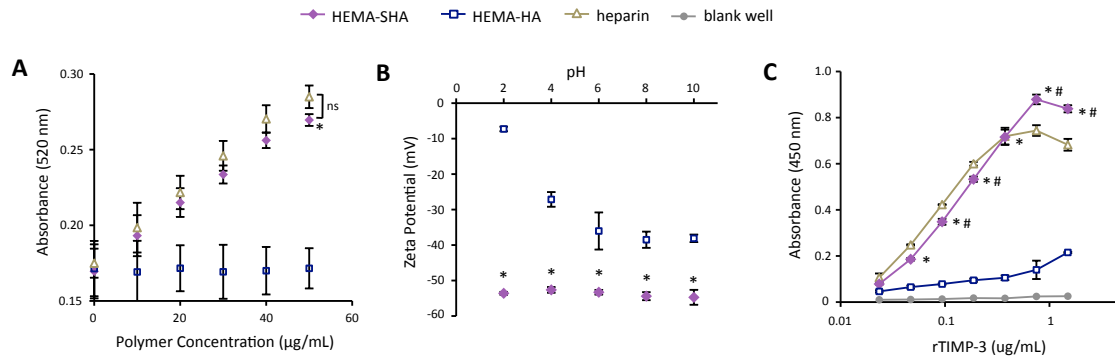
Figure 7.4. Characterization of HEMA-SHA macromers. (A) Sulfate content was significantly increased in HEMA-SHA macromers when compared to HEMA-HA macromers, as determined by dimethylmethylene blue assay. Sulfate content of HEMA-SHA macromers was comparable to that of heparin. (B) Addition of sulfate groups significantly enhanced the negative charge of carboxylic acid-containing HEMA-HA macromers via zeta potential measurements, and (C) significantly enhanced binding to the heparin binding TIMP-3 protein. TIMP-3 binding of HEMA-SHA macromers was comparable to that of heparin, though with a significantly different binding profile. (n=3 replicates per group, mean±SD, *p<0.025 compared to HEMA-HA, #p<0.025 compared to heparin).

To assess the protein-binding characteristics of the polymers, a recombinant tissue inhibitor of matrix metalloproteinases (TIMP-3) was used as a model HBP. TIMP-3 is unique among the four known TIMPs in that it binds sulfated polymers with a high affinity[26, 27]. It naturally associates with sulfated GAGs in the ECM, so matrix presentation is thought to be important in controlling TIMP-3 activity[28]. TIMP-3 was incubated in wells with polymers adsorbed to the surface and TIMP-3 bound to the polymer-coated wells was quantified using ELISA. Using this technique, a significant increase in TIMP-3 binding was observed with HEMA-SHA polymers compared to non-sulfated HEMA-HA polymers (Figure 7.3 C). Further, HEMA-SHA polymers had comparable TIMP-3 binding to heparin, although more TIMP-3 was bound to HEMA-SHA at higher TIMP-3 concentrations. This observation could be explained by the greater M_n of HEMA-SHA compared to heparin (80kDa vs. 20kDa by GPC) as both polymers were adsorbed to the wells at the same molar concentration. In addition, differences in the sulfation pattern could affect HBP binding. For example, Hintze and coworkers showed that sulfated HA binds human transforming growth factor beta-1 (TGF-β1) with a stronger affinity than synthetically sulfated

124

chondroitin sulfate, despite having the same degree of sulfation[19]. Further, sulfated HA was shown to have different binding specificities for human plasma proteins than heparin[29]. Therefore, while HEMA-SHA was shown to bind a HBP (TIMP-3) in this study, further investigation into protein binding specificity of HEMA-SHA polymers is warranted for specific HBPs.

HEMA-SHA Incorporates into Radically Crosslinked Hydrogels and Alters HBP Presentation.

While a number of heparin mimetics have been developed as antithrombotic therapeutics, very few have been crosslinked into hydrogels for application in drug delivery or tissue engineering[30-32]. After demonstrating successful synthesis of a methacrylate modified and sulfated HA macromer and its ability to bind a HBP, we crosslinked these polymers into hydrogels to encapsulate and localize HBPs. HEMA-SHA polymers were blended with HEMA-HA polymers at 10% HEMA-SHA, 90% HEMA-HA with a total polymer concentration of 4 wt% (w/v), then crosslinking was initiated with APS and TEMED redox initiators. Rheometry was used to quantify gelation, and HEMA-SHA blended hydrogels were compared to 100% HEMA-HA hydrogels. Incorporation of 10% HEMA-SHA did not significantly alter gelation, as both groups had similar storage modulus (G') profiles over time and crosslinking reached the same G' plateau after 30 min (Figure 7.5 A-B). Other ratios were also investigated (higher HEMA-SHA content); however, they led to hydrogels with statistically different mechanical properties, likely due to extensive sulfate charge repulsion and were not pursued further (results now shown).

To visualize incorporation of sulfate groups into the HEMA-SHA blended hydrogels, they were incubated with DMMB after a 2-day wash in PBS. HEMA-SHA blended hydrogels exhibited a purple color compared to blue HEMA-HA hydrogels, indicating the presence of sulfate groups (Figure 7.5 C). Further, HEMA-SHA blended hydrogels swelled significantly more than HEMA-HA hydrogels, likely due to charge repulsion within the sulfate rich hydrogels or

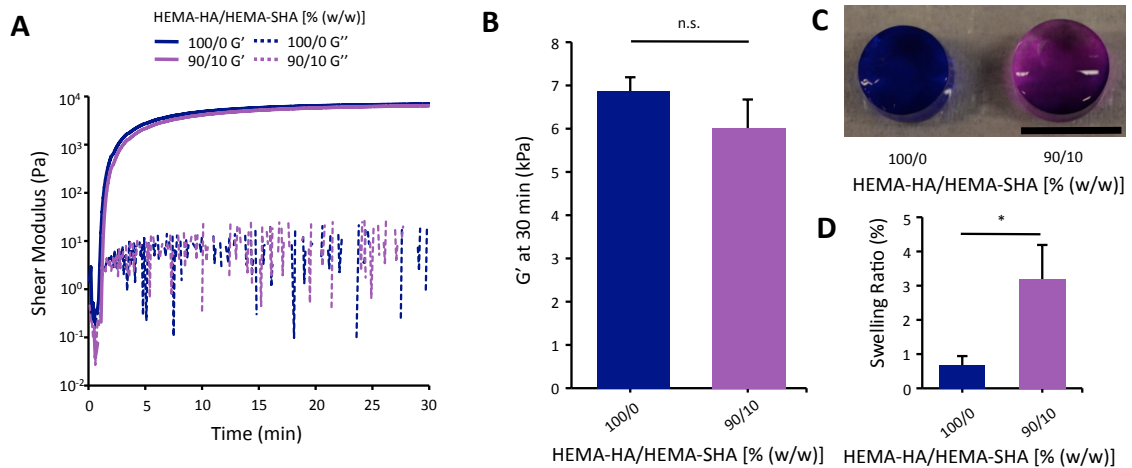increased water content due to sulfate hydrophilicity (Figure 7.5 D).

Figure 7.5. Crosslinking of HEMA-HA/HEMA-SHA hydrogels. HEMA-HA/HEMA-SHA hydrogels were crosslinked using APS/TEMED initiators and 4wt% macromers in PBS at 100/0 or 90/10 HEMA-HA/HEMA-SHA compositions (wt/wt). (A) Storage (G') and loss (G'') moduli profiles over time with and without 10% HEMA-SHA incorporation. (B) Incorporation of 10% HEMA-SHA did not significantly affect G' after crosslinking had reached a plateau at 30 min. (C) Incorporation of sulfate groups in the hydrogels was visualized using dimethylmethylene blue with purple indicative of sulfate groups (scale bar = 5mm). (D) Incorporation of sulfate groups slightly increased swelling of the hydrogels after 2 days in PBS. (n=3 replicates per group, mean±SD, *p<0.05 between groups).

Finally, to illustrate the influence of sulfate group incorporation on HBP presentation within the hydrogels, networks were formed that encapsulated either a model HBP, TIMP-3, or bovine serum albumin (BSA) and protein release and hydrogel degradation were monitored over 12 days. HEMA-SHA blended hydrogels degraded in a slightly more rapid fashion compared to HEMA-HA hydrogels (Figure 7.6 A). This observation is likely due to the increased water content of the hydrogels which enhances ester group hydrolysis of the HEMA groups. BSA release from HEMA-SHA blended hydrogels was significantly reduced from HEMA-HA hydrogel release; however, both release profiles were quite similar (~70% within 12 days), indicating little influence of sulfate groups on BSA presentation and release (Figure 7.6 B). This is not surprising as previous studies also found that albumin does not bind to sulfated HA with a high affinity[29]. However, TIMP-3 release was drastically reduced with incorporation of HEMA-

SHA polymers into the network (Figure 7.6 C). Less than 15% of the encapsulated TIMP-3 was released from HEMA-SHA blended hydrogels, whereas almost 60% was released from HEMA-HA alone hydrogels. This reduced release of TIMP-3 with the incorporation of HEMA-SHA polymers demonstrates our ability to control HBP presentation within covalently crosslinked and degradable hydrogels, simply through chemical modification of the gel precursors. This approach can be used with a variety of radically crosslinked scaffolds for drug delivery and tissue engineering applications.
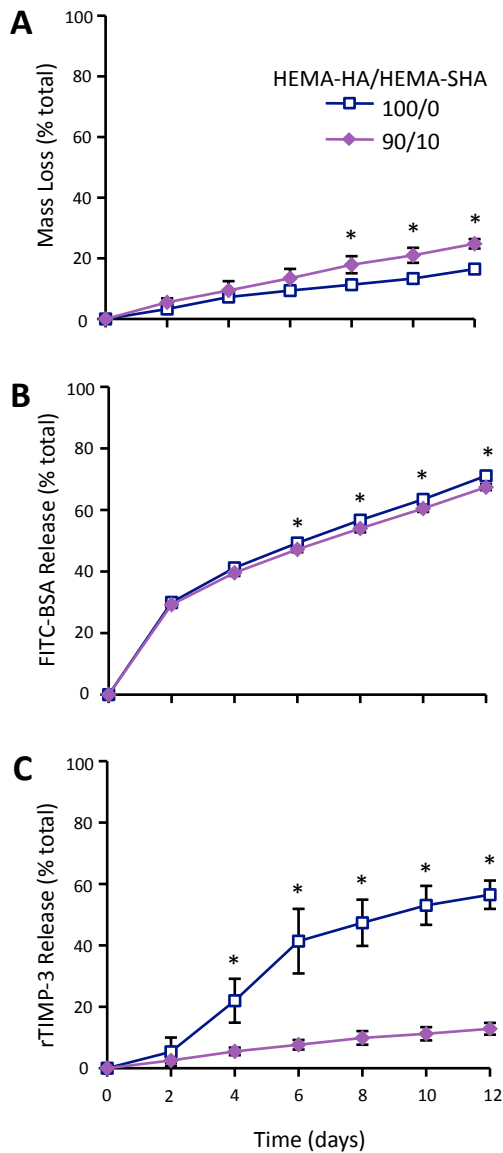
Figure 7.6. Gel degradation and encapsulated protein release. (A) Gel mass loss as determined by uronic acid content. Incorporation of HEMA-SHA macromers significantly enhanced hydrolytic degradation of the hydrogels over 2 weeks. Encapsulated FITC-BSA (B) and heparin-binding TIMP-3 (C) release from hydrogels of HEMA-HA alone or incorporating HEMA-SHA macromers. Encapsulated TIMP-3 release was reduced by over 40% with incorporation of HEMA-SHA macromers. (n=3 replicates per group, mean±SD, *$p<0.05$ between groups).

7.4. References

1. Burdick JA, Prestwich GD. Hyaluronic acid hydrogels for biomedical applications. *Adv Mater*.23:H41-56
2. Laurent TC, Fraser JR. Hyaluronan. *FASEB J*. 1992;6:2397-2404
3. Yamada T, Kawasaki T. Microbial synthesis of hyaluronan and chitin: New approaches. *J Biosci Bioeng*. 2005;99:521-528
4. Guvendiren M, Burdick JA. Stiffening hydrogels to probe short- and long-term cellular responses to dynamic mechanics. *Nat Commun*.3:792
5. Khetan S, Guvendiren M, Legant WR, Cohen DM, Chen CS, Burdick JA. Degradation-mediated cellular traction directs stem cell fate in covalently crosslinked three-dimensional hydrogels. *Nat Mater*.12:458-465
6. Purcell BP, Elser JA, Mu A, Margulies KB, Burdick JA. Synergistic effects of sdf-1alpha chemokine and hyaluronic acid release from degradable hydrogels on directing bone marrow derived cell homing to the myocardium. *Biomaterials*.33:7849-7857
7. *Heparin - a century of progress*. New York: Springer.
8. Raghow R. The role of extracellular matrix in postinflammatory wound healing and fibrosis. *FASEB J*. 1994;8:823-831
9. Ilan N, Elkin M, Vlodavsky I. Regulation, function and clinical significance of heparanase in cancer metastasis and angiogenesis. *Int J Biochem Cell Biol*. 2006;38:2018-2039
10. Sakiyama-Elbert SE, Hubbell JA. Development of fibrin derivatives for controlled release of heparin-binding growth factors. *J Control Release*. 2000;65:389-402
11. Nie T, Baldwin A, Yamaguchi N, Kiick KL. Production of heparin-functionalized hydrogels for the development of responsive and controlled growth factor delivery systems. *J Control Release*. 2007;122:287-296
12. Nakamura S, Ishihara M, Obara K, Masuoka K, Ishizuka T, Kanatani Y, Takase B, Matsui T, Hattori H, Sato T, Kariya Y, Maehara T. Controlled release of fibroblast growth factor-2 from an injectable 6-o-desulfated heparin hydrogel and subsequent effect on in vivo vascularization. *J Biomed Mater Res A*. 2006;78:364-371
13. Guerrini M, Beccati D, Shriver Z, Naggi A, Viswanathan K, Bisio A, Capila I, Lansing JC, Guglieri S, Fraser B, Al-Hakim A, Gunay NS, Zhang ZQ, Robinson L, Buhse L, Nasr M, Woodcock J, Langer R, Venkataraman G, Linhardt RJ, Casu B, Torri G, Sasisekharan R. Oversulfated chondroitin sulfate is a contaminant in heparin associated with adverse clinical events. *Nature Biotechnology*. 2008;26:669-675
14. Gandhi NS, Mancera RL. Heparin/heparan sulphate-based drugs. *Drug Discov Today*.15:1058-1069
15. Petit E, Papy-Garcia D, Muller G, Courtois B, Caruelle JP, Courtois J. Controlled sulfatation of natural anionic bacterial polysaccharides can yield agents with specific regenerating activity in vivo. *Biomacromolecules*. 2004;5:445-452
16. Nagira T, Nagahata-Ishiguro M, Tsuchiya T. Effects of sulfated hyaluronan on keratinocyte differentiation and wnt and notch gene expression. *Biomaterials*. 2007;28:844-850
17. Hintze V, Moeller S, Schnabelrauch M, Bierbaum S, Viola M, Worch H, Scharnweber D. Modifications of hyaluronan influence the interaction with human bone morphogenetic protein-4 (hbmp-4). *Biomacromolecules*. 2009;10:3290-3297
18. Yamada T, Sawada R, Tsuchiya T. The effect of sulfated hyaluronan on the morphological transformation and activity of cultured human astrocytes. *Biomaterials*. 2008;29:3503-3513
19. Hintze V, Miron A, Moeller S, Schnabelrauch M, Wiesmann HP, Worch H, Scharnweber D. Sulfated hyaluronan and chondroitin sulfate derivatives interact differently with human transforming growth factor-beta1 (tgf-beta1). *Acta Biomater*.8:2144-2152
20. Hempel U, Hintze V, Moller S, Schnabelrauch M, Scharnweber D, Dieter P. Artificial extracellular matrices composed of collagen i and sulfated hyaluronan with adsorbed transforming growth factor beta1 promote collagen synthesis of human mesenchymal stromal cells. *Acta Biomater*.8:659-666

21.   Farndale RW, Buttle DJ, Barrett AJ. Improved quantitation and discrimination of sulphated glycosaminoglycans by use of dimethylmethylene blue. *Biochim Biophys Acta*. 1986;883:173-177

22.   Mahoney DJ, Whittle JD, Milner CM, Clark SJ, Mulloy B, Buttle DJ, Jones GC, Day AJ, Short RD. A method for the non-covalent immobilization of heparin to surfaces. *Anal Biochem*. 2004;330:123-129

23.   Bourin MC, Lindahl U. Glycosaminoglycans and the regulation of blood coagulation. *Biochem J*. 1993;289 (Pt 2):313-330

24.   Maccarana M, Casu B, Lindahl U. Minimal sequence in heparin/heparan sulfate required for binding of basic fibroblast growth factor. *J Biol Chem*. 1993;268:23898-23905

25.   Powell AK, Fernig DG, Turnbull JE. Fibroblast growth factor receptors 1 and 2 interact differently with heparin/heparan sulfate. Implications for dynamic assembly of a ternary signaling complex. *J Biol Chem*. 2002;277:28554-28563

26.   Yu WH, Yu S, Meng Q, Brew K, Woessner JF, Jr. Timp-3 binds to sulfated glycosaminoglycans of the extracellular matrix. *J Biol Chem*. 2000;275:31226-31232

27.   Troeberg L, Mulloy B, Ghosh P, Lee MH, Murphy G, Nagase H. Pentosan polysulfate increases affinity between adamts-5 and timp-3 through formation of an electrostatically driven trimolecular complex. *Biochem J*.443:307-315

28.   Leco KJ, Khokha R, Pavloff N, Hawkes SP, Edwards DR. Tissue inhibitor of metalloproteinases-3 (timp-3) is an extracellular matrix-associated protein with a distinctive pattern of expression in mouse cells and tissues. *J Biol Chem*. 1994;269:9352-9360

29.   Satoh TN, K; Nagahata, M; Teramoto, A; Abe, K. The research on physiological property of functionalized hyaluronan: Interaction between sulfated hyaluronan and plasma proteins. *Polym. Adv. Technol.* 2004;15:720-725

30.   Kim SH, Kiick KL. Heparin-mimetic sulfated peptides with modulated affinities for heparin-binding peptides and growth factors. *Peptides*. 2007;28:2125-2136

31.   Freeman I, Kedem A, Cohen S. The effect of sulfation of alginate hydrogels on the specific binding and controlled release of heparin-binding proteins. *Biomaterials*. 2008;29:3260-3268

32.   Chang CW, Hwang Y, Brafman D, Hagan T, Phung C, Varghese S. Engineering cell-material interfaces for long-term expansion of human pluripotent stem cells. *Biomaterials*.34:912-921

CHAPTER 8

On-demand delivery of TIMP-3 from matrix metalloproteinase degradable hydrogels attenuates post myocardial infarction remodeling

8.1. Introduction

Excessive extracellular matrix (ECM) proteolysis by matrix metalloproteinases (MMPs) is a hallmark of many human disease states including chronic inflammation, tumor progression, and cardiovascular disease[1]. MMPs hydrolyze peptide bonds with a high level of amino acid specificity and regulation. Under normal physiological conditions, MMP activity is precisely controlled to maintain a low level of structural protein, cell receptor, and growth factor turnover. However, following a stimulus such as an injury, there is a loss of control over MMP activity which causes maladaptive changes to tissue architectures and functions, often resulting in the progression of disease[2].   For example, MMP levels are elevated in patients following a myocardial infarction (MI) and are associated with adverse left ventricle (LV) remodeling[3]. Increased MMP activity was directly measured within the human myocardium following myocardial arrest and reperfusion[4]. Further, experimental models involving transgenic deletion of specific MMPs and systemic administration of pharmacologic MMP inhibitors have demonstrated that MMPs are important contributors to multiple aspects of adverse global LV remodeling including LV wall thinning, volume dilation, and ultimately dysfunction[5-8]. While systemic administration of pharmacologic MMP inhibitors has shown efficacy in attenuating post MI remodeling in pre-clinical animal models of MI, off-target effects have limited their success in recent clinical trials[9]. Therefore, strategies that localize physiological concentrations of MMP inhibitors to regions of MMP overexpression and limit spill over into the systemic circulation would provide a safe and effective strategy to attenuate post MI remodeling by targeting MMP activity.

Wilson and colleagues recently showed that MMP elevation is highly localized to ischemic tissue within the MI region following experimental MI in pigs[10]. While MMP levels increased dramatically, levels of their inhibitors, tissue inhibitors of MMPs (TIMPs), decreased significantly within the MI region. TIMPs inhibit MMP activity by forming non-covalent complexes with MMPs in a 1:1 stoichiometry, blocking the MMP catalytic domain and preventing proteolysis. With the exception of TIMP-1, TIMPs are known to inhibit all of the 25 known MMPs, and studies have identified unique roles and functionalities of each of the four TIMPs[11]. In the context of post MI remodeling, TIMP-3 has been shown to play a particularly important role. For example, myocardial TIMP-3 levels were significantly reduced in contradistinction to elevated myocardial MMP levels in patients with end-stage heart failure[12]. In addition, transgenic TIMP-3 deletion in experimental animal models caused adverse LV remodeling and accelerated progression to heart failure following MI[13-15].

We therefore chose to evaluate the ability of a recombinant TIMP-3 to attenuate adverse LV remodeling through local MMP inhibition in a large animal model of MI. Critical to the success of this approach is a safe and flexible delivery platform that locally releases TIMP-3 to the MI region while minimizing systemic off-target effects. Injectable hydrogels have recently been developed for the therapeutic delivery of molecules to the heart following MI[16]. In these systems, therapeutic molecules are encapsulated in a polymer matrix and released locally over time to sustain target levels of a molecule in the myocardium. Polymer concentration, polymer-molecule interactions, hydrophobic effects, and gel degradation collectively determine molecule diffusion from the gel. While these parameters can be controlled to engineer a gel formulation with a desired TIMP-3 release profile, studies have shown that post MI MMP expression profiles are dynamic and vary from patient to patient. In some patients, MMP expression was endogenously restored from day 1 to day 5 following MI, while in others a persistent or elevated MMP-9 signal from day 1 to day 5 was accompanied by a 3-fold end-diastolic volume increase at day 28[3].

Therefore, while MMP overexpression is an important target towards attenuating post MI remodeling, it is difficult to choose a single TIMP-3 release profile suitable for every patient. One way to overcome these limitations is to design responsive gels that alter molecule release rates in response to external stimuli. Specifically, hydrogels with MMP-cleavable crosslinks allow encapsulated molecules to be released in response to local MMP activity[17,18]. Utilizing this approach would effectively dose TIMP-3 release in response to MMP activity.

One challenge towards realizing on-demand TIMP-3 delivery is to minimize passive TIMP-3 release from the gels (i.e., in the absence of MMP activity). TIMP-3 is unique among the TIMPs in that it is found bound to the ECM of tissues while the other three TIMPs are presented as soluble proteins[19]. Specifically, TIMP-3 binds to sulfated glyocosaminoglycans with a high affinity through an abundance of positively charged lysine and arginine residues exposed on the protein surface[20,21]. TIMP-3 binding to the ECM is thought to facilitate local MMP inhibition in tissues, and recent studies have shown that sulfated polymers enhance TIMP-3 binding affinity for specific MMPs[22]. Therefore, we developed injectable gels with a negatively charged polysaccharide backbone to mimic native TIMP-3-ECM interactions and minimize passive diffusion of TIMP-3 from the gels. MMP-cleavable crosslinks were incorporated to liberate bound TIMP-3 in the presence of local MMP activity. Further, we utilized conjugation and crosslinking chemistries to form gels rapidly upon injection into the myocardium that are stable in the absence of MMP activity to further prevent the passive release of TIMP-3 from the injection site. We demonstrate that this TIMP-3 delivery strategy effectively inhibits MMP activity within the MI region without further damaging the myocardium or raising systemic TIMP-3 levels. Finally, we show attenuated post MI LV remodeling through significant increases in LV wall thickness and ejection fraction in a large animal model of MI.

8.2. Methods

HA-maleimide synthesis.

74kDa sodium hyaluronate (NaHy, Lifecore) was first converted to a tetrabutylammonium (TBA) salt of HA (HA-TBA) by mixing NaHy with an ion exchange resin in DI water for 8hrs at RT. The resin was then filtered from the aqueous solution and the solution was pH'd to 7.02 with TBAOH, frozen and lyophilized.   HA-TBA was dissolved in DMSO and then reacted with N-(2-aminoethyl)maleimide trifluoroacetate salt (Sigma) in the presence of benzotriazol-1-yloxytris(dimethylamino)-phosphonium hexafluorophosphate for 2hrs at RT. The reaction solution was then dialyzed against DI water for 14 days, frozen and lyophilized. Percent maleimide modification of HA was determined to be 35% of the HA repeat units by normalizing the area under the maleimide ^{1}H peak to the aminomethyl protons on the HA backbone.

Solid-phase peptide synthesis.

Peptides were synthesized with the MMP-cleavable sequence GCNSGGRMSMPVSNGG-Hyd where C is the cysteine used for coupling to a maleimide functionalized HA and Hyd is the hydrazide for gel crosslinking with an aldehyde functionalized HA. The solid-phase resin (Rink Amide MBHA resin, 100-200 mesh, Novabiochem) was deprotected with 20% (v/v) piperidine in N,N-dimethylformamide (DMF) solution and Fmoc protected amino acids (Novabiochem) were activated with HBTU (Novabiochem) in 0.4 M N-methylmorpholine in DMF prior to reaction with deprotected resin. Amino acids were reacted at 4x excess to solid-phase resin using an automated solid phase peptide synthesizer (PS 3, Protein Technologies, Inc.). After completion, the polypeptide was cleaved from the resin with a 90% trifluoroacetic acid, 5% tri-isopropylsilane, 5% water solution for 3 hrs at room temperature. The polypeptide was then precipitated in ethyl ether solution at -80°C for 2 hrs, spun down and dried against vacuum pump pressure overnight. Matrix-assisted laser desorption/ionization-Time of Flight (MALDI-TOF) mass spectroscopy was used

to verify successful polypeptide mass based on theoretical calculation.

Synthesis and characterization of polymers.

HA-peptide-hydrazide polymers were synthesized by coupling a cysteine terminated peptide to HA-maleimide by mixing at a 4:1 molar ratio, cysteine:maleimide in PBS for 4hrs at 4°C. The polymer was purified by dialysis against a 20 mM NaCl solution for 4 days, then DI water for 3 days, frozen and lyophilized.   HA-aldehyde was synthesized by mixing NaHy (350kDa, Lifecore) at 1 % (w/v) and sodium periodate (IO_4) in DI water at a molar ratio of 1:2 HA:IO_4 for 2hrs at RT. The reaction was stopped by adding 10% (v/v) ethylene glycol to the reaction, dialyzing against DI water for 5 days, freezing and lyophilizing. DS-ald was synthesized in a similar fashion except DS (Sigma) was reacted with IO_4 at a molar ratio of 2:1 DS:IO_4 for 5hrs at RT. Percent aldehyde modification was quantified using a TNBS colorimetric assay as previously described[24].

Rheometry.

To form gels, ALD (2.4% HA-ald, 1.4% DS-ald (w/v)) and HYD (3.2% (w/v) HA-peptide-hyd) modified polymers were dissolved in PBS, mixed 1:1 and gelation characteristics were quantified by monitoring the storage (G') and loss (G'') moduli with time using an AR2000ex Rheometer (TA Instruments) at 37°C under 1% strain and 1 Hz.

Gel degradation and molecule release studies.

FITC-BSA or rTIMP-3 was mixed with the ALD precursor solution and gels were formed as described above in cylindrical molds for 30 min at 37°C. Gels were incubated in PBS supplemented with 1% BSA for FITC-BSA studies or TTC buffer (50mM Tris-HCl, 1mM $CaCl_2$, 0.05% triton x-100, pH 7.5) for rTIMP-3 studies at 37°C. After a wash, enzymes (collagenase type 4, Worthington or rMMP-2, R&D Systems) were added every 2 days and buffers were collected and stored at -20°C prior to analysis. Uronic acid content was analyzed to

calculate gel mass loss[25], FITC-BSA fluorescence was analyzed to measure release, and an ELISA was used to measure rTIMP-3 content (R&D Systems).

rTIMP-3 activity and binding assays.

rTIMP-3-His (Amgen, Inc.) activity was quantified by its ability to inhibit rMMP-2 (R&D Systems) activity using an MMP cleavable fluorogenic substrate (R&D Systems). Serial dilutions of rTIMP-3 were added to 4nM activated rMMP-2 in TTC buffer, incubated for 2hrs at 37°C, then the fluorogenic substrate was added and fluorescence kinetics were measured over 5 min with a microplate reader (Tecan). rTIMP-3 binding to polysaccharide polymers was evaluated with a solid-phase binding assay. HA-ald, DS-ald, and heparin (Sigma) at 2.5µM in PBS were coated overnight at 25°C on to heparin binding plates (BD Life Sciences)[26]. Wells were washed in TNC buffer (50 mM Tris/HCl, 150 mM NaCl, 10 mM $CaCl_2$, 0.05 % Brij-35 and 0.02 % sodium azide) containing 0.1 % Tween 20 between each subsequent incubation. Wells were blocked with 0.2% gelatin in TNC buffer and then incubated with rTIMP-3-His (0.02-3µg/mL in blocking solution for 3 h at 37°C). Bound rTIMP-3-His was detected using a biotin labeled antibody against the 6xHis tag on rTIMP-3 (Abcam, catalogue number ab27025, for 3 h at 37∘C), followed by streptavidin coupled to horseradish peroxidase (R&D Systems) for 1h at 37°C. Hydrolysis of a 1:1 mixture of H_2O_2 and tetramethylbenzidine was measured at 450 nm using a microplate reader (Tecan).

MI induction and gel injections.

Yorkshire pigs (n=7, 25kg, Hambone Farms, Orangeburg, SC) were anesthetized with isoflurane (2%), and through a left thoracotomy, the LV free wall was exposed. A 2 cm square calibrated grid was sutured below the origin of the first two obtuse marginal arteries of the circumflex artery (OM1 and OM2), which provided for a total of 9 distinct injection sites within a targeted 2X2 cm region of myocardium. OM1 and OM2 were ligated to induce an MI, and

characteristic ECG changes occurred, but electrical cardioversion and/or defibrillation were not required, and past studies demonstrated that this technique creates a uniform and consistent MI[8].   Referent controls were instrumented in a similar fashion with the exception of coronary artery ligation. Pigs were randomized to receive injections of saline (MI only), gel alone (gel), or gel with rTIMP-3 (gel/rTIMP-3). For gel injections, the ALD (2.4% HA-ald, 1.4% DS-ald (w/v)) and HYD (3.2% (w/v) HA-GCNSGGRMSMPVSNGG-hyd) precursors solutions were mixed in a sterile fashion, drawn into separate 1mL syringes, and injected into the mid-myocardium of each target site using a FibriJet blending connector (Nordson Micromedics, SA-3670) with a 27G needle. For gel/rTIMP-3 group, rTIMP-3 was mixed into the ALD precursor (20μg rTIMP-3/100μL ALD). Successful injections were confirmed by visualization of an opacification of the epicardial surface at the point of myocardial injection.

Blood analysis.

Pigs were instrumented as described in the preceding section with the addition of a vascular access catheter placed in the descending aorta and connected to a subcutaneous port (6 Fr., SlimPort,Bard Access Systems, Salt Lake City). Blood samples (5 mL) were collected from the subcutaneous port 1, 3, 7 and 14 days post-MI. The referent controls were again instrumented in an identical manner with the exception of MI induction. The collected blood samples were centrifuged and the decanted plasma subjected to ELISA for troponin-I (Pig Cardiac Troponin-I, KT-474, Kamiya Biomedical Co) and C-reactive protein (CRP; Porcine CRP ELISA, IPGCRPKT, Innovative Research Inc.).

LV assessment with echocardiography.

Animals were sedated (20 mg valium, PO, Elkin-Sinn) and two-dimensional echocardiographic studies (GE VIVID 7 Dimension Ultrasound System: M4S 1.5-4.3 MHz active matrix array sector transducer probe) were performed to calculate LV dimensions and ejection fraction. Echocardiography

measurements were taken 1 day prior to MI induction, and then again 1, 3, 7 and 14 days following MI.

Interstitial MMP activity.

After 14 days post MI, the pigs were anesthetized with sufentanyl (2µg/kg IV, Baxter Healthcare), morphine sulfate (3mg/kg/h IV, Elkin-Sinn), and isoflurane (1%, 3 L/min O_2, Baxter Healthcare), and mechanically ventilated. The LV was exposed through a sternotomy, a microdialysis probe (20 kDa, outer diameter of probe shaft 0.77mm; CMA/Microdialysis, North Chelmsford, MA) placed within the MI region, and infused with the MMP fluorescent substrate (5 µL/min) as previously validated[3,4]. The dialysate was then subjected to fluorometry, which reflected interstitial MMP activity, and these values were normalized to referent control values and expressed as a percent. Following these measurements, the LV was harvested, separated into MI and remote regions (area served by left anterior descending artery), and prepared for biochemical analysis.

Data and statistical analysis.

Statistical analyses were performed using STATA statistical software. LV geometry, function, and area within the markers were compared between the control and MI groups using a one-way analysis of variance (ANOVA). Post-hoc separation following ANOVA was performed using pairwise comparisons with a Bonferroni analysis (prcomp module, STATA).   The interstitial global MMP activity was evaluated by ANOVA and subsequently compared against the control values of 100% by a Student's t-test. For TIMP-3 levels and plasma troponin and CRP concentrations, values from each group were first evaluated by ANOVA, and then a post-hoc separation following ANOVA was performed using pairwise comparisons with a Bonferroni analysis. For PCR measurements, a multi-way ANOVA (MANOVA) was performed, evaluating for treatment dependent, MI dependent, and region dependent effects. Post-hoc separation following MANOVA was performed using pairwise comparisons with a Bonferroni

analysis. Results are presented as a mean ± standard error of the mean (SEM), and values of $p < 0.05$ were considered to be statistically significant.

8.3. Results and Discussion

Gel design for MMP-responsive rTIMP-3 delivery

The main criteria used in designing a gel formulation for rTIMP-3 delivery were 1) a gel that crosslinks upon injection through a syringe, 2) stable gels that degrade only in the presence of MMP activity, and 3) minimal passive release of encapsulated rTIMP-3 (i.e., in the absence of MMP activity). To this end, we developed a three-macromer system that utilizes the chemical versatility of polysaccharide backbones (Figure 8.1 a). Polysaccharides were chemically modified to contain either aldehyde (ALD) or hydrazide (HYD) functional groups to form gels in a one-step condensation reaction, with water as the only byproduct (Figure 8.1 b). Hyaluronic acid (HA) was used as a template for both ALD and HYD modifications due to the well-defined size ranges of commercially available HA, the previous use of HA in biomedical applications, and the abundance of diol and carboxylic acid groups necessary for ALD and HYD modifications, respectively. Dextran sulfate (DS) was also incorporated into the gels through ALD modification of its diol groups to act as a heparin mimetic to immobilize encapsulated heparin-binding proteins[23]. ALD modification of HA and DS were evaluated separately as each polysaccharide contains a different number of diol groups amendable to aldehyde modification (Figure 8.2).
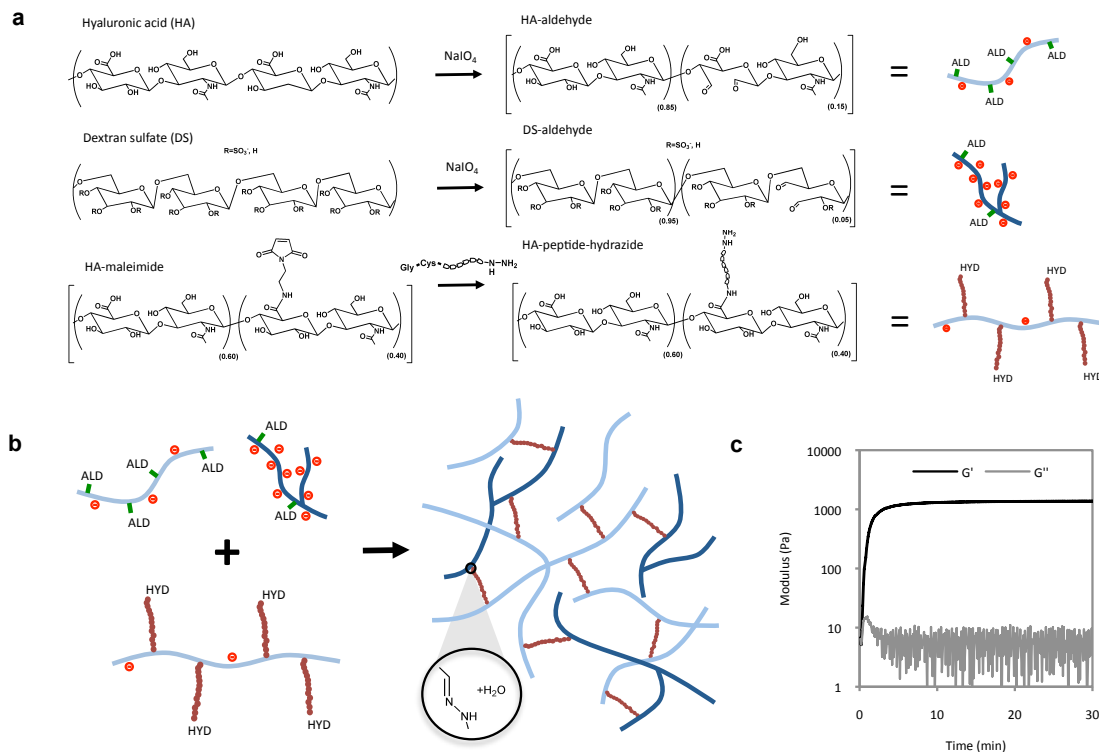
Figure 8.1. Injectable hydrogels with peptide crosslinks. (a-b) HA and DS polymers were modified with aldehyde (ALD) groups and HA polymers were modified with a peptide containing an hydrazide (HYD) group to form hydrogels through stable hydrazone bond formation. (c) Upon mixing ALD and HYD polymers, robust hydrogels formed rapidly as evidenced by development of storage (G') and loss (G'') moduli over time.
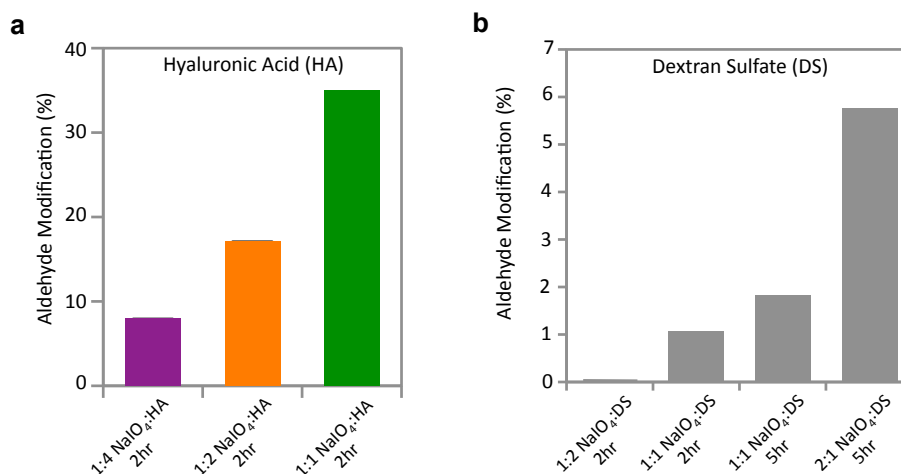

Figure 8.2. Aldehyde modifications. Aldehyde groups were synthesized on HA (a) and DS (b) polymers using sodium periodate ($NaIO_4$) oxidation of diols. Different reaction conditions were chosen for each polymer due to differences in the amount of diol groups per polymer.

Further, converting diols to aldehydes through periodate oxidation is known to degrade polysaccharides, so a large molecular weight (MW) HA (~350kDa) was chosen to provide sufficient HA-ald MW to allow formation of robust gels for rTIMP-3 encapsulation. Reaction conditions for HA-ald were chosen to balance aldehyde modification and macromer MW as periodate concentration both increased aldehyde modification and decreased HA MW in a dose-dependent manner (Figure 8.3). Reaction conditions for DS-ald were chosen to provide sufficient aldehyde modification to crosslink DS-ald into the gel.
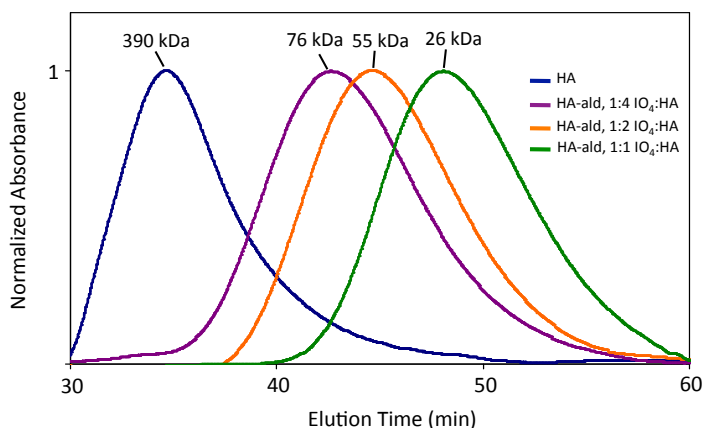

Figure 8.3. Periodate polymer degradation. HA polymers degraded due to non-specific reactions during the oxidation reaction. Values reported are number-averaged molecular weights (M_n) as determined by gel permeation chromatography.

MMP-specificity was incorporated into the gels by generating MMP-cleavable peptides with a terminal HYD functional group using solid phase peptide synthesis. In addition, a thiol containing cysteine was incorporated into the MMP-cleavable peptides, opposite of the HYD group to facilitate thioether linkage to a maleimide functionalized HA (MAHA) in a one-step click reaction (Figure 8.1). Finally, hydrophilic serine (S) and asparagine (N) spacers were incorporated between the reactive groups (cysteine and hydrazide) and the MMP-cleavable peptides to improve solubility for passage through a syringe. Successful synthesis of the designed peptide was verified with MALDI (Figure 8.4 a) and peptide coupling to MAHA was verified by complete consumption of the characteristic maleimide peak from ^{1}H NMR (Figure 8.4 b). Percent

140

maleimide modification of HA (and therefore HYD modification) was controlled through the concentration of N-(2-Aminoethyl)maleimide during MAHA synthesis. The thioether coupling chemistry was chosen for its stability in water to prevent non-specific hydrolysis of the gels. The designed formulation enabled rapid crosslinking of gels upon mixing ALD and HYD modified macromers as evidenced by development of the elastic component (G') of the complex modulus using rheometry (Figure 8.1 c). The gels reached a plateau G' of approximately 1.5 kPa, at which point the gels are robust, nearly elastic solids.
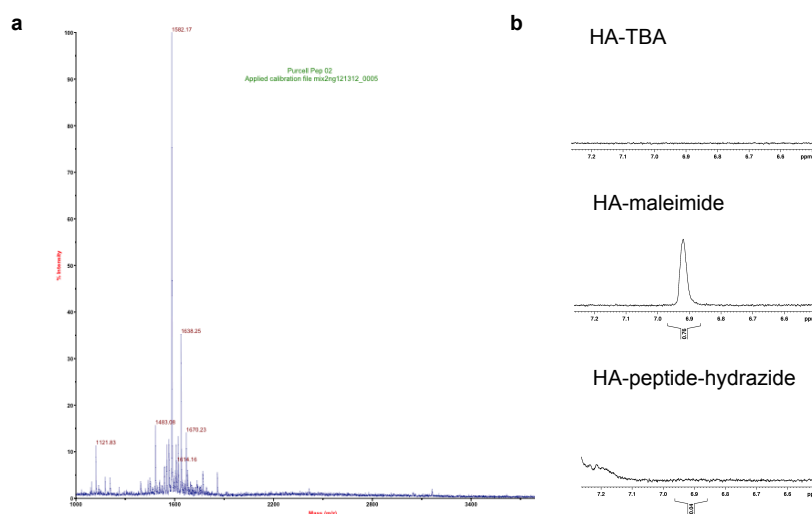

Figure 8.4. Peptide synthesis and coupling. (a) Peptide synthesized through solid-phase peptide synthesis was analyzed using MALDI-TOF mass spectroscopy to verify mass. (b) Peptide coupling to maleimide functionalized HA was verified by loss of peak characteristic of maleimide protons using ^{1}H NMR.

To demonstrate MMP-sensitivity, gels containing a peptide sequence that is cleaved by MMPs (GGRMSMPV) were incubated in buffer with varying concentrations of active MMPs and uronic acid content in the buffer was measured over time to calculate gel mass loss. In the absence of active MMPs, the gels were stable over the 12-day study (Figure 8.5 a). In a 20 U/mL enzyme concentration, the gels degraded in a near-linear fashion with very little gel remaining after 12 days. In 200 U/mL, the gels completely degraded in 2 days. To evaluate the applicability of the gels for MMP-triggered release of encapsulated molecules, FITC-BSA was encapsulated in the gels and release

was quantified in buffer with varying concentrations of active MMPs. Encapsulated FITC-BSA release followed the gel degradation behavior in a similar MMP-dependent manner (Figure 8.5 b).
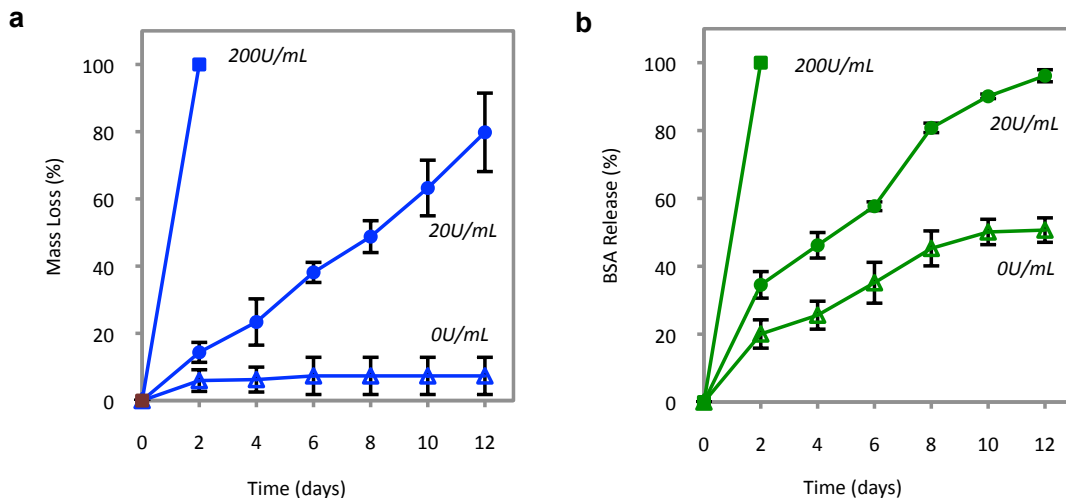

Figure 8.5. MMP-trigged molecule release. Hydrogels with the MMP-cleavable GGRMSMPV peptide in the crosslink were incubated in different concentrations of collagenase type 4. (a) Hydrogels were stable in the absence of enzyme activity and degraded in response to enzyme concentration. (b) Encapsulated FITC-BSA released in proportion to hydrogel degradation. (mean±SD, n=3 hydrogels per condition).

rTIMP-3 delivery with MMP-cleavable gels

TIMP-3 was chosen for local delivery post-MI in part because of its unique ECM-binding property. This allowed us to design ECM mimetic gels to encapsulate and immobilize rTIMP-3 until they are released by MMP-mediated gel degradation. To this end, DS was incorporated into the gel formulation to mimic sulfated GAGs, the major component of the ECM responsible for TIMP-3 binding, due to its susceptibility to aldehyde modification through diol oxidation. Binding of rTIMP-3 to DS-ald was evaluated using a solid-phase binding assay. rTIMP-3 bound to DS-ald with a much greater capacity than to HA-ald, and approached the capacity of rTIMP-3 binding to heparin (Figure 8.6 a). Importantly, rTIMP-3 binding to DS-ald did not reduce rTIMP-3 inhibition of active MMPs (Figure 8.6 b). rTIMP-3 inhibited 4nM rMMP-2 with a half maximal inhibitory concentration of 17±4 ng/mL (0.7±0.2 nM) with 50 μg/mL DS-ald in solution compared to 28±7 ng/mL (1.2±0.3 nM) without DS-ald in solution

(p=0.07). Previous studies found that a stretch of basic amino acids responsible for TIMP-3 binding to sulfated GAGs is opposite to the TIMP-3 reactive site that interacts with MMPs [21]. Therefore, utilizing polysaccharides that mimic sulfated GAGs allows localization of TIMP-3 without altering its inhibitory properties. Indeed, encapsulating rTIMP-3 in the crosslinked polysaccharide gels limited diffusion of rTIMP-3 from the gel (Figure 8.6 c), where less than 20% of encapsulated rTIMP-3 was released over the 14-day study.
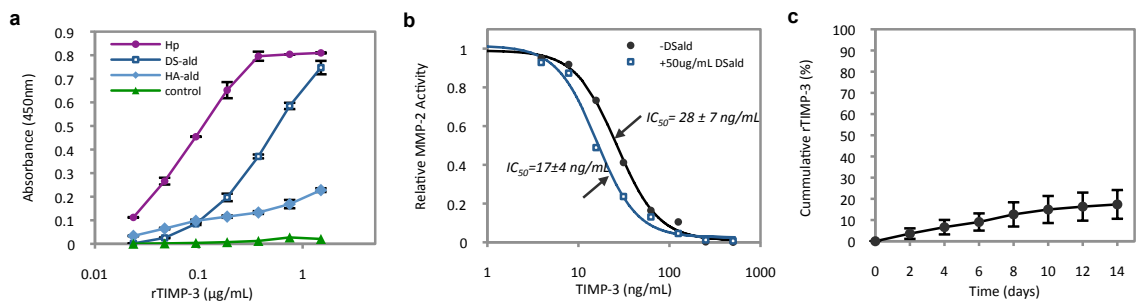

Figure 8.6. Polymer binding to rTIMP-3. (a) rTIMP-3 bound to polymer coated wells detected with ELISA. rTIMP-3 bound to DS-ald with a greater capacity than HA-ald, and approached rTIMP-3 binding to heparin. (b) rTIMP-3 activity measured by its ability to inhibit a 4 nM rMMP-2 solution. rTIMP-3 binding to DS-ald did not affect rMMP-2 inhibition. (c) Release of rTIMP-3 encapsulated in ALD+HYD hydrogels was limited to less than 20% by incorporating sulfated DS-ald.

While using MMP activity to trigger release of molecules encapsulated in gels has been performed previously[17,18], using MMP activity to trigger release of MMP inhibitors, and therefore using MMP activity to trigger its own inhibition, is a novel concept. To investigate this unique feedback system, gels with and without encapsulated rTIMP-3 were incubated in 20nM active rMMP-2. Gels without rTIMP-3 degraded within 2 days in the MMP buffer, while gels with encapsulated rTIMP-3 degraded in a linear fashion for over 14 days (Figure 8.7a). This reduction in gel degradation rate observed with rTIMP-3 encapsulation indicates that encapsulated rTIMP-3 remains active and is inhibiting rMMP-2 activity as rMMP-2 is degrading the gel (Figure 8.7 b). Further, as rMMP-2 was refreshed every 2 days to account for enzyme stability (Figure 8.8), a sufficient amount of active rTIMP-3 remained bound in the gel for the entire 14 day study, otherwise

the gel would rapidly degrade in similar fashion to the gels without rTIMP-3. These results demonstrate a novel approach of locally delivering rTIMP-3 by designing injectable gels containing MMP-cleavable crosslinks, where the local presence of active MMPs controls the release of encapsulated rTIMP-3, and therefore MMP inhibition.
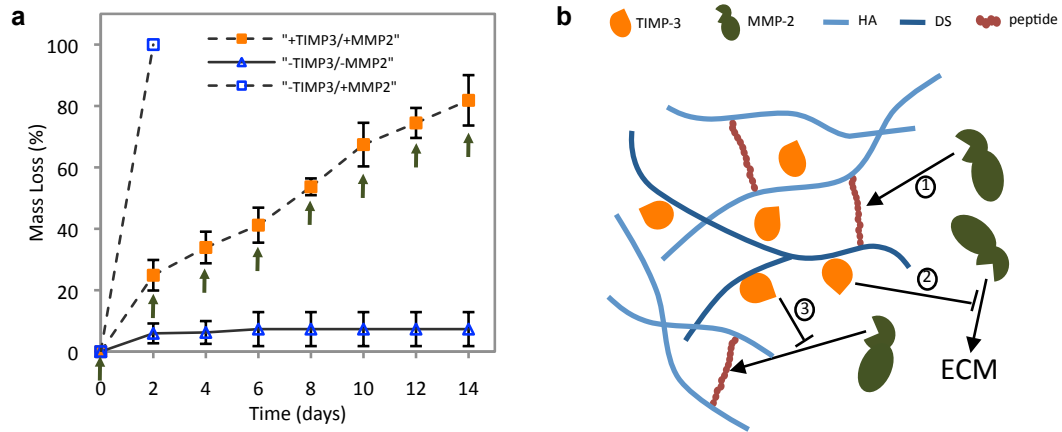

Figure 8.7. MMP-triggered release of rTIMP-3. (a) Hydrogels with (filled symbols) and without (open symbols) encapsulated rTIMP-3 were incubated with (squares) or without (triangles) rMMP-2. rMMP-2 was added every two days (indicated by green arrows). Encapsulated rTIMP-3 attenuated MMP-2 mediated hydrogel degradation, confirming activity of rTIMP-3 across the 14-day study. (b) In this system, rMMP-2 degrades the hydrogel crosslinks (1), liberating bound rTIMP-3, inhibiting rMMP-2 activity (2), and attenuating further hydrogel degradation (3).
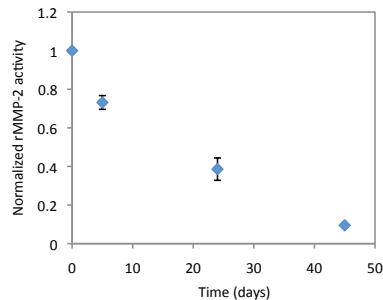
Figure 8.8. rMMP-2 activity. Activity of rMMP-2 decreases to less than 10% of its initial level immediately after activation in buffer.

Effectiveness of rTIMP-3 delivery in vivo

  To assess the effectiveness of our rTIMP-3 delivery system in the setting of MI, a large animal model of MI was employed that allows for regional quantification of MMP expression and activity, along with functional outcomes of post MI LV remodeling[10]. Following MI induction in pigs, gels were injected

144

at 9 equally spaced sites within a 2cm x 2cm grid in the MI region (Figure 8.9 a). A dual-barreled syringe was utilized to blend ALD and HYD polymers in equal ratios immediately prior to entering the tissue for *in situ* gelation.

Following rTIMP-3 delivery, blood samples were taken after 1, 3, 7, and 14 days and analyzed for TIMP-3 concentrations. Importantly, there was no observed increase in systemic TIMP-3 levels with local delivery of rTIMP-3 to the MI region using our injectable gels compared to MI only and gel injection alone (Figure 8.9 b). To quantify MMP activity within the MI region, a previously validated microdialysis technique was utilized that perfuses the myocardial interstitium with an MMP cleavable substrate and measures fluorescence as the substrate is cleaved[4]. Using this technique, MMP activity was observed to significantly increase in the MI region following MI induction (Figure 8.10). Interestingly, injection of the MMP degradable gels alone significantly reduced MMP activity within the MI region, potentially due to a "sink effect" where the cleavable peptide substrate is cleaved by active MMPs, reducing substrate hydrolysis elsewhere. However, rTIMP-3 delivery from the MMP degradable gels further reduced MMP activity within the MI region.

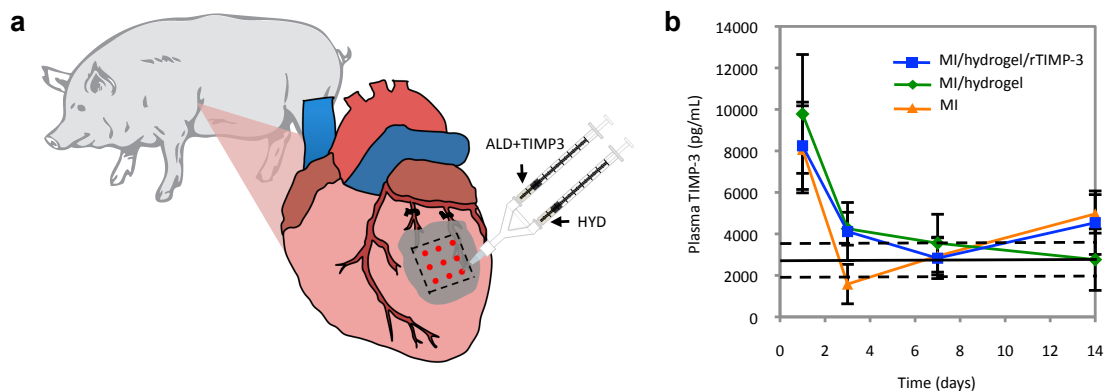**Figure 8.9. Hydrogel mediated rTIMP-3 delivery.** (a) Hydrogels were formed *in situ* by utilizing a dual barrel syringe to mix the ALD and HYD polymers at the injection site. (b) Hydrogel mediated delivery of rTIMP-3 prevented a systemic increase in rTIMP-3 levels. (mean±SD; MI n=5; MI/hydrogel n=6; MI/hydrogel/rTIMP-3 n=5; p>0.05 between groups across all time points; horizontal lines represent non-MI control ± 95% CI, n=16;)
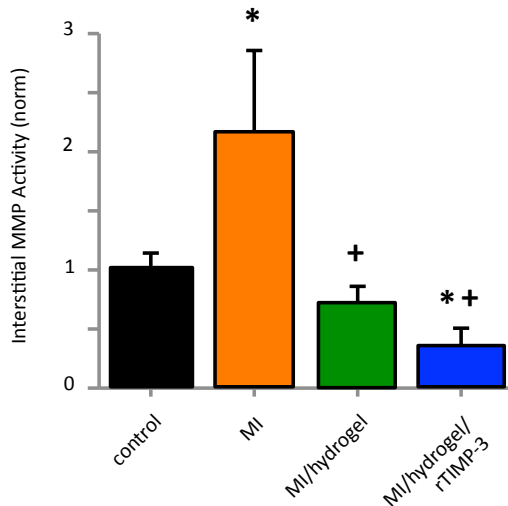
Figure 8.10. Post MI MMP activity. Interstitial microdialysis of a fluorogenic MMP cleavable substrate showed a significant increase in MMP activity in the MI region of pigs. Injection of the hydrogel alone significantly reduced MMP activity. Encapsulation of rTIMP-3 further reduced MMP activity. (mean±SD; control n=4; MI n=5; MI/hydrogel n=6; MI/hydrogel/rTIMP-3 n=4; *p<0.05 vs. control; +p<0.05 vs. MI)

Experimental MI induction caused a gradual reduction in LV function, as indicated by a declining ejection fraction (EF) and a progressive increase in pulmonary capillary wedge pressure (PCWP) (Fig 8.11 a-b). Coinciding with declining LV function were significant changes in LV geometry as indicated by progressive LV wall thinning and LV dilation (Fig 8.11 c-d). rTIMP-3 delivery from the injectable gels significantly increased LV wall thickness compared to MI only and significantly reduced LV end diastolic volume (LVEDV) compared to gel alone. Further, rTIMP-3 delivery significantly improved LV function as evidenced by significant increases in EF and decreases in PCWP compared to MI only and gel alone control groups.

Our results demonstrate the utility of injectable gels to locally deliver TIMPs and inhibit excessive MMP activity by restoring myocardial MMP/TIMP balance following MI. This is the first proof-of-concept demonstration of designing MMP-degradable gels to release an MMP inhibitor in the presence of MMP activity to limit off-target effects of MMP inhibitors, which have been clinically problematic. The successful demonstration of this technology in attenuating post MI remodeling in a large animal model warrants further pre-clinical investigation as it could ultimately provide a safe and effective therapy to treat patients in the clinical setting of acute MI.
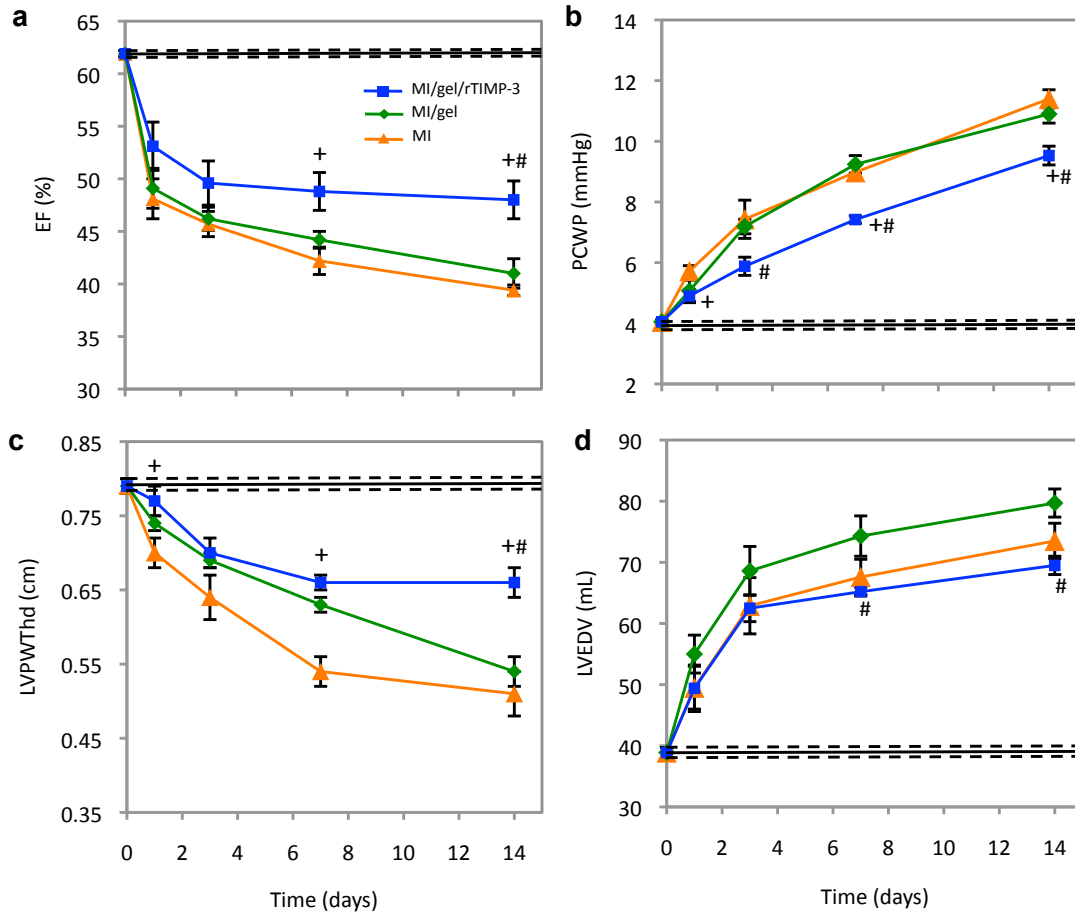
Figure 8.11. LV function and geometry post MI. Serial LV echocardiography measurements were collected over the 14 day study to assess LV function (a-b) and geometry (c-d). (a) Progressive decrease in ejection fraction (EF) was observed following MI induction, and rTIMP-3 delivery from injectable hydrogels significantly attenuated this decline. (b) Progressive increase pulmonary capillary wedge pressure (PCWP) was observed following MI induction, which was significantly attenuated with rTIMP-3 delivery. (c) Progressive thinning of the LV wall posterior wall thickness at diastole (LVPWThd) was significantly attenuated with rTIMP-3 delivery. (d) Progressive dilation of the LV end diastolic volume (LVEDV) was significantly attenuated compared to injection of the hydrogels alone. (mean±SEM; MI n=5; MI/hydrogel n=6; MI/hydrogel/rTIMP-3 n=5; +$p < 0.05$ compared to MI; #$p < 0.05$ compared to MI/hydrogel; horizontal lines represent non-MI controls ± 95% CI)

8.4. References

1. Fingleton B. Matrix metalloproteinases as valid clinical targets. *Curr Pharm Des*. 2007;13:333-346
2. Visse R, Nagase H. Matrix metalloproteinases and tissue inhibitors of metalloproteinases: Structure, function, and biochemistry. *Circ Res*. 2003;92:827-839
3. Webb CS, Bonnema DD, Ahmed SH, Leonardi AH, McClure CD, Clark LL, Stroud RE, Corn WC, Finklea L, Zile MR, Spinale FG. Specific temporal profile of matrix metalloproteinase release occurs in patients after myocardial infarction: Relation to left ventricular remodeling. *Circulation*. 2006;114:1020-1027
4. Spinale FG, Koval CN, Deschamps AM, Stroud RE, Ikonomidis JS. Dynamic changes in matrix metalloprotienase activity within the human myocardial interstitium during myocardial arrest and reperfusion. *Circulation*. 2008;118:S16-23
5. Ducharme A, Frantz S, Aikawa M, Rabkin E, Lindsey M, Rohde LE, Schoen FJ, Kelly RA, Werb Z, Libby P, Lee RT. Targeted deletion of matrix metalloproteinase-9 attenuates left ventricular enlargement and collagen accumulation after experimental myocardial infarction. *J Clin Invest*. 2000;106:55-62
6. Matsumura S, Iwanaga S, Mochizuki S, Okamoto H, Ogawa S, Okada Y. Targeted deletion or pharmacological inhibition of mmp-2 prevents cardiac rupture after myocardial infarction in mice. *J Clin Invest*. 2005;115:599-609
7. Rohde LE, Ducharme A, Arroyo LH, Aikawa M, Sukhova GH, Lopez-Anaya A, McClure KF, Mitchell PG, Libby P, Lee RT. Matrix metalloproteinase inhibition attenuates early left ventricular enlargement after experimental myocardial infarction in mice. *Circulation*. 1999;99:3063-3070
8. Mukherjee R, Brinsa TA, Dowdy KB, Scott AA, Baskin JM, Deschamps AM, Lowry AS, Escobar GP, Lucas DG, Yarbrough WM, Zile MR, Spinale FG. Myocardial infarct expansion and matrix metalloproteinase inhibition. *Circulation*. 2003;107:618-625
9. Renkiewicz R, Qiu L, Lesch C, Sun X, Devalaraja R, Cody T, Kaldjian E, Welgus H, Baragi V. Broad-spectrum matrix metalloproteinase inhibitor marimastat-induced musculoskeletal side effects in rats. *Arthritis Rheum*. 2003;48:1742-1749
10. Wilson EM, Moainie SL, Baskin JM, Lowry AS, Deschamps AM, Mukherjee R, Guy TS, St John-Sutton MG, Gorman JH, 3rd, Edmunds LH, Jr., Gorman RC, Spinale FG. Region- and type-specific induction of matrix metalloproteinases in post-myocardial infarction remodeling. *Circulation*. 2003;107:2857-2863
11. Brew K, Nagase H. The tissue inhibitors of metalloproteinases (timps): An ancient family with structural and functional diversity. *Biochim Biophys Acta*.1803:55-71
12. Fedak PW, Altamentova SM, Weisel RD, Nili N, Ohno N, Verma S, Lee TY, Kiani C, Mickle DA, Strauss BH, Li RK. Matrix remodeling in experimental and human heart failure: A possible regulatory role for timp-3. *Am J Physiol Heart Circ Physiol*. 2003;284:H626-634
13. Fedak PW, Smookler DS, Kassiri Z, Ohno N, Leco KJ, Verma S, Mickle DA, Watson KL, Hojilla CV, Cruz W, Weisel RD, Li RK, Khokha R. Timp-3 deficiency leads to dilated cardiomyopathy. *Circulation*. 2004;110:2401-2409
14. Tian H, Cimini M, Fedak PW, Altamentova S, Fazel S, Huang ML, Weisel RD, Li RK. Timp-3 deficiency accelerates cardiac remodeling after myocardial infarction. *J Mol Cell Cardiol*. 2007;43:733-743
15. Kassiri Z, Defamie V, Hariri M, Oudit GY, Anthwal S, Dawood F, Liu P, Khokha R. Simultaneous transforming growth factor beta-tumor necrosis factor activation and cross-talk cause aberrant remodeling response and myocardial fibrosis in timp3-deficient heart. *J Biol Chem*. 2009;284:29893-29904
16. Tous E, Purcell B, Ifkovits JL, Burdick JA. Injectable acellular hydrogels for cardiac repair. *J Cardiovasc Transl Res*.4:528-542
17. Segers VF, Tokunou T, Higgins LJ, MacGillivray C, Gannon J, Lee RT. Local delivery of protease-resistant stromal cell derived factor-1 for stem cell recruitment after myocardial infarction. *Circulation*. 2007;116:1683-1692

18.   Salimath AS, Phelps EA, Boopathy AV, Che PL, Brown M, Garcia AJ, Davis ME. Dual delivery of hepatocyte and vascular endothelial growth factors via a protease-degradable hydrogel improves cardiac function in rats. *PLoS One*.7:e50980

19.   Leco KJ, Khokha R, Pavloff N, Hawkes SP, Edwards DR. Tissue inhibitor of metalloproteinases-3 (timp-3) is an extracellular matrix-associated protein with a distinctive pattern of expression in mouse cells and tissues. *J Biol Chem*. 1994;269:9352-9360

20.   Yu WH, Yu S, Meng Q, Brew K, Woessner JF, Jr. Timp-3 binds to sulfated glycosaminoglycans of the extracellular matrix. *J Biol Chem*. 2000;275:31226-31232

21.   Lee MH, Atkinson S, Murphy G. Identification of the extracellular matrix (ecm) binding motifs of tissue inhibitor of metalloproteinases (timp)-3 and effective transfer to timp-1. *J Biol Chem*. 2007;282:6887-6898

22.   Troeberg L, Mulloy B, Ghosh P, Lee MH, Murphy G, Nagase H. Pentosan polysulfate increases affinity between adamts-5 and timp-3 through formation of an electrostatically driven trimolecular complex. *Biochem J*.443:307-315

23.   Huang M, Vitharana SN, Peek LJ, Coop T, Berkland C. Polyelectrolyte complexes stabilize and controllably release vascular endothelial growth factor. *Biomacromolecules*. 2007;8:1607-1614

24.   Su WY, Chen YC, Lin FH. Injectable oxidized hyaluronic acid/adipic acid dihydrazide hydrogel for nucleus pulposus regeneration. *Acta Biomater*.6:3044-3055

25.   Bitter TM, H. M. . A modified uronic acid carbazole reaction. *Anal Biochem*. 1962;4:330-334

26.   Mahoney DJ, Whittle JD, Milner CM, Clark SJ, Mulloy B, Buttle DJ, Jones GC, Day AJ, Short RD. A method for the non-covalent immobilization of heparin to surfaces. *Anal Biochem*. 2004;330:123-129

27.   Mukherjee R, Rivers WT, Ruddy JM, Matthews RG, Koval CN, Plyler RA, Chang EI, Patel RK, Kern CB, Stroud RE, Spinale FG. Long-term localized high-frequency electric stimulation within the myocardial infarct: Effects on matrix metalloproteinases and regional remodeling. *Circulation*.122:20-32

CHAPTER 9

Conclusions and Limitations

The work presented in this dissertation illustrated the utility of injectable hydrogels based on the molecule hyaluronic acid (HA) to engineer the left ventricular (LV) remodeling process that occurs following a myocardial infarction (MI) by encapsulating and locally delivering therapeutic proteins to the MI region. Specifically, HA hydrogels were designed and implemented for the delivery of two therapeutic proteins: stromal cell-derived factor-1 alpha (SDF-1a) and tissue inhibitor of matrix proteinases-3 (TIMP-3), and a range of *in vitro* and *in vivo* studies were implemented to understand how the controlled delivery of proteins through electrostatic interactions and hydrogel degradation influence therapeutic outcomes. The following sections summarize the conclusions and limitations of each Aim, as well as present a prospective on future directions for this area of research.

9.1. <u>Specific Aim 1</u>: Demonstrate that local rSDF-1α delivery from HA hydrogels homes mobilized bone marrow derived cells (BMCs) to the heart following MI.

Conclusions: Both rSDF-1α and the crosslinkable HA macromer stimulated BMC chemotaxis up to 4-fold *in vitro* through CXCR4 and CD44 receptor signaling, respectively. Moreover, the HEMA-HA macromer bound rSDF-1α with a dissociation constant of 36±5 μM through electrostatic interaction. When formed into hydrogels via photo-initiated crosslinking, release of encapsulated rSDF-1α and crosslinked HA were sustained for over 7 days, and these molecules significantly increased BMC chemotaxis *in vitro*. When applied to the heart following experimental MI in mice, the HA hydrogel containing rSDF-1α significantly increased the number of systemically infused BMCs in the heart by ~8.5 fold after 7 days over untreated controls, likely through both systemic and

local effects of released molecules. We conclude that sustained release of rSDF-1α and HA from our photo-crosslinked HA hydrogels enhances circulating BMC homing to the remodeling myocardium better than delivery of rSDF-1α alone.

Limitations: While our finding that SDF-1α release from HA hydrogels enhances BMC homing through both SDF-1α and HA activities is significant, several experimental variables limit the implications of this result. First, it was necessary to deliver BMCs to the animals and this was completed 3 hrs following MI induction. Although this was necessary to quantify homing to the heart, the approach here was not intended to investigate injected cell therapies, but rather the influence of the delivered molecule alone. Also, during this acute stage of post MI remodeling, the endothelium of the coronary vasculature is activated with adhesion molecules to regulate cell trafficking to the remodeling myocardium[1]. While delivering SDF-1α and HA during this phase enhanced engraftment of BMCs, whether or not SDF-1α and HA delivery at a more chronic stage would have the same effect is unclear. Therefore this therapeutic strategy may be limited to acute post MI remodeling. Further, since a heterogeneous population of BMCs was used to model cell homing, it is unclear which populations of cells responded to local molecule delivery and in this Aim, we did not investigate the actual influence of the homed cells on LV remodeling. Therefore, we can only speculate about what effect the responsive cells would have on post MI remodeling. Finally, while recruiting endogenous populations of progenitor cells to repair the heart is an attractive strategy to avoid *ex vivo* cell manipulations, progenitor cell numbers have been shown to decline with age[2-4], and therefore the endogenous capacity for regeneration in older patients may be a limiting factor in the translation of this approach.

9.2. <u>Specific Aim 2</u>: Assess the therapeutic benefit of engineered SDF-1α analogue (ESA) delivery from injectable HA hydrogels post MI.

Conclusions: Encapsulating ESA in redox-initiated HEMA-HA hydrogels

sustained ESA release for over 4 weeks as the hydrogels degraded *in vitro*. Interestingly, aggregates of ESA were observed dispersed throughout the gel suggesting the engineered protein is less water-soluble than native SDF-1α, but remained active in enhancing progenitor cell chemotaxis over the 4-week *in vitro* study. Further, endothelial progenitor cell (EPC) chemotaxis to molecules released from the hydrogel alone was significantly enhanced, consistent with the finding in Aim 1 that HA released from the degradable HA hydrogels provides a cue for cell migration. When delivered to the heart within injectable hydrogels following MI induction in rats, near-IR tagged ESA was detected for over 3 weeks in the heart using transthoracic optical microscopy, consistent with *in vitro* release kinetics. Injection of the HA hydrogels alone significantly reduced LV fibrosis and dilation and significantly improved cardiac output (CO) and LV end-systolic pressure volume relationship (ESPVR). Further, significant increases in CXCR4+ cell and capillary densities were observed with hydrogel injection alone. However, delivery of ESA from hydrogels further reduced adverse LV remodeling with significant reductions in LV fibrosis and wall thinning, and significant increases in CO, ejection fraction (EF) and ESPVR compared to gel injection alone. Further, ESA delivery significantly increased CXCR4+ cell densities in the myocardium. We conclude that injectable HA hydrogels allow for sustained delivery of ESA to the myocardium post MI, and this approach effectively attenuates adverse LV remodeling in a rat model of MI through both hydrogel bulking and SDF-1α/CXCR4 homing effects.

Limitations: While this study provided a strong proof-of-concept that injectable HA hydrogel mediated delivery of ESA significantly attenuates post MI remodeling in rats, several experimental variables limit the implications of this finding. First, it is important to note that while a fluorescent ESA signal was detected in the heart for over 3 weeks following hydrogel injection, this does not confirm activity of delivered ESA for over 3 weeks *in vivo*. The engineered ESA is still susceptible to protease degradation; therefore, additional studies are warranted to investigate duration of active ESA *in vivo.* Second, the hydrogels

152

with encapsulated ESA were delivered immediately following MI. As described in the limitations to Aim 1, this time period may be optimal to enhance recruitment of endogenous cells, and therefore the positive findings reported here may not be generally applied to clinical situations where treatment modalities must be effective in the setting of chronic heart failure. In addition to providing a SDF-1α signal in the early stages of post MI remodeling, the injected hydrogels provide mechanical support to the ischemic myocardium and therefore may be more effective in attenuating LV remodeling when applied directly following MI induction. Therefore, the results from this Aim must be considered in an acute MI context. For both Aims 1 and 2, a further limitation exists in that each injection technique required direct injection either on or within the infarct tissue from a syringe, rather than through a percutaneous delivery approach. This may limit the patient population that could undergo such a process for hydrogel injection.

9.3. <u>Specific Aim 3</u>: Investigate the effect of local TIMP-3 release from injectable HA hydrogels on MMP activity and LV remodeling following MI

Conclusions: HEMA-HA macromers bound rTIMP-3 with a dissociation constant of 3.8±0.3 µM through electrostatic interaction. When encapsulated in redox-initiated HEMA-HA hydrogels, rTIMP-3 release was sustained for over 2 weeks *in vitro*. When delivered to the myocardium following experimental MI in pigs, a detectable rTIMP-3 signal was still present at the injection sites after 7 days, indicating that rTIMP-3 release was sustained for at least 7 days from injectable HA hydrogels *in vivo*. This delivery approach effectively inhibited MMP activity within the MI region compared to MI only and hydrogel alone control groups. By restoring the TIMP/MMP balance, infarct expansion was abrogated, LV dilation reduced by ~20%, and ejection fraction increased by ~20% when compared to MI only 14 days post MI (p<0.05). Further, smooth muscle actin content indicative of myofibroblast proliferation increased and pro-inflammatory cytokine levels were reduced within the MI region 14 days post MI with TIMP-3

delivery. These changes were not associated with a significant increase in collagen accumulation compared to hydrogel delivery alone. We conclude that these results provide the first proof of concept that local and sustained delivery of a recombinant TIMP from injectable HA hydrogels can effectively attenuate the adverse post MI remodeling process in a large animal model of MI by normalizing MMP activity and pro-inflammatory cytokines, and inducing contractile myofibroblast proliferation.

Limitations: While it is clear from this study that local delivery of rTIMP-3 from injectable HA gels has beneficial effects on post MI remodeling, the mechanism for this benefit remains associative. rTIMP-3 delivery inhibited MMP activity, altered fibroblast phenotype, and attenuated cytokine signaling within the MI region; therefore, it is difficult to speculate about which has the largest impact on the remodeling process. Further, while observing these beneficial results in a large animal model of MI is a significant step towards translating this therapeutic approach to humans, the hydrogels were injected immediately following MI induction, which may not be possible in a clinical scenario. However, since ECM turnover is important for adequate wound healing following MI[5,6], early MMP inhibition may not necessarily be optimal. Therefore, additional studies are warranted that examine the optimal window for localized modulation of TIMP levels within the MI region, with respect to providing maximal prevention of adverse remodeling and minimal interference with the necessary wound healing response. Further, rTIMP-3 was chosen for its strong binding to the ECM[7-9] and its critical role in post MI remodeling[10-12], however the three other TIMPs could also be suitable candidates for therapeutic delivery post MI. In addition, while communications with collaborating laboratory (F.G. Spinale) revealed that injections of rTIMP-3 alone had little effect of post MI remodeling, adding this treatment group would better illustrate the importance of sustaining rTIMP-3 levels in the myocardium with injectable hydrogels. Finally, additional dose-titration studies will be required to determine the minimal threshold levels of rTIMP-3 release in order to significantly affect LV regional geometry and function

post MI while limiting off target effects.

9.4. <u>Specific Aim 4</u>: Develop sulfated HA macromers to incorporate high TIMP-3 binding affinity into injectable HA hydrogels.

Conclusions: We developed sulfated and vinyl modified HA macromers by first synthesizing HEMA-HA, then sulfating primary hydroxyls along the HA backbone through nucleophilic substitution with SO_3 (HEMA-SHA). The sulfation reaction did not alter HEMA group modification and therefore HEMA-SHA macromers could be readily incorporated into HEMA-HA gels by simply blending the two macromers together at a desired ratio and initiating crosslinking with free radical initiators. Sulfate content of HEMA-SHA macromers was significantly greater than HEMA-HA, and comparable to sulfate content of heparin. In addition, HEMA-SHA bound rTIMP-3 with an affinity comparable to heparin, and could be covalently incorporated into hydrogels without altering hydrogel crosslinking. Once incorporated into the hydrogels, HEMA-SHA significantly reduced encapsulated rTIMP-3 release (~15% compared to 60% total release) over 14 days. We conclude that these sulfated HA macromers provide a useful way to introduce heparin-binding features into radically crosslinked HA hydrogels without altering hydrogel architectures, and can therefore be applied in a wide range of radically crosslinked HA hydrogel systems, including injectable hydrogels for localized rTIMP-3 delivery.

Limitations: While we showed comparable rTIMP-3 binding to sulfated HA macromers and heparin, the differences in sulfation pattern between the two polymers is likely to alter the library of proteins they bind[13]. Therefore, further investigation into protein binding specificity of HEMA-SHA polymers is warranted. In addition, these hydrogels would be exposed to a wide-range of proteins *in vivo*, and binding endogenously expressed proteins could affect biological processes. Therefore, demonstrating biocompatibility of injectable HEMA-SHA blended gels *in vivo* in the context of the intended therapeutic application is important. Further, the high concentration of highly acidic sulfate groups on the

HEMA-SHA polymers could affect the viability of cells encapsulated in HEMA-SHA blended hydrogels. Therefore, cell viability studies in a range of HEMA-HA/HEMA-SHA ratios is important towards cellular applications of these hydrogels.

9.5. <u>Specific Aim 5</u>: Engineer injectable HA hydrogels with MMP sensitive degradation to allow for localized TIMP-3 delivery as a function of MMP expression within the MI region.

*Conclusions***:** In order to form HA hydrogels with MMP degradable crosslinks upon injection through a syringe, a two component, aldehyde (ALD) and hydrazide (HYD) macromer system was developed. This system allowed for rapid crosslinking of stable hydrogels upon mixing ALD and HYD macromers, and limited passive rTIMP-3 release by incorporation of ALD functionalized dextran sulfate (DS) macromers for strong rTIMP-3 binding in the hydrogels. In the presence of 20 nM rMMP-2, the hydrogels degraded over 14 days, releasing encapsulated rTIMP-3 in response to MMP-2. However, hydrogels without encapsulated rTIMP-3 completely degraded in two days in 20 nM rMMP-2, indicating that the encapsulated rTIMP-3 remains active as it is bound in the hydrogel over the 14-day study as it attenuates MMP-mediated degradation. Regional injection of the hydrogel alone immediately following MI induction in pigs normalized MMP activity in the MI region to baseline values at 14 days post MI, potentially by acting as a sink for active MMPs as the MMP-degradable crosslinks were cleaved. However, delivery of the hydrogel alone did not significantly attenuate LV remodeling as measured by LV wall thickness, LV end-diastolic volume (LVEDV), pulmonary capillary wedge pressure (PCWP), and ejection fraction (EF). Regional delivery of rTIMP-3 encapsulated in the hydrogels further reduced MMP activity within the MI region compared to hydrogel alone injections, and significantly attenuated LV remodeling as evidenced by significant increases in LV wall thickness, EF, and PCWP compared to MI only and hydrogel alone controls, and a significant decrease in

LVEDV compared to hydrogel alone controls. Further, these beneficial effects on LV function were observed without an increase in systemic rTIMP-3 levels with gel/rTIMP-3 delivery to the heart. We conclude that MMP-triggered release of rTIMP-3 with injectable MMP-degradable hydrogels is an effective strategy to attenuate adverse LV remodeling while avoiding systemic concentrations of MMP inhibitors.

Limitations: While rTIMP-3 delivery from MMP degradable hydrogels significantly attenuated post MI remodeling, interstitial MMP activity was not significantly different with rTIMP-3 delivery compared to hydrogel delivery alone. Therefore additional studies are warranted to investigate other biological effects of rTIMP-3 as in Aim 3. Further, as discussed in the limitations of Aim 3, delivering an MMP inhibitor very early following MI may prevent ECM turnover necessary for wound healing; therefore, additional studies are warranted to find an optimum window following MI for this therapeutic strategy. In addition, delivery of this therapy immediately following MI may not be relevant to clinical scenarios of chronic MI. Also, serial echocardiography measurements revealed progressive decline in LV function in all groups over the two week study, therefore longer term studies are warranted to see if therapeutic effects are maintained at later time points. Finally, as demonstrated in Aim 3, injection of hydrogels alone has beneficial effects on post MI remodeling by bulking and mechanically supporting the myocardium. Little effect was observed in this Aim with hydrogel injection alone; therefore, hydrogels that degrade to release encapsulated molecules may not be as optimal as they lose their mechanical properties over time.

9.6. Future Directions

Based on the limitations of the studies performed in this dissertation, there are numerous avenues of future exploration related to HA hydrogels for the delivery of therapeutic proteins.

For all Aims in which hydrogels were injected immediately following MI,

application of the hydrogel systems in chronic models of MI (injections weeks to months following MI induction) would lead to a better understanding of the therapeutic window available to deliver hydrogels and encapsulated proteins post MI. In addition, percutaneous delivery of the hydrogels through catheter technologies would allow therapeutic application of the hydrogels and proteins in a larger population of patients where a thoracotomy is not part of the current clinical treatment. Finally, different doses of encapsulated proteins (SDF-1α and TIMP-3) would identify optimal conditions for stimulating cell homing and MMP inhibition.

For SDF-1α delivery, animal models with labeled bone marrow would allow a more mechanistic understanding of the contribution of homed cells towards myocardial repair. In addition, animal models with humanized bone marrow would better assess the therapeutic potential of sustained SDF-1α delivery in patients.

For TIMP-3 delivery, longer therapeutic studies would better elucidate whether early MMP inhibition delays the progression of LV remodeling or permanently interrupts remodeling events. Further, injectable hydrogels with peptide crosslinks that degrade at different rates could be explored to identify an optimal rate of MMP-triggered TIMP-3 release. In addition, to maintain hydrogel bulking while delivering TIMP-3 on demand, inter-penetrating networks of an MMP degradable phase and a stable phase could be constructed.

Finally, the hydrogels developed in this dissertation could be explored for the delivery of a wide range of therapeutic proteins and combinations thereof by simply mixing the reconstituted proteins with the hydrogel precursor solution.

9.7. References

1.	Abbott, J. D.; Huang, Y.; Liu, D.; Hickey, R.; Krause, D. S.; Giordano, F. J., Stromal cell-derived factor-1alpha plays a critical role in stem cell recruitment to the heart after myocardial infarction but is not sufficient to induce homing in the absence of injury. *Circulation* **2004,** 110, (21), 3300-5.

2.	Vaziri, H.; Dragowska, W.; Allsopp, R. C.; Thomas, T. E.; Harley, C. B.; Lansdorp, P. M., Evidence for a mitotic clock in human hematopoietic stem cells: loss of telomeric DNA with age. *Proc Natl Acad Sci U S A* **1994,** 91, (21), 9857-60.

3.	Conboy, I. M.; Conboy, M. J.; Smythe, G. M.; Rando, T. A., Notch-mediated restoration of regenerative potential to aged muscle. *Science* **2003,** 302, (5650), 1575-7.

4.	Fuller, J., Hematopoietic stem cells and aging. *Sci Aging Knowledge Environ* **2002,** 2002, (25), pe11.

5.	Ertl, G.; Frantz, S., Healing after myocardial infarction. *Cardiovasc Res* **2005,** 66, (1), 22-32.

6.	Cleutjens, J. P.; Kandala, J. C.; Guarda, E.; Guntaka, R. V.; Weber, K. T., Regulation of collagen degradation in the rat myocardium after infarction. *J Mol Cell Cardiol* **1995,** 27, (6), 1281-92.

7.	Leco, K. J.; Khokha, R.; Pavloff, N.; Hawkes, S. P.; Edwards, D. R., Tissue inhibitor of metalloproteinases-3 (TIMP-3) is an extracellular matrix-associated protein with a distinctive pattern of expression in mouse cells and tissues. *J Biol Chem* **1994,** 269, (12), 9352-60.

8.	Yu, W. H.; Yu, S.; Meng, Q.; Brew, K.; Woessner, J. F., Jr., TIMP-3 binds to sulfated glycosaminoglycans of the extracellular matrix. *J Biol Chem* **2000,** 275, (40), 31226-32.

9.	Lee, M. H.; Atkinson, S.; Murphy, G., Identification of the extracellular matrix (ECM) binding motifs of tissue inhibitor of metalloproteinases (TIMP)-3 and effective transfer to TIMP-1. *J Biol Chem* **2007,** 282, (9), 6887-98.

10.	Fedak, P. W.; Smookler, D. S.; Kassiri, Z.; Ohno, N.; Leco, K. J.; Verma, S.; Mickle, D. A.; Watson, K. L.; Hojilla, C. V.; Cruz, W.; Weisel, R. D.; Li, R. K.; Khokha, R., TIMP-3 deficiency leads to dilated cardiomyopathy. *Circulation* **2004,** 110, (16), 2401-9.

11.	Tian, H.; Cimini, M.; Fedak, P. W.; Altamentova, S.; Fazel, S.; Huang, M. L.; Weisel, R. D.; Li, R. K., TIMP-3 deficiency accelerates cardiac remodeling after myocardial infarction. *J Mol Cell Cardiol* **2007,** 43, (6), 733-43.

12.	Kassiri, Z.; Defamie, V.; Hariri, M.; Oudit, G. Y.; Anthwal, S.; Dawood, F.; Liu, P.; Khokha, R., Simultaneous transforming growth factor beta-tumor necrosis factor activation and cross-talk cause aberrant remodeling response and myocardial fibrosis in Timp3-deficient heart. *J Biol Chem* **2009,** 284, (43), 29893-904.

13.	Satoh, T. N., K; Nagahata, M; Teramoto, A; Abe, K, The research on physiological property of functionalized hyaluronan: interaction between sulfated hyaluronan and plasma proteins. *Polym. Adv. Technol.* **2004,** 15, 720-725.